Aachener Verfahrenstechnik Series
AVT.CVT – Chemical Process Engineering
Volume 3 (2020)

Axel Böcking

Membrane Transport Properties and Process Design in Nanofiltration with Organic Solvents and Aqueous Solvent Mixtures

Membrane Transport Properties and Process Design in Nanofiltration with Organic Solvents and Aqueous Solvent Mixtures

Transporteigenschaften von Membranen und Prozessdesign in der Nanofiltration mit organischen Lösungsmitteln und wässrigen Lösungsmittelgemischen

Von der Fakultät für Maschinenwesen
der Rheinisch-Westfälischen Technischen Hochschule Aachen
zur Erlangung des akademischen Grades
eines Doktors der Ingenieurwissenschaften genehmigte Dissertation

vorgelegt von

Axel Böcking

Berichter:
Univ.-Prof. Dr.-Ing. Matthias Wessling
Univ.-Prof. Dr.-Ing. habil. Jens-Uwe Repke

Tag der mündlichen Prüfung: 27.01.2020

Diese Dissertation ist auf den Internetseiten der Universitätsbibliothek online verfügbar.

Berichte aus der Verfahrenstechnik

Axel Böcking

Membrane Transport Properties and Process Design in Nanofiltration with Organic Solvents and Aqueous Solvent Mixtures

Shaker Verlag
Düren 2020

Bibliographic information published by the Deutsche Nationalbibliothek
The Deutsche Nationalbibliothek lists this publication in the Deutsche Nationalbibliografie; detailed bibliographic data are available in the Internet at http://dnb.d-nb.de.

Zugl.: D 82 (Diss. RWTH Aachen University, 2020)

Printed in Germany.

ISBN 978-3-8440-7397-3
ISSN 0945-1021

Shaker Verlag GmbH • Am Langen Graben 15a • 52353 Düren
Phone: 0049/2421/99011-0 • Telefax: 0049/2421/99011-9
Internet: www.shaker.de • e-mail: info@shaker.de

Danksagung

Die Abfassung einer Dissertationsschrift ist stets ein Produkt aus der Zusammenarbeit eines Einzelnen mit Vielen. Allen, die mich bei der Arbeit an meiner Dissertation auf unterschiedlichste Art und Weise unterstützt haben, möchte ich an dieser Stelle danken.

Ganz besonderen Dank gilt Prof. Dr.-Ing. Matthias Wessling für die fachliche Betreuung der Arbeit sowie die motivierenden und offenen Gespräche während meiner Zeit am Lehrstuhl für chemische Verfahrenstechnik der RWTH Aachen University.

Ebenso bedanke ich mich bei Prof. Dr.-Ing. habil. Jens-Uwe Repke für die Übernahme des Koreferats und Begutachtung der vorliegenden Arbeit.

Mein Dank gilt auch meinen ehemaligen Kollegen für die angenehme Arbeitsatmosphäre am Lehrstuhl und die vielen hilfreichen unterstützenden Beiträge und Diskussionen. Insbesondere sind an dieser Stelle Benedikt Aumeier, Burkhard Ohs, Johannes Kamp, Stefanie Kriescher und John Linkhorst zu nennen, die mich selbst nach meiner Zeit am Lehrstuhl durch Kritik und Korrekturen unterstützten. Zudem bedanke ich mich bei allen meinen ehemaligen Bürokollegen sowie den Kollegen aus der ehemaligen “SusPro”-Gruppe des Lehrstuhls für andauernde Hilfe und förderliche Diskussionen zu Forschungsfragen und Konferenzbeiträgen. Weiterhin bedanke ich mich für unersetzliche Hilfe bei Susanne Offermann die im Sekretariat des Lehrstuhls als gute Seele mit allen möglichen Belangen von wissenschaftlichen Mitarbeitern und Studenten betraut wird und immer beste Lösungen findet (auch auf unzähligen Baubesprechungen!). Nicht zu vergessen ist auch die Buchhaltung, Helga Walbert und Regina Hetzel, die mich stets sicher bezüglich Projektfinanzierung und HiWi-Geldern unterstützten, sowie Karin Faensen, die für neue Standards der Arbeitssicherheit in den CVT-Laboren sorgt.

Ganz besonderen Dank gilt auch den vielen helfenden Händen an der AVT die einen den Servicebetrieb aufrechterhalten und erst gute wissenschaftliche Arbeit ermöglichen. Die Rede ist von den AVT-lern aus den Werkstätten (mechanische und elektrische), dem Zentral-Labor und dem

IT-Service die stets hilfreich und schnell Probleme beseitigen.

Unvergessen bleiben auch meine zahlreichen Studenten und Projektpartner, die mich forderten und damit auch fördertern.

Einen erheblichen Teil meiner Zeit am Lehrstuhl war ich im Neubau-Projekt der AVT-Lehrstühle involviert. Auch für die zahlreichen über den Tellerrand reichenden Erfahrungen, die ich dabei sammelte möchte ich mich insbesondere bedanken bei: Simon Roth, Robert Keller, Jörn Viell, Peter Peters, Frau Pilic und Frau Fischbach und Herrn Wuttke. Sie und alle weiteren Partner im Bauprojekt sorgten dafür, dass der Neubau der AVT-Lehrstühle, das “Center for Next Generation Processes and Products” = das NGP^2 im Februar 2017 bezogen werden konnte. Bedanken möchte ich mich auch bei meiner Vorgängerin in der lehrstuhlseitigen Projektleitung Fee Pitsch und bei Thomas Harlacher für diese verantwortungsvolle Aufgabe und der Beantwortung aller Fragen bezüglich vergangener Bauphasen.

Im Privaten danke ich meiner Familie und meinen Freunden, die mir ebenfalls stets zur Seite stehen und mich unterstützen. Auch sorgen sie immer wieder für Abwechslung und Zerstreuung, wenn man sie benötigt.

Schließlich danke ich meiner Frau Katja Böcking für ihre unendliche Geduld und ihrem unermüdlichen Antrieb. Ihr habe ich mit Abstand die meisten Nerven abverlangt und wäre ohne ihre motivierende Art wohl nie zu einem Schluss gekommen.

Es bleibt Magie,
auch wenn man eine Erklärung dafür hat.

- Terry Pratchett

Contents

Abstract

Nanofiltration processes are energy saving and product-friendly. However, many effects and phenomena are still hidden or not understood. In particular, for processes with organic solvents as process medium has lacked standardized measuring methods and reliable data. Further, findings are rare from the combination of aqueous nanofiltration (aq. NF) and organic solvent nanofiltration (OSN).

Collaborative tests were performed with partners at various research institutions to standardize an experimental procedure. The results were statistically evaluated. The assessment certified high-quality data as an outcome of the standardized method. A process design optimization for membrane cascades was carried out with the statistical data. It showed that small differences affect a possible process configuration. Subsequently, five optimization scenarios were used to investigate the design of an OSN cascade. As a unique condition, at least one of the solutes had a negative retention value. This condition means that the membrane did not retain this substance. The solute instead accumulated in the permeate. The achievable selectivity is dependent on the mutual distance of the respective retentions. Also, their position on the retention scale is significant. The experiments were continued in the field of Solvent tolerant nanofiltration (STNF). The polymeric membranes used were developed for the OSN or aq. NF. Water was successively added to the organic solvent to create an appropriate process medium. The dominant effects changed in solvent mixtures with an ethanol content of between $60\,\mathrm{wt}\%$ and $80\,\mathrm{wt}\%$. This result applied for charged and uncharged solutes. Similar, a ceramic membrane type was used, which was coated with polyelectrolytes in water. This membrane type had previously only been used in the aq. NF. The retention and flux results were explained by the cononsolvency effect combined with the polarity effect of the solution. Cononsolvency were traced back to the disturbing of hydrogen bonds.

This thesis proves the quality of retention and flow data from the standardized method. This quality provides the necessary reliability to spread the technology of OSN and STNF. Even small data deviations can lead to a changed optimal process setup. The selectivity in such a configuration depends on the difference in retention and the position on retention scale. Process performance can be varied by adding water or an organic solvent to the process fluid. In mass transfer through membranes are also little known or unknown effects involved. Such effects have been demonstrated in experiments, e.g., cononsolvency or preferential solvation.

Zusammenfassung

Nanofiltrationsprozesse sind energiesparend und produktschonend. Viele Effekte und Phänomene sind jedoch noch unbekannt oder nicht verstanden. Insbesondere bei Prozessen mit organischen Lösungsmitteln als Medium fehlen standardisierte Messverfahren und zuverlässige Daten. Darüber hinaus sind Ergebnisse aus der Kombination von wässriger (aq. NF) und organophiler Nanofiltration (OSN – Englisch: Organic Solvent Nanofiltration) selten.

Diese Dissertation zeigt die, in Zusammenarbeit mit verschiedenen Forschungseinrichtungen, durchgeführten Tests zur Standardisierung einer experimentellen Messmethode. Die statistische Auswertung der Ergebnisse bescheinigte qualitativ hochwertige Daten. Mit der standardisierten Methode können hervorragend Daten reproduziert werden. Ebenso wurde mit den Ergebnissen das Prozessdesign für Membrankaskaden optimiert. Es zeigte sich, dass bereits kleine Unterschiede eine mögliche Prozesskonfiguration beeinflussen. Anschließend wurden fünf Optimierungsszenarien verwendet, um das Design einer OSN-Kaskade zu untersuchen. Als besondere Bedingung hatte mindestens einer der gelösten Stoffe einen negativen Rückhalt. Dies bedeutet, dass die Membran diese Substanz nicht zurückgehalten, sondern der gelöste Stoff sich stattdessen im Permeat angesammelt hat. Die erreichbare Selektivität ist nicht nur vom Abstand der jeweiligen Rückhalt-Werte zueinander abhängig, sondern auch von ihrer Position auf der Rückhalt-Werte-Skala. Die Experimente wurden im Bereich der sogenannten „solvent tolerant nanofiltration“ (STNF) fortgesetzt. Dafür wurden Polymer-Membranen verwendet, die für die OSN oder aq. NF entwickelt wurden. Dem org. Lösungsmittel wurde sukzessive Wasser zugesetzt. Die dominanten Effekte änderten sich bei Gemischen mit einem Ethanolgehalt zwischen 60 und 80 wt%. Die Änderungen wurden sowohl für geladene als auch für ungeladene gelöste Stoffe beobachtet. Außerdem wurde ein keramischer Membrantyp verwendet, der mit Polyelektrolyten in Wasser beschichtet wurde. Dieser Membrantyp wurde bisher nur in der aq. NF verwendet. Die Rückhalt- und Flussergebnisse wurden durch die Polarität der Lösung in Kombination mit dem „Cononsolvency“-Effekt erklärt. Dieser Effekt wurde dabei auf die Störung der Wasserstoffbindungen im Medium zurückgeführt.

Die Dissertation beweist die Qualität der Rückhalt- und Fluss-Daten aus der standardisierten Methode. Diese Qualität bietet die notwendige Sicherheit, um die Technologien (OSN und STNF) in der Industrie zu etablieren. Schon kleine Datenabweichungen können zu einer veränderten optimalen Prozessgestaltung führen. Die Selektivität in einer Prozesskaskade hängt von der Differenz der Rückhalte und der Position auf der Rückhalt-Werte-Skala ab. Die Prozessleistung kann durch Zugabe von Wasser oder einem org. Lösungsmittel verändert werden. Beim Stoffaustausch durch Membranen sind auch wenig bekannte oder unbekannte Effekte beteiligt. Solche Effekte wurden in Experimenten nachgewiesen, z.B. „Cononsolvency“ oder bevorzugte Solvatisierung.

1 Introduction

1.1 Motivation

Our industrial society has a responsibility to future generations. Prosperity is based on globally available resources and secure, reliable and affordable energy supply. Besides, such energy savings and resource conservation result in a reduction of CO_2 emissions. For sustainable use of energy, it is not only the energy production that must be considered but also the entire energy chain from production to use by the consumer. The intelligent use of energy also offers significant potential for the conservation of resources [Unit2015]; [Euro2010]; [Blum2017]; [Bart2016]; [SusC2018]. In general, we have to improve the handling and recovery of resources continuously.

Therefore, the redesign and new approaches for production processes in classical process engineering are of great importance. Separation processes (especially thermal separation processes) are the most energy intensive processes in the chemical, petrochemical and pharmaceutical industries. These processes have a significant energy saving potential and account for 50 % to 90 % of total production costs [Mart2012]. Politics has already recognized this and reacts supportively with new goals for the most efficient and ecological use of raw resources and energy.

In Germany the "energy Concept for an environmentally friendly, reliable and affordable energy supply" was developed in 2010 [BMWi2010]. This concept is to be understood as a guideline for reliable, economical and environment-friendly energy supply in future. To achieve these ambitious goals, the German government expanded its energy and climate policy in 2011 by promoting research and developments in sustainable energy technologies. This strategic approach is laid down in the "6th Energy Research

Programme of the Federal Government" [BMWi2011]. Besides, the funding initiatives are regularly evaluated and, for example, published in the "Bundesbericht Energieforschung 2018" [BMWi2018].

With a contribution of 45 %, industry, commerce, trade, and services are major energy consumers in Germany [BMWi2011]; [AGEB2018] . Therefore, they are of central importance for the implementation of energy system transformation and climate protection. Under the heading "3.1.3 Energy efficiency in industry, commerce, trade, and services" the funding areas for the chemical industry can be found. Such areas include "reducing the use of energy in the process" and "optimizing existing processes."

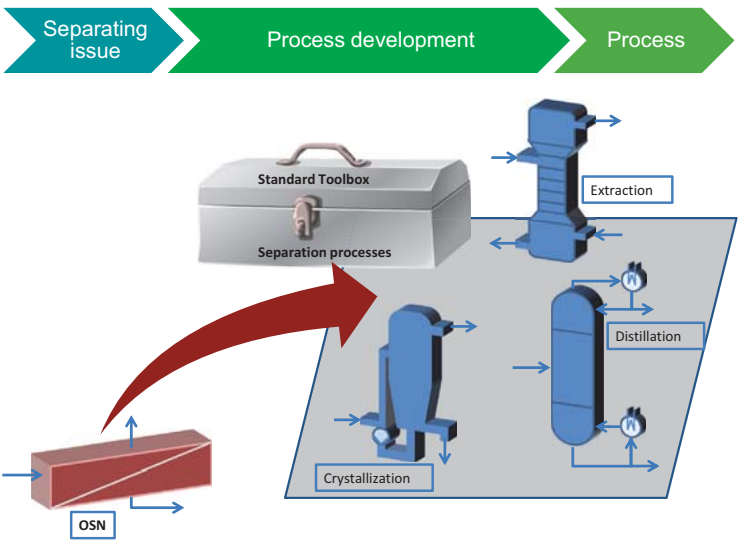

Figure 1.1: The overall ambition of the ESIMEM project: Integration of the OSN technology into the "standard toolbox" of separation processes.

Intensive energy savings and recovery of essential chemicals, as well as product-friendly separation of different valuable substances in the process streams, can be realized by membrane processes. Accordingly, research projects in this area are being supported. The collaborative project "Energy Efficient Material Separation in the Chemical and Pharmaceutical Industries by Membrane Processes" (ESIMEM) was established as part of

the funding program "Energy Saving and Energy Efficiency." The ESIMEM project is located in the field of nanofiltration with the ambition to enable OSN technology to be integrated into a standard process toolbox (Figure 1.1). To compete with the traditional processes, process developers have to evaluate the applicability of the OSN process early. Accordingly, a reliable, standardized method for determining the separation properties of membranes was the primary objective. The progress and outcome of this project mainly resulted in this dissertation.

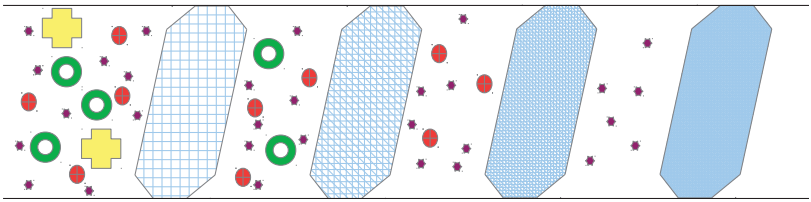

Process	Microfiltration	Ultrafiltration	**Nanofiltration**	Reverse osmosis
Pore size	~ 0,1 µm	~ 0,01 µm	**~ 0,001 µm**	~ 0,0001 µm
Pressure	0,3 - 3 bar	0,5 - 10 bar	**3 - 60 bar**	10 - 200 bar
Retention of	Particles Bacteria	Proteins Polymers	**Org. molecules** **200 - 1000 kg kmol^{-1}**	Salts

Figure 1.2: Pressure-driven membrane processes in liquid phase.

Nanofiltration is a membrane process that is positioned between ultrafiltration with porous membrane structures and reverse osmosis with dense membrane structures. In this intermediate range, substances above approximately $200\,\mathrm{kg\,kmol^{-1}}$ are retained which typically requires a pressure of $3\,\mathrm{bar}$ to $60\,\mathrm{bar}$ (Figure 1.2). The selective mass transport through the membrane is based on steric effects, but also intermolecular interactions and electrostatic interactions.

A distinction is made between aqueous nanofiltration (Aq. NF), organic solvent nanofiltration (OSN), and solvent tolerant nanofiltration (STNF) depending on the medium treated by nanofiltration.

1.2 Nanofiltration processes

Membrane processes are mainly used for the separation, concentration, and recovery of valuable materials. The most common are three-end processes (or modules) with a feed stream, a retentate stream, and a permeate stream. The semipermeable structures of the membranes allow selective separation of substances with similar properties. The difference in chemical potential between the retentate and permeate side causes the driving force [Meli2007]. In particular, the difference in concentration and pressure, as well as the affinities between the substances, are essential for nanofiltration processes described in the chapters of this thesis.

Polymeric membranes can be used in all nanofiltration processes. Three key advantages of polymer membranes are the often simple large-scale production process, large membrane areas with small modules, and good commercial availability. Three disadvantages of membranes made of polymers are the limited chemical and thermal stability as well as the necessity to use often harmful chemicals during production.

Besides polymeric membranes, developments have been made in the field of ceramic membranes for use in nanofiltration applications [Marc2013]; [Marc2014]. For instance, layer-by-layer methods (LbL) can be used to upgrade ceramic porous micro- or ultrafiltration membranes [Menn2016b]. With this method, a coating of the basic structure is applied which can be tailored to the process requirements and conditions.

The main advantages of ceramic membranes are high chemical and thermal stability coupled with no swelling or compression. Their disadvantages include a complex and energy-intensive manufacturing processes and less understood transport phenomena.

Aqueous nanofiltration is the most widespread nanofiltration process. It is mainly used in drinking water production and water purification [Van 2008]; [Moha2015]; [Oatl2017].

In contrast, the OSN is still in its incubation phase. Consequently, the demand for new innovative membrane materials and sophisticated predictive models is accompanied by a request for standardized experimental

procedures and thus high data quality. The latter enables a faster and more reliable process design. As a result, more and more OSN processes can be implemented. Some applications for these processes can be found in the pharmaceutical industry and the production of specialty chemicals. However, the possibilities for applications of this technology are continously growing and become gradually available in other areas as well [Vand2008]; [Peev2010]; [Marc2014].

So far, significantly less research has been conducted on STNF processes. Nevertheless, these processes also gain a growing interest in the industry. For example, agrochemicals and specialty chemicals can benefit from these processes. In their production, mixtures of water and organic solvents as process streams exist in many cases [Post2015]; [Mert2018].

1.3 Scope of this work

This thesis presents investigations in nanofiltration with organic solvents in the medium. Both organic solvent nanofiltration (OSN) and solvent tolerant nanofiltration (STNF) are addressed.

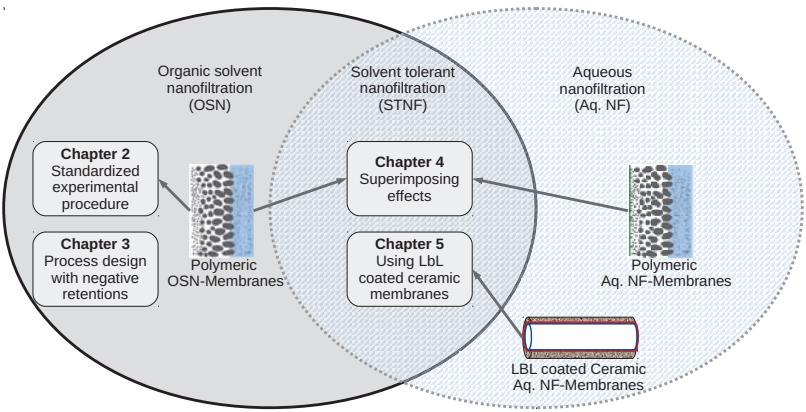

Figure 1.3: Outline of this thesis.

Initially, issues in the OSN and the modeling of such processes are discussed. The following chapters cover the field of STNF. This research field

was entered by adding water to the solvent system. The results from the first STNF experiments inspired the experimental investigation of coated ceramic membranes. Such membranes were developed for aqueous nanofiltration. Hence, this time, the addition of organic solvents to the originating solvent system (water) leads to investigations in STNF. Beyond the experimental results, an outlook is gained on the application of this membrane type in OSN processes (Figure 1.3).

In **chapter 2**, the standardized ESIMEM-procedure for the experimental characterization of OSN membranes is proposed. This standardized process is an important step within the community to generate reliable and high-quality data for the development of new membrane processes. Solvents (ethanol, isopropyl alcohol (IPA), butanone (MEK), ethyl acetate, toluene, and heptane) and dissolved solutes (polystyrene (PS), alkanes, sucrose octaacetate (SOA), poly-(methylmethacrylate) (PMMA)) are categorized and combined to ideal model systems. With experimental test series in different research facilities and industrial development laboratories, the always occurring deviations and possible sources of errors were determined. As a result, the effects of the statistical deviations on the process design are presented.

Chapter 3 addresses emerging questions on the ideal connection of membrane cascades in OSN. The process design is optimized in several scenarios in which combinations of negative and positive retentions are applied. Several retention differences of two solutes are considered as well as the shift of a constant retention difference on the retention scale. In each case, the model found the optimal configuration for a membrane cascade with three stages and showed how the connections change due to the selected conditions.

Chapter 4 continues on the experimental part. The solvent is extended by another component so that now both, water and organic solvents, are contained. As the organic component ethanol or n-methyl-2-pyrrolidone (NMP) are used. Salts and water-soluble polymers (polyethylene glycols (PEGs)) are applied as dissolved substances. The retention and flux measurements should determine which effects occur and how these superim-

pose each other.

In the penultimate chapter (**chapter 5**) a coated ceramic membrane is used. Such membranes were previously used in aqueous nanofiltration by Menne et al. [Menn2016b]. The ceramic supporting structure of the membrane offers various possibilities in the production of nanofiltration membranes and some advantages compared to the conventional polymer or ceramic membranes. The application of these membranes in water-solvent mixtures has not been investigated previously and is therefore presented here for the first time.

1

2 Can the variance in membrane performance influence the design of organic solvent nanofiltration processes?

This chapter has been published as:
Axel Böcking, Velichka Koleva, Jan Wind, Yvonne Thiermeyer, Stefanie Blumenschein, Rebecca Goebel, Mirko Skiborowski, Matthias Wessling
Can the variance in membrane performance influence the design of organic solvent nanofiltration processes?, Journal of Membrane Science, 2019
DOI: 10.1016/j.memsci.2018.12.077

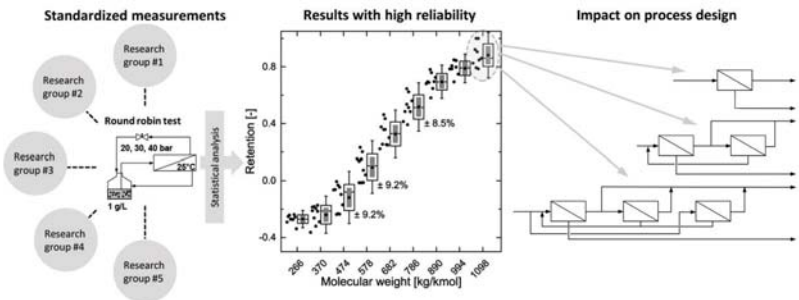

Investigation and evaluation of a standardized experimental procedure for the characterization of polymeric membranes used in organic solvent nanofiltration.

2.1 Introduction

Taking membrane research from its initial phase of concept development, material and membrane design into process development requires substantial resources and time. This is not special but true for many innovations starting with an innovation trigger. This is also known as the Gartner Hype Cycle [Lind2003]. Judgment of the quality of the innovation trigger occurs often through reproducibility and applications studies and generally also creates - after a peak of inflated expectations - a trough of disillusion.

In membrane research, the innovation trigger is assumed to occur through the availability of new materials and membranes made thereof. Yet, it is often not well known how statistically significant the mass transport properties of new membrane materials and new membrane products are. In a recent meta-study for example [Liu2016], published in this journal with more than 3000 references, the authors pose the fundamental questions (a) whether there is an average proton conductivity for Nafion membranes, (b) how the proton conductivity due to Nafion modification has evolved over past 10 years, (c) which additives really contribute to a conductivity increase, (d) how temperature or humidity affect conductivity. While such questions are not scientifically inspiring and do not initiate a new hype cycle, such questions are important in order to understand and judge the significance of a new material or membrane type. Here we pose similar questions with respect to the statistical significance and comparability of characterization methods to quantify mass transport properties for membranes used in organic solvent nanofiltration. As opposed to the meta-study, we have chosen to engage different labs and research groups with comparable analytical infrastructure, to use a round robin test evaluating the results of a developed standard experimental procedure. This leads to conclusions on standard deviations in flux and retention values in a complex parameter space for different membrane materials in various solvent/solute systems.

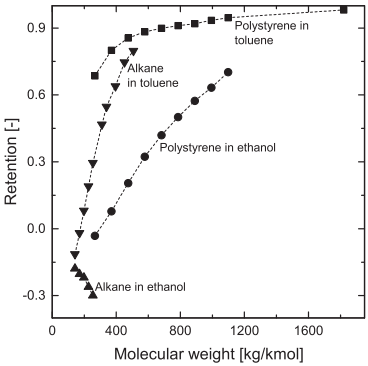

Figure 2.1: Retention measurements using different solvents and solutes for PuraMem® S600 at 30 bar and 25 °C show different behaviour of the membrane.

2.2 Background

Organic solvent nanofiltration (OSN) became a new member of the family of pressure-driven membrane processes by the discovery of solvent resistant membranes. Up to now, a great number of various applications were developed since the production and reactions in organic solvents comprises a wide range [Marc2014]; [Peev2010]. Although OSN is still in the focus of industry as an energy-efficient separation process, there are only a few established plants [Cupe2015]; [Blum2015]; [Have2017]. However, the progress in the investigation of this field is still growing, and the challenges include a wide spectrum of different issues. For instance, the community knows that flux and retention depends on the interaction of solutes, solvents, and membranes [Yang2001]; [Geen2005a]; [Zwij2012]; [Post2016]; [Solt2016]; [Schm2013]; [Hoss2016]. Stamatialis et al. [Stam2006] suggested a three-dimensional space of properties determining the mass transport properties of solvent and solute transport.

Due to this complex interplay, the molecular weight cut off (MWCO), defined as the molecular weight that is rejected by 90 %, also depends on the system of compounds. Figure 2.1 shows retention curves for PuraMem®-S600 at 30 bar in two different solvents using two different solutes. It

demonstrates the strong dependence of the functional membrane characteristic on the used compounds.

Nevertheless, the MWCO is measured and determined for OSN membranes in many different ways, and no standard test system is established [Post2013]; [Dave2017]; [Li2009]; [Silv2015]. See Toh et al. [See 2007] proposed first to standardize the method for a membrane characterization measurement of the MWCO in OSN. The idea was to use a homologous series of polystyrene oligomers which are soluble in many organic solvents to find the MWCO and possibly recognize leak flux. In fact, lot of data can be found in the literature for commercially available and new developed membranes [Bast2017]. These data are commonly presented as individual or a few measurements, and often it is not stated if the data are reproducible.

This diversity of methods and lack of information about comparability and reproducibility is delicate for research as well as an industrial application of the technology, since it complicates and delays a possible commercialization of new membranes. In addition, it poses a risk to process design since data for specific products have to be retested and evaluated. Thus, the expansion of OSN plants in real processes slows down and turns out of focus of the process designer. However, Schmidt et al. [Schm2014] have offered a process design workflow for general new OSN processes, and there exist manuals to support membrane experiments for process design [Cupe2012]. These approaches are indeed steps towards a higher acceptance of OSN in industry, though we still owe a proof of accuracy for results from membrane characterization experiments. Also, Shi et al. [Shi2017] conclude that new research in module and process design is necessary besides new membrane materials to achieve for example ultra-high permeance. Marchetti, Peeva, and Livingston [Marc2017] point out the selectivity challenge in OSN and suggest that process engineering solutions lead to a need of standardized procedures for membrane characterization. In their general review of data quality, Keller et al. [Kell2017] highlight the importance of data quality and especially accuracy and precision as important elements for a correct interpretation and evaluation of experimental results.

In order to achieve this aim and to follow the recommendations of Shi et al. [Shi2017] and Marchetti, Peeva, and Livingston [Marc2017], a consortium of research groups and industrial partners has been formed, working on a comparison and validation of experimental results. The main objective of this consortium is to define and assess a standard experimental procedure for several chemical systems. The standardized procedure should enable an estimation to determine whether (new) membranes/materials are suitable for process design. For this purpose, results for a membrane must ideally exist for a similar chemical model system. We categorized the solvents and solutes to combine ideal model systems. The results from the experimental plan ought to be comparable and reliable between different institutions. Therefore, we performed extensive round robin testing to show for the first time the comparability and reliability of such measurements by cooperative experiments. Subsequently, we evaluated the results of the standardized procedure with statistical methods. Furthermore, additional bilateral cooperative tests were performed for other chemical systems and evaluated accordingly as well. During the development of the standardized procedure different sources for occurring errors, caused e.g. by the different analytic methods, were identified and ruled out. For an evaluation of the comparability of the measurements at the different locations, a statistical analysis is indispensable to avoid arbitrary criteria. The error estimation enables end-users to select suitable membranes more quickly. Besides, it allows membrane manufacturers to judge faster whether it is economically viable to bring newly developed membranes to production. The present work is consequently of major importance for the transfer of research results in the field of membrane development to later processes and the evaluation in industry.

Table 2.1: Properties of the selected test solvents for the experimental standard procedure [Smal2012]; [Hans2007].

	Hansen Solubility Parameter						
	δ_{tot}	δ_d	δ_p	δ_h	ϵ_r	Polarity	
Solvent	$[MPa^{1/2}]$				$[-]$	E_T^N [%]	Category
Ethanol (EtOH)	26.52	15.8	8.8	19.4	22.4	65.4	protic-polar
Isopropyl alcohol (IPA)	23.58	15.8	6.1	16.4	18.3	54.6	protic-moderate polar
Butanone (MEK)	19.05	16.0	9.0	5.1	18.5	32.7	aprotic-polar
Ethyl acetate (ESTP)	18.15	15.8	5.3	7.2	6.02	23	aprotic-moderate polar
Toluene	18.16	18.0	1.4	2.0	2.38	9.9	aprotic-non polar
n-Heptane	15.3	15.3	0.0	0.0	1.92	1.2	aprotic-non polar

2.3 Experimental standard measurement procedure

Materials and categorization

An appropriate categorization usable for test systems has to be as simple as possible and as accurate as necessary. Following this maxim, we decided to categorize the solvents in protic and non-protic solvents. In protic solvents, we extended the category with two degrees of polarity and for non-protic solvents with three degrees of polarity. Therefore, the normalized polarity index of Reichardt [Reic1994] supplies the values. The same as the polarity, in this way a wide range of the Hansen-Solubility parameter [Hans2007] and the relative permittivity [Smal2012] is covered. Overall, six solvents were chosen to define the set of ideal test-solvents (Table 2.1), of which ethanol and toluene were used as solvents in the round robin tests. The purity of all solvents used is ACS grade. The supplier of the solvents could be chosen individually by the contributors.

The categorization of solutes is much more complicated than for the solvents because of the multitude of possible compounds and functional groups. Additional to a classification of the structure, polarity and molecular weight, it is beneficial to give the branch of industry in which the solutes and related solutes are often used. Supplementary, we take solubility, analyzability, and costs into account. Thereby, the solute groups are chosen in such a way that either MWCO curves or individual retention as indicator for estimations on real substances can be measured.

Table 2.2 shows three solute groups defined with the solute properties for the ideal test systems. All solute substances used are of ACS grade purity. The contributors used as solutes in the round robin tests polystyrene oligomer mixtures containing PSS-ps560 and PSS-ps1.8k (Polymer Standards Service GmbH, Mainz, Germany) with a molar mass distribution from 266 to 1800 kg/kmol. The bilateral cooperative test systems consisted of these polystyrene oligomers in the remaining solvents from Table 2.1 as well as n-alkanes (Thermo Fisher Scientific Inc.) and sucrose octaacetate

Table 2.2: Properties of the selected test solutes for the experimental standard procedure [Post2013]; [Shi2015]; [Li2011]; [Wypy2016].

Solute group (Category)	Selected examples	Mw [kg/kmol]	Structure	Polarity	Branch of industry
n-Alkane	Decane - Hexatriacontane	ca. 140 - 500	Linear	Non-polar	Petrochemistry
Sugar and Derivative sugar	Sucrose octaacetate (SOA)	677	Branched out widely	Moderate polar	Food- and agricultural chemistry
Polymer	Polystyrene (PS), Poly-(methyl methacrylate) (PMMA)	ca. 200 - 2000	Linear	PS: non-polar PMMA: moderate polar	Commodity chemicals and polymer chemistry

(SOA) (Merck KGaA) in each solvent and poly-(methyl methacrylate) (Polymer Standards Service GmbH) in each solvent. We selected the solute combinations concerning solubility and simple analysis assuming that solute/solute interactions have no significant influence on the measurements [Hoff2015].

The OSN membranes can be distinguished in terms of membrane material and membrane type [Marc2014]. For the standard measurement procedure development, we focused on polymeric membranes and tested several integrally skinned asymmetric membranes as well as some thin film composite membranes. Four different membranes were used in the round robin test by each contributor: DuraMem® 200 and 300 (polyimide-based membranes), PuraMem® S600 and a PDMS membrane (both with silicone-based separation layer). DuraMem® and PuraMem® membranes are products of Evonik Resource Efficiency GmbH and the Helmholtz-Zentrum Geesthacht provided the PDMS membrane. The membranes with a polyimide-based separation layer are suitable for applications in polar solvents (e.g. ethanol) whereas the silicone-based membranes are more appropriate for nonpolar solvents (e.g. toluene). Therefore, the particular membranes selection covers a broad range of possible membrane uses (e.g. solvents and solutes with different physico-chemical properties).

While the different partners were performing the same experiments, there were important differences in the experimental set-ups and the analytical methods. Some set-ups are commercially available (e.g., METcell cross flow set-up from Evonik Resource Efficiency GmbH), some are tailor-made by an equipment manufacturer, and one is self-constructed. Therefore, membrane test cells with different geometry (round cells, rectangle cells) and scale were applied throughout the tests. The active membrane areas used vary between 50 and 100 cm^2 per module. Test system volume, control instruments (pressure, temperature, flow) and analytical devices were various too. This is representative for the diversity that is present not only in the scientific community, but also in industrial laboratories. The diversity brings, naturally, a high number of important factors that can potentially contribute to differences in the experimental results. Such results might even lead to

different conclusions. Therefore, it is indispensable to implement a standard measurement procedure, as well as to evaluate the variance in the obtained results, as has been done in the scope of the current study.

Experimental standardized procedure

All contributors unified the measurement procedure together. At least two identical membrane coupons were tested at the desired conditions. Usually the testing cells were connected in parallel. The DuraMem® and PuraMem® membranes were pre-washed using the process solvent until $5\,ml\,cm^{-2}$ permeate was collected or permeate became colorless. This procedure is necessary to prepare the membrane for its use, by removing the conditioning agent from its surface. Furthermore, the solvent treatments of the membranes have to be equal since they have a major impact on the membrane performance [Raza2017]. The membrane performance was determined by measuring the pure solvent permeate flux and the retention of different molecules (markers) in different solvents.

Figure 2.2 illustrates the agreed process conditions of the experimental standardized procedure. The pure solvent flux measurements were carried out at a pressure of $20\,bar$ and $30\,bar$, a temperature of around $25\,°C$ and a cross-flow velocity of $1\,m\,s^{-1}$. Flux was measured by collecting $5\,ml$ of permeate sample. The amount of collected permeate was controlled with a mass balance (especially important by low permeate flux and high volatile solvent). Also, measured flux values of electronic flow meters were validated by this method.

For the retention measurements, samples were taken at the same process conditions as in the permeation measurements. The process pressure was sequentially increased (20-30-40 bar) whereby permeate and retentate samples were taken at the end of each pressure step. The solute concentration in the feed mixtures was kept constant during the experiments (continues permeate return) at a maximum of $1\,g\,L^{-1}$ for each used solute group.

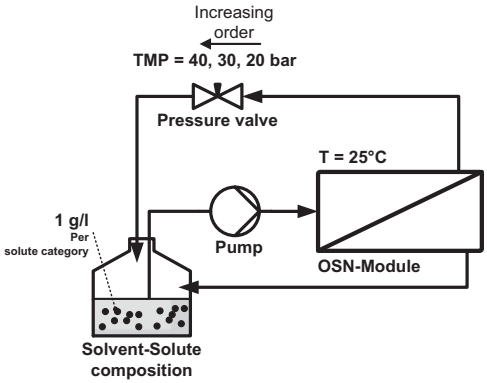

Figure 2.2: Schematic illustration of the experimental standardized procedure.

Following the membrane manufacturer recommendation, polyimide-based membranes were operated under pressure for 4 h before taking samples for flux and retention measurements. The time is required for the membrane to reach the steady state of its performance and abating representative results accordingly. When silicone-based membranes were applied, the time for compaction was set to 2 h. Permeate and retentate samples were taken simultaneously to determine the membrane retention. The retention was calculated by:

$$R_i = 1 - \frac{c_{i\,(Permeate)}}{c_{i\,(Retentate)}} \tag{2.1}$$

Analytic methods

Evonik, Merck and TU Dortmund University applied the high-performance liquid chromatography (HPLC-method) described by See Toh et al. [See 2007] after all round robin tests and for tests with Poly-(methyl methacrylate) (PMMA). The existing facilities of the partners were used. The used HPLC device at Merck KGaA, for example, is an HPLC Hitachi LaChrom® (Hitachi High Technologies America, Illinois, USA) equipped with an UV-vis detector. RWTH Aachen University and the Helmholtz-Zentrum Geesthacht (HZG) used a gel permeation chromatography (GPC) method to determine

the concentrations of the polystyrene oligomers and PMMA. The GPC were executed with a UV/vis detector and minimum two columns (SDV, 100 Å pore size, 3 µm particles, 8.0x300mm (IDxlength), Polymer Standards Service GmbH, Mainz, Germany). Tetrahydrofuran (AnalaR) was used as mobile phase, and the UV detector was set at the same wavelength as in the HPLC-method (264 nm). The solvent had to be evaporated from the samples before analysis, and the solutes had to be re-dissolved in the mobile phase. These steps were carried out in a very cautious way (evaporating at low temperature, accurate re-dissolving) to minimize loss of solute. Samples from tests with alkanes and sugar were analyzed by gas chromatography as described by Postel et al. [Post2013]. The used GC device is dependent on the contributor. At RWTH, for example, a GC 6890 system (Agilent, CA, USA) with liquid autosampler and flame ionization detector (FID) was used. An Agilent 19091J-413 HP-5 column was used coated with 5 % phenyl methyl siloxane, 30 m length, 0.32 mm inner diameter and 0.25 mm thickness.

In order to compare the analytical technique used by the partners, they mutually exchange samples (permeate and retentate) during the experimental phase and re-analyze these in their laboratory. The resulting retention curves were compared and an analytical error was calculated.

2.4 Statistical analysis and evaluation

While it is often stated that comparable results have been obtained in different studies, these statements are qualitative and therefore subjective. To avoid such subjectivity and allow for a meaningful quantitative reference, we considered a statistical evaluation of the results. Thus, we defined a degree of congruence. The difference between a random sample and a reference or confidence intervals compared to each other are typically used. Confidence intervals should give the precision of an estimated value. However, real values for flux or solute retention cannot be determined because of the limited influenceable structure of membranes.

We considered confidence intervals, stated at the 95 % confidence level,

as a measure of precision. The arithmetic mean values for flux and retention measurements were determined based on the taken samples, and the related confidence intervals were calculated. As result there is a $95\,\%$ probability that such an estimated interval contains the real value. Furthermore, intervals with a breadth of one (estimated) standard deviation (1σ) are reported to relate the obtained data points to the probabilistic distribution of measured values. The smaller the interval, the more narrow is the expected distribution.

Obvious single outliers and failed tests had to be identified and removed from the database prior to the statistical evaluation. Failed tests were recognized by an overall visible lower retention or a significantly higher flux value compared to the parallel tested module. They could occur by sealing problems (leak flux) inside the membrane module, membrane defects or contamination of the samples before analyzing. These tests were repeated to get a reliable database with minimum 18 raw data points for every single pure solvent flux and nine raw data points for retention of each molecular weight. The amount of samples arose from the number of parallel tested membranes and contributors with the assumption of one failed test. For flux measurements this number were doubled since higher deviations were expected. In total, this approach generated at least 81 data points for retention curves measured in ethanol and 90 data points for retention curves measured in toluene.

The calculation of the standard deviation and the confidence intervals was based on the assumption that the given samples (data points) are unbiased, independent and statistically normally distributed [Walt1997]. Further we had to notice that the original variance is unknown. Hence, the variance s^2 with the unbiased sample variance arise from:

$$s^2 = \frac{1}{n-1}\sum(x_i - \bar{x})^2 \tag{2.2}$$

n is the number of measurements, x_i, and $\bar{x}$ are the individual measured values and the related mean value, respectively. The standard deviation σ is accordingly the square root of the variance s^2. Due to the limited sample

size, the confidence interval calculation uses the student's t-distribution, considering the $(1-\alpha/2)$ quantile of t. The quantile is tabled in the literature [Mein2006]. Thus, the confidence intervals result from:

$$\left[\bar{x} - t_{(1-\alpha/2)}\frac{s}{\sqrt{n}}; \bar{x} + t_{(1-\alpha/2)}\frac{s}{\sqrt{n}}\right] \tag{2.3}$$

With this way of calculation, the range of reliable mean values is determined. Confidence intervals from future experiments can overlap and therefore narrow the range in regard to a real value. However, the primary objective of this study is to define a standard experimental procedure and perform a statistical analysis of the obtained results, allowing for a representative retrospective on reported data in literature. The effort of the contributors to generate comparable results become apparent in the standard deviations of the data points. Assuming an exact normal distribution of the measurement data, reflecting random differences of the membrane material (e.g. thickness of the active layer) it is expected that $95\,\%$ of all measurements will be located in the vicinity of the interval with 2σ range around the real mean. Thus, almost all of the measurements should be located within a range of two (estimated) standard deviation, around a value within the confidence interval of the mean.

In addition, tests of normality evidenced the assumption of statistic normally distributed data. The gathered results were tested on normal distribution with the methods of Anderson-Darling (a Goodness-of-Fit-Test) [Ande1952]; [Step2004] and Shapiro-Wilk (an omnibus test) [Shap1965]; [Roys1995]; [Rahm1997]. The Shapiro-Wilk-Test analyzes the variance. Data are normally distributed if the estimated variance is near the hypothetical variance of the normal distribution. With the Anderson-Darling-Test data are sorted and transformed into a uniform distribution. The distance to the hypothetical normal distribution is, in this case, the critical value. Normal distribution was granted if the results passed both sensitive tests.

The bilateral cooperative test systems cannot be compared in this way, since only two contributors measured the data. In these cases, minimum four data points are available, which is too few for a reasonable calculation

of confidence intervals. The results comply with our claims if the deviation of each data point to the related ones is less or equal than the deviation between the data points in the round robin tests.

Superstructure optimization

In order to evaluate the effect of the extent of uncertainty related to the experimentally determined performance metrics, different scenarios are evaluated within a superstructure optimization approach considering a sampling within the ranges of the determined confidence intervals around the estimated mean values. The superstructure represents a so-called state-space approach [Baga1992] and builds on a previous implementation for the optimization of reverse osmosis processes for seawater desalination [Skib2012]. Similar superstructures have been used for the optimization of gas permeation processes for natural gas upgrading [Scho2015] and nitrogen removal from natural gas [Ohs2016].

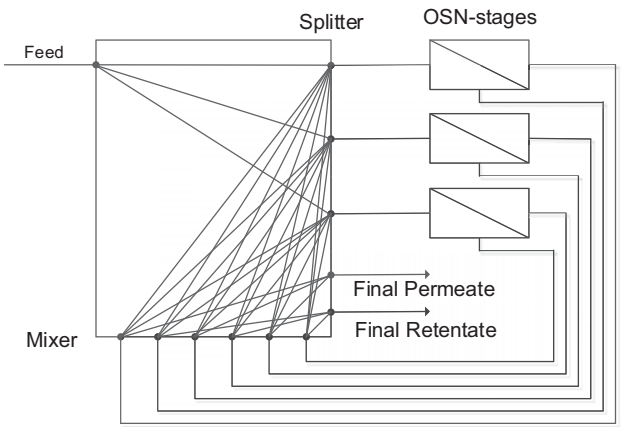

Figure 2.3: Superstructure for membrane network optimization.

An illustration of the superstructure, which consists of a generic distribution network and three OSN membrane stages is provided in Figure 2.3. The distribution network allows distribution of the entering streams, which are the overall feed stream and all product streams from the membrane stages, to all outgoing streams that are the feed streams of the OSN stages and the final permeate and retentate product streams. Thereby any kind of combination between the different membrane stages is possible. The performance of each membrane stage is modeled based on the available performance metrics from the experimental data, which are an overall flux as well as solute-specific retention. Furthermore, a concretization of the membrane stage concerning 100 finite elements is performed to account for the composition changes along the membrane length.

However, a constant performance regarding the experimentally determined values is assumed, and concentration polarization and pressure drop are neglected since no information on module geometry and hydrodynamics is considered. Operating temperature and pressure are also fixed to the experimental conditions, such that only the membrane area remains as a degree of freedom for every membrane stage. For the current study a maximum membrane area of $50\,m^2$ per stage and a total of three possible stages was considered. The objective of the optimization is to perform a specific separation, concerning purity and recovery constraints, with a minimum number of membrane stages and membrane area.

The superstructure optimization model is implemented in the general modeling framework GAMS as a mixed integer nonlinear programming problem (MINLP). The discrete decisions account for the existence of the different membrane stages, for which additional Big-M constraints enforce a minimum feed flowrate for existing membranes, while further constraints introduce additional cuts to eliminate topologically equivalent solutions by enforcing a specific order on the available membrane stages [Skib2012]. This is important to avoid multiplicity of equivalent optima in the solution space, which severely complicates global deterministic optimization. The resulting MINLP is solved using the global deterministic solver ANTIGONE to determine the best possible solution.

2.5 Results and discussion

Considering the spent effort devoted to the standardized experimental procedure and the validation of the analytic methods, it can be concluded that the obtained results of the round robin test are a best case representative for the diversity of measurements in diverse laboratories. Differences are quite normal since locations, set-ups, measurement devices, analytic methods, time of measurements and experimenter vary from each other. The contributors endeavored to operate as equal as possible to ensure that the experimental procedure became a standard in functional membrane characterization.

Comparison of analytic methods

Testing identical samples in different laboratories resulted in a minimal data points variation. Figure 2.4 shows two diagrams with four exemplary retention curves for the comparison of the analytical methods at different laboratories. The retention of the different styrene oligomers is plotted versus their molecular weight. Single occasional outliers could be identified by comparing the curves. The reason for the apparent deviations at $266\,\mathrm{kg\,kmol^{-1}}$ was the more sensitive evaluation of the small peaks obtained by analyzing the retentate and permeate samples. The biggest differences between the measured retention values, excluding outliers are only about $6\,\%$, proving the comparability of the analytic methods.

Pure solvent flux

Figure 2.5a shows the results plotted in a box plot (left part for toluene fluxes, right part for ethanol fluxes) for each membrane to display the distribution and differences of the data. Toluene fluxes could be measured only with PuraMem® S600 and PDMS membranes. DuraMem® series membranes showed very low or no permeation with toluene. Ethanol fluxes, however, were measured with all selected membranes. One point worthy of note, is the different scales on the flux axes. Figure 2.5b illustrates the

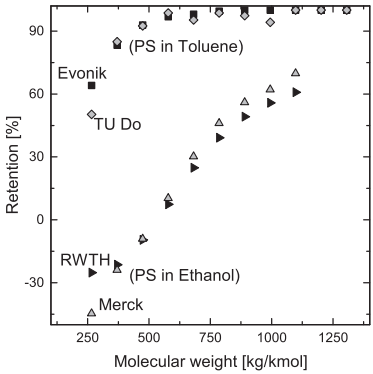

(a) Retention measurements with the PDMS membrane.
Evonik ■ and TU Do ◇ used samples with toluene as solvent (sampling at 30 bar).
Merck △ and RWTH ► used samples with ethanol as solvent (sampling at 30 bar).

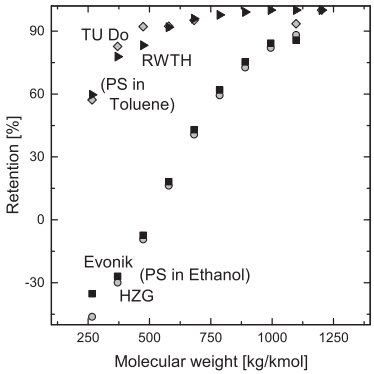

(b) Retention measurements with the PuraMem® S600.
TU Do ◇ and RWTH ► used samples with toluene as solvent (sampling at 20 bar).
Evonik ■ and HZG ◯ used samples with ethanol as solvent (sampling at 40 bar).

Figure 2.4: Comparison of analytic results from retention measurements with the PDMS membrane and PuraMem® S600

meaning of the boxplots, in which the dots represent the measured fluxes while the white boxes indicate the standard deviation as 1σ interval of the measured data. The accompanying percentage gives the difference from the arithmetic average to the upper or lower value of the range. Inside the boxes the line and the dot are the median and the arithmetic average of the data respectively. Above and below, the whiskers show the 2σ interval. The grey colored boxes represent the calculated confidence intervals (Eq. 2.3). The horizontal spread of the data dots is plotted this way to avoid overlap of too many points for the same membrane. It is randomized and has no physical meaning.

The fluxes (Figure 2.5a) for toluene are much higher than for the polar solvent ethanol. Highest fluxes with few scattering were measured for the PDMS membrane. The mean could be found at $90.5\,\mathrm{L\,m^{-2}\,h^{-1}}$ and the corresponding confidence interval is close to this value with $\pm\ 3.1\,\mathrm{L\,m^{-2}\,h^{-1}}$. The

standard deviation has limits at $\pm$ 7.3 % of the mean. The results from the flux measurements with the PuraMem® S600 membrane show wider scattering with an arithmetic average of 64.9 L m^{-2} h^{-1}. However, the breadth of the 1σ interval is $\pm$ 13.4 % of the mean and the measured data shows that only single higher and lower values lead to the comparative high deviation. The precision around the estimated mean value amounts to $\pm$ 3.8 L m^{-2} h^{-1}.

The toluene fluxes correspond to the expectations of the manufacturers. The higher fluxes through the PDMS membrane compared to those through the PuraMem® S600 membrane can be attributed to the structure and material of the membranes. The selective layer of the PDMS membrane consists of radiationally crosslinked PDMS with a thickness of 2 µm [Thie2018]. The high toluene fluxes were expected due to the small distance of the total Hansen Solubility Parameters (HSP) according to [Post2013] ($|\delta_{Membrane} - \delta_{Solvent}| = 2.73\ MPa^{0.5}$ with $\delta_{Membrane} = 15.57\ MPa^{0.5}$ for PDMS). The coated silicone-based layer of the PuraMem® S600 membrane is thin and supported by a polyimide structure. This supporting structure is much more polar than PDMS and seems to have an inhibitory effect on the nonpolar sol-

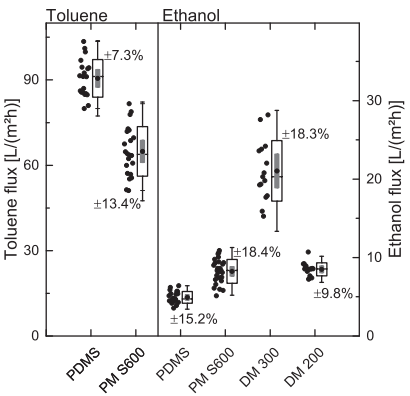

(a) Box plot and data points of pure solvent fluxes of toluene (left) and ethanol (right) at 30 bar transmembrane pressure and 25 °C.

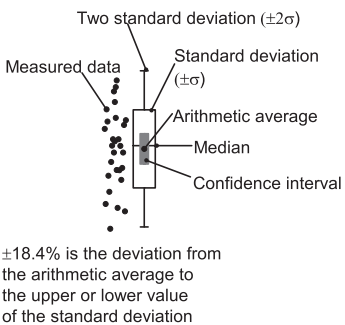

(b) Meaning behind the symbols, boxes, whiskers and numbers of the box plots.

Figure 2.5: Results of pure solvent flux measurements illustrated as box plot.

vent. Accordingly, no flux measurement through the cross-linked polyimide-based membranes DuraMem® 300 or DuraMem® 200 with toluene was possible.

Fluxes of ethanol are mostly around or below $10\,\mathrm{L\,m^{-2}\,h^{-1}}$. The lowest fluxes were measured with the PDMS membrane and the PuraMem® S600 membrane with mean values at $4.9\,\mathrm{L\,m^{-2}\,h^{-1}}$ and $8.2\,\mathrm{L\,m^{-2}\,h^{-1}}$, respectively. The limits of their 1σ intervals are around $\pm\,15.2\,\%$ and $\pm\,18.4\,\%$. Results from the confidence interval calculation show a difference from the mean value of $\pm\,0.3\,\mathrm{L\,m^{-2}\,h^{-1}}$ for PDMS membrane and $\pm\,0.6\,\mathrm{L\,m^{-2}\,h^{-1}}$ for PuraMem® S600 membrane. There is a remarkable deviation in the flux values of the DuraMem® 300 membrane. The reason for it is most likely the higher porosity of the membrane and its natural deviation from the production process. The standard deviation interval is $\pm\,18.3\,\%$ of the mean which is $21.1\,\mathrm{L\,m^{-2}\,h^{-1}}$. For this case, the confidence interval was determined at $\pm\,2.1\,\mathrm{L\,m^{-2}\,h^{-1}}$. The measurements with the DuraMem® 200 membrane resulted in a mean value of $8.5\,\mathrm{L\,m^{-2}\,h^{-1}}$ and a confidence interval of $\pm\,0.4\,\mathrm{L\,m^{-2}\,h^{-1}}$. The standard deviation has limits at $\pm\,9.8\,\%$ of the mean. For all membranes the median is close to the mean. The highest differences are $-1.1\,\mathrm{L\,m^{-2}\,h^{-1}}$ for toluene flux through the PuraMem® S600 membrane and $-0.7\,\mathrm{L\,m^{-2}\,h^{-1}}$ for ethanol flux through the DuraMem® 300 membrane.

Furthermore, Figure 2.5a shows referring to the measurements in ethanol with the PuraMem® S600 membrane more data points than for the other measurements. The reason is testings about a reasonable size of the database. For the membrane were additional measurements conducted, so the number of data points rises from 19 to 28. The arithmetic mean value changed slightly (from $8.3\,\mathrm{L\,m^{-2}\,h^{-1}}$ to $8.2\,\mathrm{L\,m^{-2}\,h^{-1}}$). The initial 1σ interval decreased as expected from ca. $\pm\,18.6\,\%$ to $\pm\,15.2\,\%$. The additional measurements show the dependency of the data gathered on the number of samples. It is evident that the chosen number of samples is sufficient. On the one hand it is high enough to calculate reasonable standard deviations and confidence intervals. On the other hand it is small enough to avoid inefficiency and insignificant interval ranges.

The fluxes of ethanol through the membranes match the expectations of the manufacturers. The fluxes are significantly lower, depending on the material of the active membrane layer. As a second factor, the degree of cross-linking and thus the tightness of the membrane is essential. It is challenging for polar substances, such as ethanol, to permeate through the two nonpolar silicone-based membranes. This low permeation results in the lowest fluxes for the PDMS membrane and only slightly higher values for the coated PuraMem® S600 membrane. In contrast to the flux measurements with toluene, the polyimide substructure of the PuraMem® S600 membrane allows a higher liquid flux for ethanol.

Besides, it is interesting to note that the flux through the PuraMem® S600 membrane corresponds approximately to that through the DuraMem® 200 membrane. According to the manufacturer, the DuraMem® 200 membrane has a lower MWCO than the PuraMem® S600. It is evident that the silicone-based coating (active membrane layer) appropriately hinders the permeation of the polar solvent, since the supporting structure of the PuraMem®-S600 membrane (produced of the same material as the DuraMem® 200) is less cross-linked and, therefore, consists of a more open structure.

The observed standard deviations of the measured flux values show that distinct differences can occur in the measurements, despite the standardized procedure. These differences can be observed especially for pure solvent fluxes. However, the differences also confirm the experience of the membrane manufacturers. As already mentioned for the DuraMem® 300, one possible origin of the deviations are the production tolerances that occur within a batch. It should also be remembered that the membranes in laboratory plants have a much smaller surface area. The membrane sample can only show an average value corresponding to the large production batches or modules if they either represent precisely the average of the batch or are measured in sufficient numbers. The low confidence intervals in combination with the close range of median and arithmetic mean demonstrate that the results provide highly precise information on flux averages. This study is unique in that the measurements were carried out at different times in different institutions. The comparison between measurements of

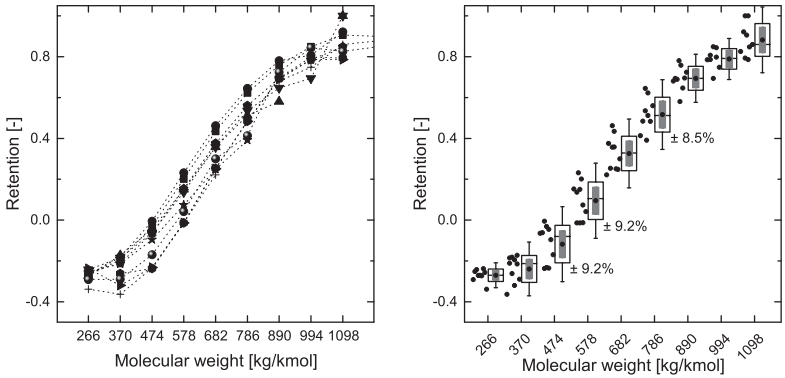

(a) Array of all measured retention curves from the round robin test with polystyrene oligomers in ethanol with the PDMS membrane. A different symbol is used for each measurement series. Obvious outliers are removed.

(b) Box plot and measured data points from the round robin test with polystyrene oligomers in ethanol with the PDMS membrane.

Figure 2.6: Results from the round robin test with the PDMS membrane and polystyrene in ethanol at 30 bar transmembrane pressure and 25 °C.

laboratory size membranes and industrial membrane modules is an interesting topic for future work.

The summary is based on 136 measurement data points, whereby 12 outliers were excluded. The breadths of all 1σ intervals are lower than $\pm 20\,\%$. Also, the mean values were estimated with a high precision. The results verify the reliability of the proposed standard experimental procedure for flux measurements.

Retention measurement

To visualize the retention measurements, we depict the results of the round robin tests in two ways (Figure 2.6). Figure 2.6a shows the array of retention curves for this test system, whereby the outliers are already excluded. The outliers were identified only with the help of the regular retention curves (the points were laying clearly outside of the curve). These outliers could also have an analytical background as previously shown in

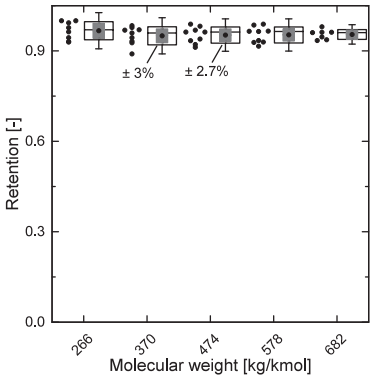

Figure 2.7: Box plot and data points of retention values from the round robin test with the DuraMem® 300 and polystyrene in ethanol at 30 bar transmembrane pressure and 25 °C.

Figure 2.4. Only six outliers out of 90 data points were identified for the system PDMS membrane-ethanol-polystyrene. The results can therefore be seen as representative. The curves are forming a belt, starting with a negative retention for the smaller molecules and ending with a retention of above 90 % for the bigger styrene oligomers, as expected. The experimental data points for the retention of each styrene (different molecular weight) adhere to a normal distribution, with the exception of the high retention values of large oligomers (R>97 %), due to the upper limit of 100 % retention. Consequently, outliers for such molecular weights are irrelevant for the results evaluation too.

The second depiction (Figure 2.6b) displays the relevant retention of the different oligomers (different molecular weight) in box plots similar to Figure 2.5b. In such diagrams, it is easier to visualize the distribution of the results. Figure 2.6b shows exemplary the box plots for the PDMS-membrane in ethanol, Figure 2.7 shows the plots for the DuraMem® 300 membrane also in ethanol and Figure 2.8 shows the plots for the PuraMem® S600 membrane in toluene.

The values on the horizontal axis are the molecular weights from the single styrene oligomers. They could be identified analytically with 266 kg kmol^{-1}

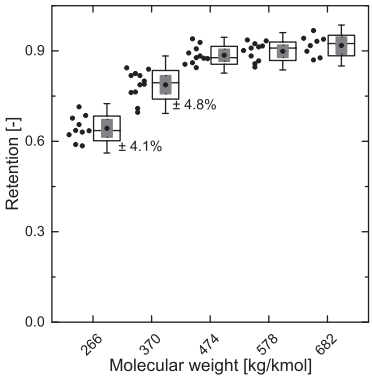

Figure 2.8: Box plot and data points of retention values from the round robin test with the PuraMem® S600 and polystyrene in toluene at 30 bar transmembrane pressure and 25 °C.

+ n · 104 kg kmol^{-1}. The boxes positions are following the retention curves. While the boxes from the system PDMS membrane-ethanol-polystyrene show the described increase of retention with increasing molecular weight of the oligomers, the boxes of the system DuraMem® 300 membrane-ethanol-polystyrene form a horizontal line above 90 % retention (Figure 2.7). Fewer oligomers could be considered in this system because of the proximity to the retention limit and the smaller MWCO in this solvent-solute combination. The system PuraMem® S600 membrane-ethanol-polystyrene (not depicted) behaved similarly as the system PDMS membrane-ethanol-polystyrene. The results from the PuraMem® S600 membrane-toluene-polystyrene experiments (Figure 2.8) shows boxes positions from characteristic retention curves as well. The increase of the retention values for the different styrene oligomers is more gradual as 60 % retention was already achieved for the smallest styrene oligomer. In this case, the system PDMS membrane-toluene-polystyrene (not depicted) behaved similarly. The retention values in all these systems were affected by the different pressure level only slightly. Changes primary occurred for the lower retention values. Positive retention values increased by increasing pressure while negative retention values decreased by increasing pressure. Regarding the scatter-

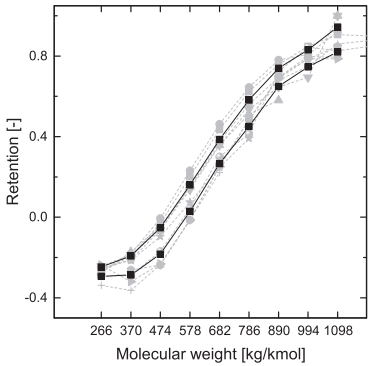

Figure 2.9: Calculated confidence intervals (■) drawn as retention curves. They are superimposed on the array of measured retention curves from the round robin test with the PDMS membrane and polystyrene in ethanol at 30 bar transmembrane pressure and 25 °C. A different symbol is used for each measurement series.

ing of the data points, no tendency could be mentioned. At first glance, the measurements seem to be comparable.

The results prove the good applicability of the developed standard testing procedure. All 1σ intervals have a low absolute range. The highest breadth is $\pm 9.2\,\%$ of the mean value at the test system PDMS membrane-ethanol. Even with Figure 2.9 it becomes apparent that all measured curves are within or close to the calculated confidence intervals. The intervals are drawn as retention curves and superimposed on the array of measured data. Thus, it shows in another way the precision of the results and the quality of a standardized experimental procedure.

The measured retentions are in line with the expectations of the membrane manufacturers. The results show that the gradient of the retention curves is dependent on the membrane for low molecular weight solutes. Oligomers with a higher molecular weight can only permeate to a small extent because of their high diffusion coefficients. The gradient at low molecular weights is highest in both toluene and ethanol for the PDMS membrane and lowest for DuraMem® 300 membrane in ethanol. Here the interactions between membrane, solute and solvent are the major factors.

The nonpolar polystyrenes dissolve and permeate preferably through

nonpolar membranes. However, increasing numbers of polar groups in a membrane, such as the DuraMem® 300 membrane, lead to a stronger permeation barrier. Concurrently, the nonpolar solutes can interact less with the polar ethanol than with the nonpolar toluene. These effects result in very high retentions even for low molecular weight oligomers using the DuraMem® 300 membrane. The high retentions are also supported by the dense membrane structure indicated in the manufacturers' MWCO specification.

The PDMS membrane, on the other hand, impedes permeation of the solvent ethanol rather than of the polystyrene. This preferential permeation leads to negative retentions for the low molecular weights. With increasing molecular weight, the steric effect of the molecules increases and leads to an increase in retention. Since a gradual increase can also be observed in toluene, it can be assumed that the steric factors of the molecules are dominant. This conclusion also corresponds to the statement from Thiermeyer, Blumenschein, and Skiborowski [Thie2018].

The polystyrenes have a high affinity to the PuraMem® S600 membrane due to the nonpolar coating. However, the affinity is weakened by the supporting structure. The same applies for the solvent toluene as described for the pure solvent fluxes. Therefore, toluene also provides higher retention for polystyrene oligomers with a lower molecular weight using the PuraMem® S600 membrane compared to the PDMS membrane. Similar to this membrane, the importance of steric effects increases with increasing molecule size. In ethanol, it is contrary for the solvent, and the nonpolar silicone-based layer hinders the flux through the membrane. These measurements showed negative retentions which were also observed for the PDMS membrane.

From the statistical evaluation, it can be seen that the results show less deviations compared to the pure solvent fluxes. The standard deviation is low and the distance between median and arithmetic mean is small. The low confidence intervals demonstrate that the standardized procedure produces precise estimates of the mean value. Accordingly, it can be assumed that similar results will be achieved with retention measurements using the

standardized procedure. Meaning that a few measurements per solute are sufficient for the characterization of a new membrane.

The retention results from the bilateral cooperative tests (performed parallel by two contributors) were compared directly for each molecular weight. Since there were only four data points for the retention of each solute, confidence intervals were not considered and no standard deviations were calculated. Figure 2.10 shows the retention of alkanes and SOA as well as PMMA in different solvents.

The depicted retention curves of alkanes and SOA were results from measurements with the PDMS membrane. In isopropyl alcohol (IPA) and ethyl acetate (ESTP) negative retention occur. With increasing molecular weight, the retention values decrease in the polar solvent IPA, whereas increase in the moderate polar solvent ESTP. As mentioned above, such negative retentions were also observed in some measurements with styrene oligomers. In the nonpolar solvent n-heptane, the measurements with alkanes resulted in only positive values as common retention curves. Affinity effects established with solubility parameter could give an explanation about

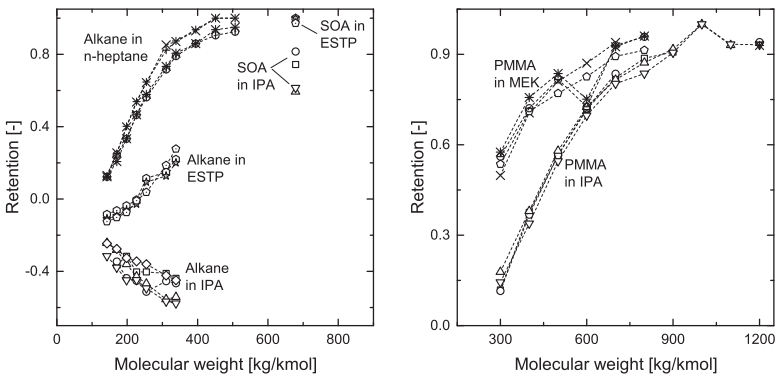

(a) Retention curves of alkane and SOA in various solvents at 30 bar transmembrane pressure and 25 °C for the PDMS membrane.

(b) Retention curves of PMMA in IPA and MEK at 30 bar transmembrane pressure and 25 °C for the PuraMem® S600 membrane.

Figure 2.10: Results from additional tests distributed to two contributors each. A different symbol is used for each measurement series.

this behaviour. Similar measurements and results were presented in Postel et al. [Post2013]. SOA is a more complex branched molecule with a higher molecular weight than the alkanes. Consequently, it can be argued that the diffusion coefficient is high compared to that of the alkanes. Furthermore, SOA is a moderately polar solute with a high acceptance for hydrogen bonds due to its excellent water solubility and the bounded oxygen. This polarity leads to the assumption of a high Hansen Solubility Parameter. For that reason a low affinity to the nonpolar PDMS membrane is expected. In this combination, similar to the polyethylene glycol retention in Postel et al. [Post2013], the size exclusion is dominant for retention in IPA and ESTP (SOA is not soluble in n-heptane).

The retention measurements of PMMA oligomers with PuraMem® S600 membranes (Figure 2.10b) results in common retention curves. The measurements with the combination butanone (MEK) and PMMA results in higher retention values than the measurements with the combination IPA and PMMA. Such lower retention values in IPA could also lead back to affinity effects, since the active layer of the PuraMem® S600 membrane is silicon based as the PDMS membrane.

The curves in both diagrams are not corrected and the plausible outliers are easily recognizable (retention curves of PMMA in butanone (MEK) or SOA in IPA). The total deviation in retention for each solute is, however, as low as the one in the round robin test. Most of the data points deviate by less than $10\,\%$ in total, and every deviation is in total less than $\pm 15\,\%$ of the arithmetic average.

Case studies

Two different case studies were investigated using the superstructure optimization approach to elucidate the effect of uncertainties of flux and retention measurement on subsequent process design. In Case Study 1 a concentration of one component with a molecular weight of $474\,\mathrm{kg\,kmol^{-1}}$ solved in ethanol is assessed, considering the experimentally determined performance metrics of the DuraMem® 300 membrane and the mixture of ethanol

with styrene oligomers. The flux across the membrane at $30\,\mathrm{bar}$ was determined to $21.052\,\mathrm{L\,m^{-2}\,h^{-1}}$ while the confidence interval was $\pm\ 2.136\,\mathrm{L\,m^{-2}\,h^{-1}}$. The retention for the styrene oligomer with a molecular weight of $474\,\mathrm{kg\,kmol^{-1}}$ was determined to $95.2\,\% \pm 2.1\,\%$.

For the optimization a feed flowrate of $100\,\mathrm{kg\,h^{-1}}$, a concentration from $0.05\,\mathrm{g\,g^{-1}}$ in the feed to $0.1\,\mathrm{g\,g^{-1}}$ in the final retentate and a solute recovery of at least $98\,\%$ was assumed.

Figure 2.11 shows three of the resulting optimal process structures, for exemplary samples within the experimentally determined confidence intervals. Depending on the selected case, significant differences in the necessary membrane area and the complexity of the process arise. While the high flux and retention values lead to a simple process in a single step, the process with the low values is much more complicated and not intuitive. The total feed is divided between a parallel module and a two-stage cascade. The permeate flow of the first stage is only partially used for the second cascade stage. The retentate streams from the module operated in parallel and the second cascade stage are fed back to the feed of the cascade, before the first stage. Output streams from the process are the retentate stream from the first cascade stage and the combined permeate streams from all membrane modules. Overall nine different scenarios were evaluated.

As a second case study, a separation step of two solutes solved in ethanol was chosen. The solute size equals $474\,\mathrm{kg\,kmol^{-1}}$ and $1098\,\mathrm{kg\,kmol^{-1}}$. The smaller solute is assumed to be the product while the bigger solute represents an impurity. The feed contains $0.05\,\mathrm{g\,g^{-1}}$ of the product and $0.003\,\mathrm{g\,g^{-1}}$ of the impurity while the flow rate is set to $100\,\mathrm{kg\,h^{-1}}$. The final permeate needs to contain at least $98\,\%$ of the product, and the concentration of the impurity in the permeate needs to be lower than $0.001\,\mathrm{g\,g^{-1}}$. For this case study, the experimental values determined with the PDMS membrane and the mixture of ethanol with styrene oligomers are used. The flux was experimentally determined to be $4.925\,\mathrm{L\,m^{-2}\,h^{-1}} \pm 0.331\,\mathrm{L\,m^{-2}\,h^{-1}}$ at $30\,\mathrm{bar}$. The retention of the styrene oligomer with a molecular weight of $474\,\mathrm{kg\,kmol^{-1}}$ equals $-11.8\,\% \pm 6.6\,\%$ and the retention of the styrene oligomer with a

molecular weight of $1098\,\mathrm{kg\,kmol^{-1}}$ equals $88.2\,\% \pm 6.2\,\%$.

Compared to the first case study the flux is much smaller, and additionally, the experimentally determined confidence intervals are broader. Overall 27 different combinations of flux and retentions were evaluated, all of which represent samples within the ranges of the experimentally determined confidence intervals. Three of the determined optimal process structures for the second case study are depict in Figure 2.12. This case study also shows clear differences in the necessary membrane area and the interconnection concepts. The value combination of high flux and retentions far from each other lead to a simple single-stage membrane process with a small membrane area. On the other hand, lower flux values and a narrower retention range between the individual solutes result in a substantially more complex two-stage process. In this process, the main feed is divided between the two stages, with part of the permeate from the first stage supplementing the feed of the second stage. The feed of the first stage is also fed with the retentate of the second stage. The output streams are the retentate of the first stage and a mixture of the permeates of the two stages.

Both case studies demonstrate the dependency of a subsequent process design on accurate information of the membrane performance. A consistent determination and reporting of the data quality, as indicated in the current study, is, therefore, an essential component for the further development and dissemination of OSN processes.

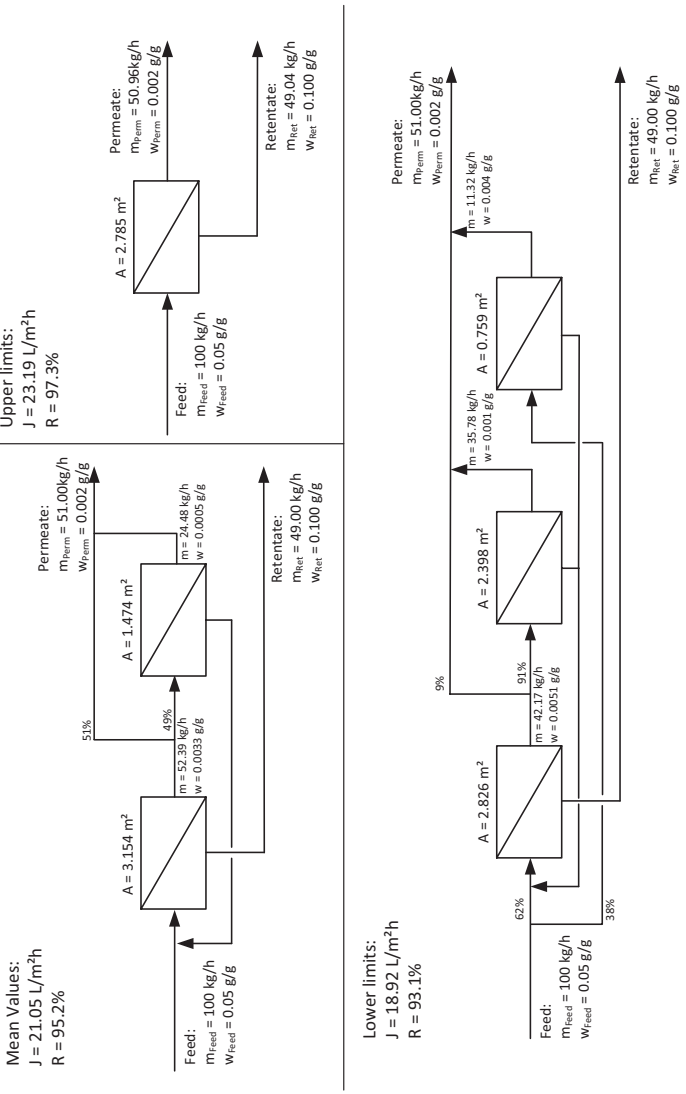

Figure 2.11: Case study 1: Three optimized process structures for different flux and retention combinations from the test system DuraMem® 300-ethanol-polystyrene (Mw = 474 kg kmol^{-1}) at 30 bar and 25 °C.

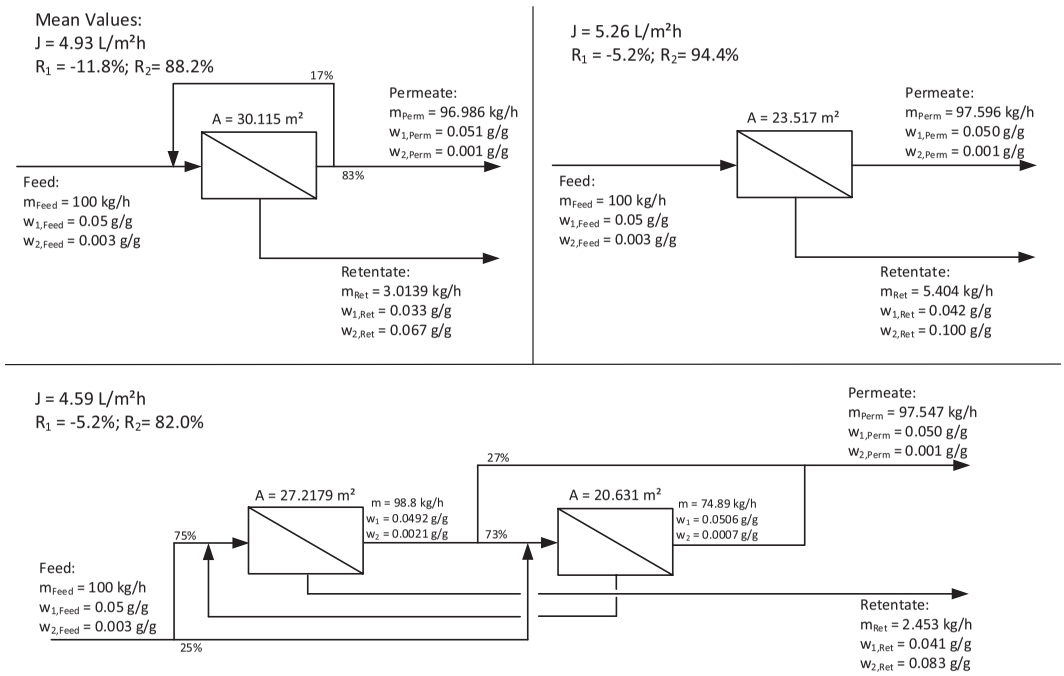

Figure 2.12: Case study 2: Three optimized process structures for different flux and retention combinations from the test system PDMS membrane-ethanol-polystyrene (Mw = 474 kg kmol^{-1} as product and 1098 kg kmol^{-1} as impurity) at 30 bar and 25 °C.

2.6 Conclusion

The data quality of results from membrane characterizations has never been stated as a basis for the OSN users. This uncertainty hinders the progress in finding one or more reasonable standard systems for OSN membrane characterization. Such standardized procedure can simplify the assessment of membrane performance and their applicability in real separation processes. As a result, the process design of a OSN plant in industrial scale would be less difficult and troublesome.

In this study, we demonstrate the reliability and reproducibility of a standardized experimental procedure to improve and accelerate process design for OSN applications. The procedure was applied with different test and analytical equipment, for several solvents, membranes, and solutes.

The results from the round robin test were statistically evaluated. The calculations for pure solvent flux and retention measurements demonstrate that the precision of the determined mean values from the experiments are high and the standard deviations reasonable. Therefore, the deviation of the data is low enough to permit the assumption of comparable results in future tests by using the standardized experimental procedure.

Using the statistically quantified information on the accuracy of the determined experimental flux and retention values, we further demonstrated the effect of these uncertainties on subsequent process design. The two investigated case studies confirmed the importance of an accurate assessment of data quality and accuracy. The standardized procedure for membrane characterization experiments should help to assess future results better and apply statistical methods. Then data from different sources and their reliability can be used in optimal process design.

Further results with other test systems confirm the reliability of the method and emphasize the comparability of the obtained results.

Considering all results, we showed that the proposed standard experimental procedure, used in a conjunction with the categorized test systems, enable generating comparable and reliable membrane performance data. Prospectively, this procedure can become a standard to characterize OSN

membranes and give credible performance information. Nevertheless, further investigation on this field is desirable. A development of heuristic method for membrane selection could promote and strengthen the method. Furthermore, it can help with its reliable results to reveal correlations in the complex solvent-solute-membrane system in future work.

3 Organic solvent nanofiltration membrane cascades for separation of solutes with positive and negative retentions

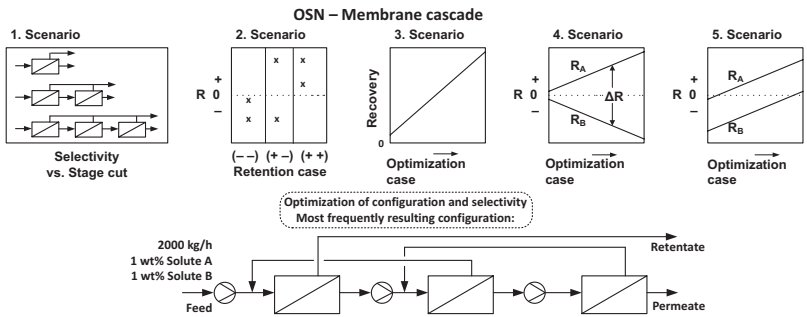

Five scenarios are used to investigate the influence of negative retention on the optimal process configuration and selectivity considering the power demand.

3.1 Introduction

Separation processes, such as the recovery of organic solvents, are the main energy consumers in the chemical industry. Thus, organic solvent nanofiltration as energy efficient separation method has become increasingly popular and has aroused particular attention in the industry [Marc2014]; [Blum2015]; [Cupe2015]; [Have2017]; [Lopr2017]. In addition to the challenges already known from other membrane processes, an unusual phenomenon has frequently been observed: negative retention [Post2013]; [Zeid2013]; [Solt2016]. Such negative retentions occur if the solute preferably dissolves in the membrane material. As a result, the solute accumulates in the permeate. However, so far only few processes are known that take advantage of the enrichment of a solute in the permeate [Volk2014].

Most membrane processes require more than a single-stage process to achieve both high recovery and purities. Modeling and simulation of membrane processes allow investigating a huge number of possible membrane configuration and identifying efficient process designs. Hence, modeling is essential to connect the membrane stages most efficiently.

This study aims to understand the optimization of a membrane cascade. Recently Böcking et al. [Böck2019] showed the influence of statistical variance in membrane performance on process design. In this work, also negative retentions for the solutes have been observed. However, the influence of and potential benefits of negative retention on the process design has not been investigated yet. Therefore, we investigate the effect of negative retentions on the process design for the first time.

- What happens with the optimal process design if one or both of the solutes have negative retention?
- What influence does the distance between the retentions have?
- Is there a transition point in the process design if a constant retention difference on the retention scale is shifted from positive to negative?

The development and implementation of processes are usually associated with many difficulties. This is especially true if the processes are not yet

part of the standard repertoire and if phenomena are not yet fully understood. To answer these questions, we use a superstructure optimization approach based on mixed-integer nonlinear programming (MINLP). This method enables to identify the best process case from a large number of possible processes. Values of measurements from [Post2013] with the solutes PEG 400, stearic acid and hexadecane in the solvents toluene and methanol are used for case studies.

3.2 Background

Membrane cascades enhance the selectivity and overall retention. In particular, this is necessary to improve solvent recovery and separation of substances with similar retentions. So far, process designs are mainly investigated by laboratory experiments with small controllable cascades and simulations. Simulations of mass transport at the membrane scale initially precede the simulation of a cascade at the process scale. Such simulations are used to predict the permeate concentrations and thus the retention.

Usually, three model types are used for mass transport through nanofiltration membranes. (a) Irreversible thermodynamic models, (b) pore-flow models, and (c) solution-diffusion models ([Marc2014]). In the irreversible thermodynamic models, the membranes are treated as a black box. Since a forced thermodynamic disequilibrium enables nanofiltration, free energy dissipates continuously and entropy increases in the system ([Blum2016]). Based on these considerations, Kedem and Katchalsky [Kede1958] first developed a model to describe water desalination, which was further developed by Spiegler and Kedem [Spie1966].

The other models take membrane properties into account. The pore-flow models assume a porous membrane structure, and the solution-diffusion models a dense membrane structure. In the pore-flow models, the chemical potential is changed across the membrane due to a pressure gradient. This assumption allows calculating the solvent flux $J_{Solvent}$ with the Hagen-

Poiseuille (Equation 3.1) or Carman-Kozeny-correlation (Equation 3.2).

$$J_{Solvent} = \frac{r_{pore}^2 \epsilon}{8\tau\eta} \frac{\Delta p_{eff}}{l} \tag{3.1}$$

$$J_{Solvent} = \frac{\epsilon^3}{K_{Car}\eta A_{SV}^2 (1-\epsilon)^2} \frac{\Delta p_{eff}}{l} \tag{3.2}$$

In these equations, r_{pore} denotes the pore radius, ϵ the porosity of the membrane, τ the tortuosity, and η the solvent viscosity. Δp_{eff} is the effective pressure difference, calculated with the transmembrane pressure difference and the difference of the osmotic pressure, by $\Delta p_{eff} = \Delta p - \Delta\pi$. The membrane thickness is l, the Carman-Kozeny-constant is K_{Car}, and the surface-area-to-volume ratio is A_{SV}. Solute fluxes are described with empirical model equations that are always dependent on the material system ([Marc2014]; [Blum2016]).

In solution-diffusion models, mass transport occurs in 3 steps. First, the substances dissolve in the membrane. Second, the substances diffuse through the membrane matrix, and in the third step, the substances desorb on the permeate side of the membrane. If there is no pressure gradient, mass transport can be described with Fick's law ([Marc2014]; [Post2014]). With the usual pressure gradients in nanofiltration, the mass transport (flux of substance i) results in Equation 3.3.

$$J_i = \frac{D_i K_{sorp,i}}{l} (c_{i,ret} - c_{i,perm} e^{-\nu_i \Delta p_e ff/(R_g T)}) \tag{3.3}$$

Here D is the diffusion coefficient, K_{sorp} the sorption coefficient, $c_{i,ret}$, and $c_{i,perm}$ the respective concentration at the surface of the membrane on the retentate side and the permeate side. ν is the molar volume, R_g the ideal gas constant, and T the temperature.

The usual solution diffusion model is extended by combining pore-flow models with solution diffusion models to the solution diffusion model with imperfections. Thereby additional less ideal spots are inserted through which substances can be transported convectively ([Marc2014]). Another

extension of the solution diffusion models considers with the Maxwell-Stefan equations the frictional forces between the materials and the membrane. Postel et al. [Post2014] recently applied to this extended model.

The simulations or optimizations of membrane cascades on the process scale are difficult to understand if they also contain the equations from the membrane scale. Besides, the effort is considerable, and convergence challenging. Therefore, simplifications are common, and results from simulations at membrane level or from experiments are used.

Caus et al. [Caus2009] simulated a four-stage nanofiltration cascade for the separation of xylose and maltose in water. Also, Montesdeoca et al. [Mont2016] showed experimental studies for the separation of oligosaccharides by a three-stage cascade. Chun-Te Lin and Livingston [Chun2007] conducted proof of concept experiments on OSN cascades. In particular, they investigated the solvent exchange of toluene with methanol. These conceptual results of feasibility were further confirmed in [Siew2013b] for the separation of active pharmaceutical ingredients (API) with simultaneous solvent recovery. A three-stage cascade improved the total retention (R) compared to a single-stage process from $R = 0.55$ to 0.8. The cascade could also be well controlled in the laboratory experiments. The group showed further results for membrane cascades in [Siew2013a].

In a follow-up study by Peeva et al. [Peev2014], a purity of $> 99\,\%$ for the separation of the API Roxithromycin from a potential genotoxic impurity with a two-stage cascade was achieved. The cascade can subsequently be combined with another process (e.g., an adsorption column) for solvent purification. Abejón, Garea, and Irabien [Abej2014] also investigated the separation of impurities and APIs. Methanol was used as solvent and cascades of up to five stages were simulated. Additionally, they optimized the costs based on the retentions and pressures of the individual stages.

Furthermore, Kim et al. [Kim2013] carried out experiments with two-stage cascades and developed a MATLAB model. Both experimental and simulation results underlined the importance of recycling retentate streams for high yields. Renouard, Lejeune, and Rabiller-Baudry [Reno2018] recently presented a simulation that can calculate up to 11 stages and dif-

ferent recirculations. More than 75 cascade configurations were investigated for the separation of a catalyst and an aldehyde in toluene. Also, the limitations are shown due to the ambitious separation aims which lead to unattainable concentrations in the final streams and excessive volume reduction rates.

Adi et al. [Adi2016] performed optimization of the superstructure of cascades with a MINLP for a crude oil application. Therefore, a binary mixture of heptane and hexadecane was used as the model solvent. The cascade design was optimized for maximum product purity with a given input stream.

3.3 Optimization model

The model applied in this study is a simplified model based on the work of [Ohs2016]; [Scho2015]; [Skib2012] using MINLP. The primary task of the model is to answer whether the configurations of membrane modules and total process selectivity change as a function of the retention values. Therefore, the model optimizes the superstructure of the membrane cascade when the solutes in their combination have (1) only positive retentions, (2) only negative retentions, and (3) both positive and negative retentions.

Furthermore, the interdependence of the stage cut and the selectivity is investigated. The stage cut represents the feed flow that is withdrawn on the permeate side of the membrane cascade. For example, with a feed mass flow in the cascade of $1000\,\mathrm{kg\,h^{-1}}$, a stage cut of $20\,\%$ would correspond to a permeate mass flow of $200\,\mathrm{kg\,h^{-1}}$ at the end of the cascade.

Superstructure with simplifications

The superstructure consists solely of pumps and membrane modules. Figure 3.1 shows all potential process configurations in this study. Multistage membrane cascades are challenging to control and require multiple compression. These conditions decrease the efficiency of the process [Favr2010]. Thus, the superstructure for the process is limited to three

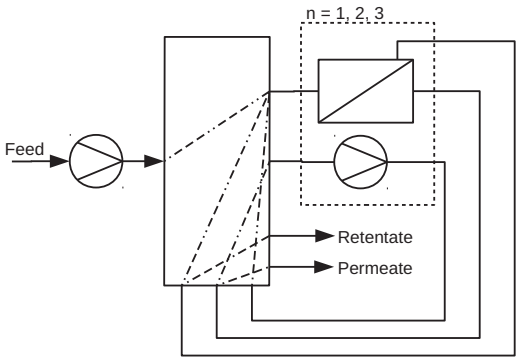

Figure 3.1: Superstructure approach for solute separation with OSN (adapted from [Scho2015]; [Ohs2016]).

stages. To reduce the computational effort, unreasonable process connections are not permitted. In particular, we defined the following logical constraints: the pressure determines the driving force. Therefore, a pump is connected to the permeate stream if it is fed to another membrane stage. Streams can both be merged and recirculated. However, the recirculations must always be connected at least to a preceding stage and thus can effectively only be realized for the second and third stage. The retentate and permeate streams cannot be split.

In each case, the system of substances is modeled with one solvent and two solutes. For the total process feed stream, it is stipulated that the two solutes (A and B) are dissolved with the same concentration of $1\,\mathrm{wt}\%$. The two solutes should be separated as best as possible using three module stages. As a measure for the separation, the selectivity S value is used:

$$S = \frac{\omega_B/\omega_A}{\omega_{B_{Feed}}/\omega_{A_{Feed}}} \tag{3.4}$$

ω_B and ω_A are the mass fraction of the solutes in the overall permeate of the process. $\omega_{B_{Feed}}$ and $\omega_{A_{Feed}}$ are the respective mass fractions in the overall

feed of the process.

The power specific selectivity is the objective function of the optimization model. It is obtained by dividing the selectivity with the power demand of the pumps. Maximizing this objective function provides insight into the process configuration to gain the highest possible selectivity at low power demand. Therefore, the model reveals the internal process streams and the quantity of the needed recycling streams. The model also gives information about the required membrane areas because these are not fixed.

Model equations

For further simplification, we assumed that the solution is ideal and the temperature constant. Pressure loss on the retentate side of the membrane is neglected. Furthermore, we do not consider possible swelling of the membranes or concentration polarization. The membrane area is not divided into discrete. Therefore, the membrane modules are treated as a black box.

The following balances apply to all single process units and the overall process. The mass balance is given by the equation:

$$\dot{m}_{in} = \dot{m}_{out1} + \dot{m}_{out2} \tag{3.5}$$

$\dot{m}$ are mass streams, “in,” “out1” and “out2” label the inlet and outlets of the single operations. For the overall feed source, the overall retentate and permeate sink and the pumps, $\dot{m}_{out2}$ is set to zero. For the overall process and the membane modules “out1” means the retentate and “out2” means the permeate.

Furthermore, the mass balance for each component can be written as follows:

$$\dot{m}_{in} \cdot w_i = \dot{m}_{out1} \cdot w_i + \dot{m}_{out2} \cdot w_i \tag{3.6}$$

w_i means the mass fraction of the separate substances.

The energy balance is implemented with:

$$\dot{m}_{in} \cdot \frac{1}{\rho_{in}} \cdot p_{in} + \Sigma P_{pu} = \dot{m}_{out1} \cdot \frac{1}{\rho_{out1}} \cdot p_{out1} + \dot{m}_{out2} \cdot \frac{1}{\rho_{out2}} \cdot p_{out2} + \Sigma \dot{Q} \quad (3.7)$$

In this equation ρ is the density of the solution. p represents the pressure, P_{pu} the power of the pumps and $\dot{Q}$ the heat flow.

The modeling of the membrane modules requires further equations. The solvent flow $J_{Solvent}$ through the membrane is calculated based on the linear ratio between flow and pressure difference Δp measured by Postel et al. [Post2013]. This simplification is possible because the solvent concentration across the membrane remains approximately constant. The pressure difference decisively determines the flux, and the other influencing factors are combined to the constant C_1. Therefore Equation 3.1 or Equation 3.2 is simplified to the empirical Equation 3.8.

$$J_{Solvent} = C_1 \cdot \Delta p \quad (3.8)$$

The solute fluxes result from the ratio of the individual fluxes J_{Solute} to the total flux through the membrane J_{Total} and the individual concentration in permeate $c_{Solute,Perm}$ to the total concentration in permeate $c_{Total,Perm}$.

$$\frac{J_{Solute}}{J_{Total}} = \frac{c_{Solute,Perm}}{c_{Total,Perm}} \quad (3.9)$$

The needed solute concentrations in the permeate result from experimentally measured or assumed retentions R by:

$$R = 1 - \frac{c_{Solute,Perm}}{c_{Solute,Ret}} \quad (3.10)$$

The fluxes, the molar masses M and the membrane area A_{Mem} determine the mass stream on the permeate side.

$$\dot{m}_{out2} = (\Sigma(J_{Solute} \cdot M_{Solute}) + J_{Solvent} \cdot M_{Solvent}) \cdot A_{Mem} \quad (3.11)$$

Mathematical problem definition

As previously stated, we used MINLP for the optimization model. The mathematical problem definition is similar to [Ohs2019]:

$$max\ f(x,y) \tag{3.12}$$

as a function of:

$$g(x,y) = 0 \tag{3.13}$$

$$h(x,y) \geq 0 \tag{3.14}$$

$$x \in X \tag{3.15}$$

$$y \in \{0;1\} \tag{3.16}$$

$f(x,y)$ represents the objective function (i.e., the power specific selectivity). $h(x,y)$ are the model equations, such as the mass balances, for the single process units and the overall process. $g(x,y)$ are the constraints which determine the boundary of the solution space. These include, e.g., the range of possible mass streams. x is the vector of process variables such as stage cut or feed concentrations. y is the vector of integer variables describing the connections within the process configuration.

The optimization model was implemented in the General Algebraic Modeling System (GAMS). Therefore, the programming is independent of the solver. The optimization task for this study was solved with the solver Branch-And-Reduce Optimization Navigator (BARON). This solver ensures the identification of a global optimum.

3.4 Case studies

This study investigates the separation of the solutes PEG 400, stearic acid and hexadecane in the solvents toluene and methanol. Postel et al. [Post2013] has presented solute data, flux data, and retentions. The data and results were measured with a development membrane from Evonik in-

dustries, which was registered as a patent by Haensel et al. [Haen2012] and is similar to PuraMem® S600. The total feed stream set in the model is $2000\,\mathrm{kg\,h^{-1}}$. Due to the measurements from Postel et al. [Post2013], the flux is adjusted to $4.9743\text{x}10^{-8}\,\mathrm{mol\,s^{-1}\,m^{-2}\,Pa^{-1}}$ if toluene is used (Retention case: (+ +)) and to $3.6848\text{x}10^{-8}\,\mathrm{mol\,s^{-1}\,m^{-2}\,Pa^{-1}}$ if methanol is used (Retention case (+ –) and (– –)). The following results have all been calculated with a feed pressure of $30\,\mathrm{bar}$ for each module stage. A and B represents the undesired solute A (higher retention value) and the desired solute B (lower retention value). The equation for the selectivity (Equation 3.4) can be simplified because of the equal concentration in the feed stream:

$$S = \frac{\omega_B}{\omega_A} \tag{3.17}$$

The optimizations are carried out for five different scenarios:

1. Stage cut scenario:

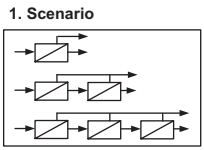

Selectivity vs. Stage cut

To gain a deeper understanding of the separation process, the dependency of the selectivity value on the stage cut for a one-, two- or three-stage process is investigated. The stage cut indicates the percentage of feed stream permeating through the membrane. The connection of the modules is predefined, i.e. the structure of the process is not optimized and the modules are always connected in series. The permeate is the feed stream of the next module (Figure 3.2). Only the retention case (+ –) with the respective values is optimized (Table 3.1) because we expected the highest selectivities in this case.

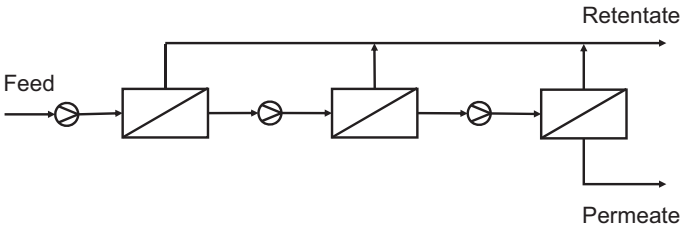

Figure 3.2: Predefined module configuration of the stage cut scenario with three stages.

Table 3.1: Retention cases and solutes with used retention values from the experimental measurements of [Post2013].

	Solute values					
Retention case	Solute A	MW_A [kg/kmol]	R_A [-]	Solute B	MW_B [kg/kmol]	R_B [-]
From experiments with methanol as solvent:						
(– –)	Stearic acid	284	-0.10	Hexadecane	226	-0.37
(+ –)	PEG 400	400	0.73	Hexadecane	226	-0.37
From experiments with toluene as solvent:						
(+ +)	PEG 400	400	0.73	Hexadecane	226	0.28

2. Experimental measured values scenario:

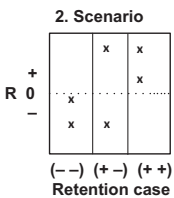

The combinations with two positive solute retentions (+ +), two negative solute retentions (– –) and one positive and one negative solute retention (+ –) are optimized. The optimal structure with the highest possible selectivity is required. The experimental measured substances from Table 3.1, flux, and retention values are used. The stage cut of the process is set at $20\,\%$ which guarantees an appropriate permeate mass stream.

3. Increasing recovery scenario:

The retention case with one positive and one negative retention value (+ –) is investigated. No stage cut is specified. Instead, the separation is investigated for different recoveries. The recovery r_{Rec} is the mass of the desired solute in the target stream (here permeate) divided by the mass in the feed stream.

$$r_{Rec} = \frac{\dot{m}_{B_{Perm}}}{\dot{m}_{B_{Feed}}} \tag{3.18}$$

The recovery is increased from 0.1 to 0.9, and the change in connection between the modules and the total selectivity is considered.

4. Rising ΔR scenario:

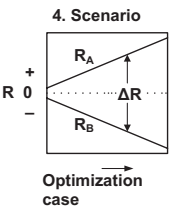

The flux data and solute data previously used (retention case (+ –)) are applied for optimization. The difference in the retention values for the two solutes ($\Delta R = R_A - R_B$) was varied in the range of $\Delta R = 0.2$ to $\Delta R = 1.8$. Therefore, the retention R_B was gradually decreased beginning at $R_B = -0.1$. Concurrent the retention R_A was gradually increased beginning at $R_A = 0.1$. The retention difference of $\Delta R = 1.8$ is reached if $R_B = -0.9$ and $R_A = 0.9$.

5. Shifting a constant ΔR scenario:

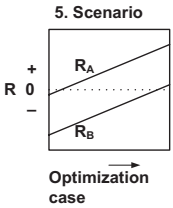

As in previous scenario, the retention case (+ –) is used but the retentions are varied. In this cases, the difference of the retentions remains constant with $\Delta R = 0.8$. This value approximately corresponds to the retention difference of PEG400 and stearic acid by the measured values from Postel et al. [Post2013] (Table 3.1). The retention difference is shifted in intervals of 0.1 from negative to positive. The higher retention value increases from $R_A = -0.1$ to $R_A = 0.9$. The lower retention value increases from $R_B = -0.9$ to $R_B = 0.1$. The effect of the position of the ΔR on the connection between the modules and the selectivity values is investigated.

In addition to the optimizations described above, the scenarios three and five were also optimized concerning only the selectivity value. This means the objective function is equal to Equation 3.17 and the power demand is not limited. The comparison of the results show the influence of minimizing the power demand, which is finally a first approximation for a cost optimization.

3.5 Results and discussion

This optimization study shows the sensitivity of the process design for different retention conditions, retention distances, and positions of the retentions on the retention scale. In scenarios two to five, the three-module stages are connected differently. Overall, nine different configurations result from the optimizations. In contrast, we specified the connections for scenario one. Thus, in scenario one, the module configuration itself is not optimized.

Stage cut scenario

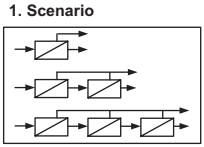

Scenario one mainly aims to develop a deeper understanding of the process and to reveal the correlation between selectivity and stage cut. This correlation is depicted in Figure 3.3 for a one-, two- and three-stage membrane processes. The connections for the three-stage process are shown in Figure 3.2. The selectivity value is maximized for a given stage cut. The optimization for a single-stage membrane process showed a more or less linear correlation. The highest selectivity value is reached at the lowest stage cut. The selectivity decreases to 1 for a stage cut of approximately $100\,\%$. For a two-stage membrane process, the selectivity value decreases exponentially towards high stage cuts. In a three-stage process, this effect is even more pronounced.

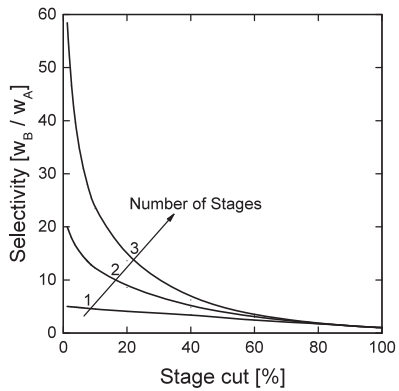

Figure 3.3: Optimization results of the stage cut scenario with one, two or three stages.

The decrease of the selectivity value with increasing stage cut was expected. At constant pressure, a higher permeate flow can only be achieved

with a larger membrane area. This point implies that the solute with higher retention also passes the membrane at a higher concentration. At a theoretical stage cut of $100\,\%$, the entire feed stream passes the membrane unit. Thus, the fraction of the solutes in the feed and the permeate stream are equal, resulting in a selectivity value of 1. If an insignificant stage cut is selected, the separation of the two substances can be potentiated by a further stage for the permeate or the shown configuration in Figure 3.2. This circumstance results in the exponential curves of these module connections. The results are in line with the results from [Siew2013a] and [Mont2016]. However, this scenario gives a first impression of how a cascade influences the separation of two different solutes. In the following, we investigate how recirculation and other process connections influence the selectivity.

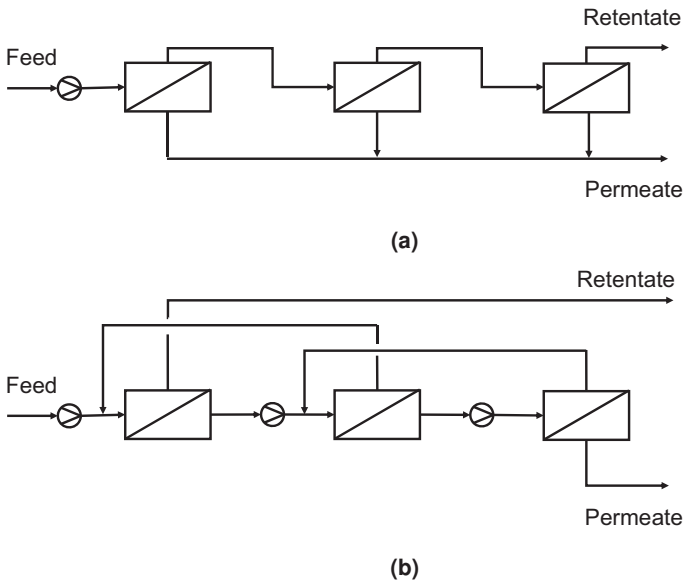

Figure 3.4: Resulting additional module configurations from the optimizations of the experimental measured values scenario.
(a) is the result for the retention case (– –),
(b) is the result for the retention case (+ –) and (+ +).
The desired solute R_B is enriched in the permeate.

Experimental measured values scenario

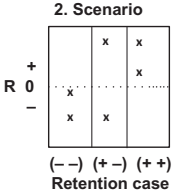

The optimizations show two different optimal configurations for the different retention cases (Figure 3.4). If both solutes have negative retentions (retention case (– –)), the configuration corresponds to a simple series connection (Figure 3.4a). For both other cases (retention cases (+ –) and (+ +)), the connections change significantly (Figure 3.4b). The mixture of the process inlet stream and the retentate stream of the second stage combine to the feed of the first membrane stage. The permeate of the first stage is mixed with the retentate of the third stage. The resulting mixed stream is then fed to the second stage. The permeate of the third stage represents the outlet of the process. The optimized membrane areas of the individual modules and the total membrane area can be taken from Table 3.2. Furthermore, the achieved selectivity value and power demand are presented in Table 3.2.

Notably, it is apparent that the selectivity value is highest for the retention case (+ –). The membrane area is the highest for this retention combination. In the retention case (– –), the selectivity value is low and almost no separation occurs.

Table 3.2: Resulting selectivities, power demands and membrane areas from the optimization of the experimental measured values scenario.

Retention case	Selectivity value [-]	Power demand [W]	Membrane area Module 1 [m^2]	Module 2 [m^2]	Module 3 [m^2]	Total [m^2]
(– –)	1.2	2031	11.0	10.2	9.6	30.8
(+ –)	59.2	5372	161.4	133.4	30.8	325.6
(+ +)	16.7	3982	27.4	26.0	8.0	61.4

The results of this scenario show that the separation of the two solutes in retention case (– –) is challenging with the given stage cut. How-

ever, it should be considered that the distance between the two retentions ($\Delta R = R_A - R_B$) is the smallest of the individual cases ($\Delta R = 0.27$). The configuration of the membrane modules corresponds to that of a single-stage process with the total membrane area. The continuous purification of the permeate does not result in a higher selectivity, which is worthwhile relative to the power demand. Instead, a membrane area as small as possible for the fixed stage cut is chosen. Accordingly, the lowest possible flux through the membrane is favored. Therefore, the question arises whether the ΔR is responsible for the configuration. Resulting, the second question occurs at which ΔR value the "transition point" concerning the configuration exists.

For the retention case (+ –), the ΔR is the highest ($\Delta R = 1.1$). The continuous purification of the permeate is combined with the recycle of the retentate. This recirculation allows for larger membrane areas. Thus the material flow can be treated while keeping the stage cut constant. The power demand increases due to the necessary pressure increase of the permeate. Concurrent, the selectivity for this retention case rises rapidly. As a result, the relative value of selectivity to power demand is higher. In the third retention case (+ +), the same configuration is optimal. Here the ΔR has a value of 0.45. It is clearly below the value of retention case (+ –) and only slightly above that of (– –). Initially, this result indicates that the value of ΔR is the decisive factor. Though, the position of ΔR on the retention scale can also influence the configuration. Based on the scenario results, we investigate where the maximum power demand with a stage cut of $20\,\%$ on the ΔR scale lays. Thus, a possible maximum would exist regarding the recirculation. The selectivity should be as high as possible relating to the power demand.

Increasing recovery scenario

Increasing the recovery rate of R_B in the permeate results in four different optimal configurations. With a recovery of 0.1 up to 0.4, the configuration from Figure 3.4b is applied. The setup from Figure 3.4a is calculated as optimum with a recovery of 0.5 to 0.7. At 0.8 and 0.9 recovery, new connections are found with the optimization model (Figure 3.5). The configuration lead-

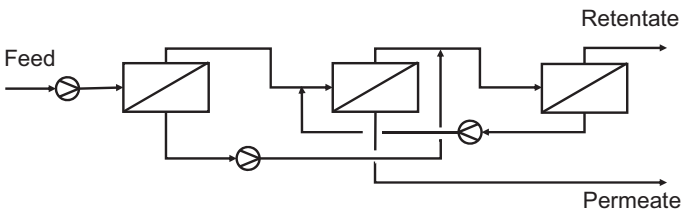

(a) Recovery rate: 0.8; Objective function: power specific selectivity

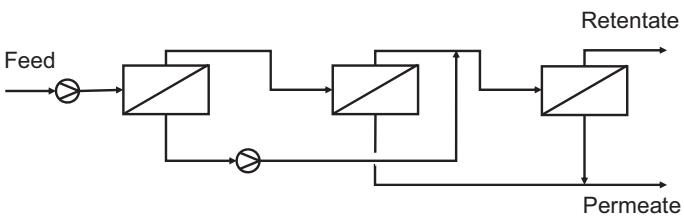

(b) Recovery rate: 0.9; Objective function: power specific selectivity

Figure 3.5: Resulting additional module configurations from the optimizations of the increasing recovery scenario in consideration of the power demand.

ing to a recovery of 0.8 of R_B in the permeate is shown in Figure 3.5a. The permeate of the first stage is combined with the retentate of the second stage to the feed of the third stage. The feed of the second stage con-

sists of the retentate of the first stage and the permeate of the third stage. The retentate of the third stage and the permeate of the second stage are ejected from the entire process. Figure 3.5b shows the process if 0.9 recovery is required. The process differs from the one in Figure 3.4a by mixing the permeate from the first stage with the retentate from the second stage. This mixture is fed to the third stage. The retentate of the third stage and the mix of the second and third stage permeate are ejected from the process.

Figure 3.6 shows the resulting selectivity, stage cut, power demand, and total membrane area for the optimizations in this scenario. Results of two different situations are depicted: the solid lines represent the optimizations with the selectivity divided by the power demand as the objective function. The dotted lines represent the optimizations with only the selectivity as the objective function. Initially, the results represented as the solid lines are discussed (Figure 3.6). The specific data for each recovery case in this situation are listed additionally in Table 3.3.

It is noticeable that the selectivity value decreases exponentially with increasingly mandatory recovery. Up to a recovery of 0.4, power demand and membrane areas increase. At 0.5 recovery, the power demand and membrane areas decrease abruptly. If higher recovery values are applied in the optimization, the membrane area rises again, as well as the power demand. The area and power demand values change significantly whenever a new configuration results from the optimization (cf. Figure 3.6).

Considering that the flux through a membrane is dependent on the pressure, the stage cut and the membrane area must be adjusted to a given recovery rate. Therefore, one or both of these variables must rise with increasing recovery at constant pressure. Increasing the stage cut expands automatically the minimum membrane area required to reach the stage cut. Conversely, the membrane area can increase without raising the stage cut, since the permeate quantity can be controlled by recirculation. The configuration depicted in Figure 3.4b leads to high selectivities for small recovery rates and can only be realized by large membrane areas. At the same time,

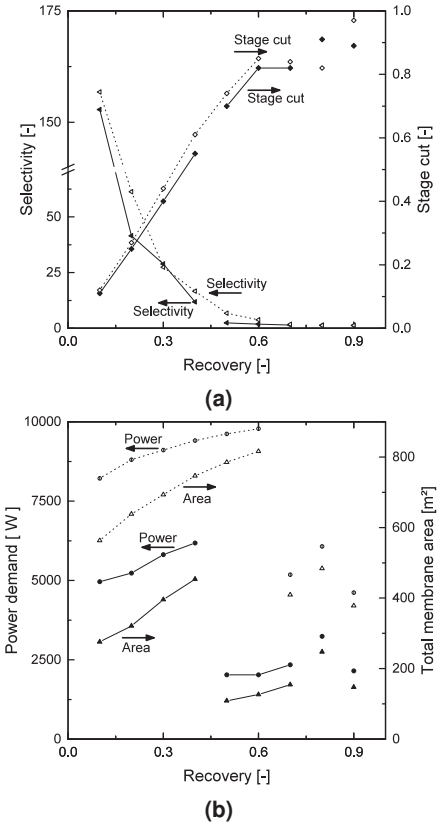

Figure 3.6: Resulting selectivity ◀, ◁ and stage cut ◆, ◇ (a) as well as power demand ●, ○ and total membrane area ▲, △ (b) for the increasing recovery scenario (scenario 3).
Solid lines with closed symbols: objective function is the selectivity divided by the power demand.
Dotted lines with open symbols: objective function is the selectivity.
The lines are interrupted when the module configuration changes.

the required recovery rate increases the stage cut. In comparison to Figure 3.3, the achievable selectivities decrease.

The optimum of the objective function can not be achieved with three pumps for a recovery rate above 0.5. Thus, the configuration changes and corresponds to a single stage process containing the total required membrane area. No pump increases the power demand, and no recirculation increases the membrane area. The area is determined completely by the stage cut. Accordingly, the selectivity has dropped as the module stages decreased virtually from 3 to 1. However, the stage cut remains constant for an increase in the recovery rate from 0.6 to 0.7, while the membrane area increases. This increase in the area can be related to the decrease in selectivity, which is feasible within the solution space. Interestingly, further changes of the configuration are obtained to achieve a recovery rate of 0.8 and 0.9.

Therefore, additional pumps are included in the configuration of the modules, and no intuitive combinations occur in the interconnection. The selectivity is near the theoretical minimum. The extremely high stage cuts require a large permeate flow. This flow is achieved by a large membrane area directly before the permeate removal. The permeate streams of the other modules are small and therefore, do not require high power demands. The combination of permeate streams and retentate streams appears not to be beneficial for the separation efficiency. However, selectivity does not matter for the optimization as it is already too low. The achievement of the mass flows to comply with the fixed stage cut primarily determines the optimization. The module connections are necessary to generate the appropriate material flow quantities through the respective membranes.

In this ‘increasing recovery scenario’, the conflict between recovery rate or stage cut and selectivity becomes clear. Intuitively, very high stage cuts and recovery rates are not reasonable due to the low selectivity. Similarly, an exceptionally high selectivity cannot be achieved due to low recovery rates.

Table 3.3: Resulting selectivities, stage cuts, power demands and membrane areas from the optimization of the increasing recovery scenario in consideration of the power demand.

Recovery case	Selectivity value [-]	Stage cut [-]	Power demand [W]	Membrane area Module 1 [m^2]	Module 2 [m^2]	Module 3 [m^2]	Total [m^2]
Optimal configuration is depicted in Figure 3.4b.							
0.1	152.83	0.11	4959	138.4	119.7	17.5	275.6
0.2	41.48	0.25	5234	150.8	131.9	38.4	321.1
0.3	28.87	0.40	5814	172.5	161.5	61.9	395.9
0.4	11.79	0.55	6181	185.9	182.7	85.1	453.7
Optimal configuration is depicted in Figure 3.4a.							
0.5	2.43	0.70	2028	38.6	27.8	42.2	108.6
0.6	1.88	0.82	2028	27.8	27.8	70.9	126.5
0.7	1.47	0.82	2344	27.8	98.7	27.7	154.2
Optimal configuration is depicted in Figure 3.5a.							
0.8	1.38	0.91	3242	43.4	140.2	63.5	247.1
Optimal configuration is depicted in Figure 3.5b.							
0.9	1.25	0.89	2150	10.7	127.9	8.6	147.2

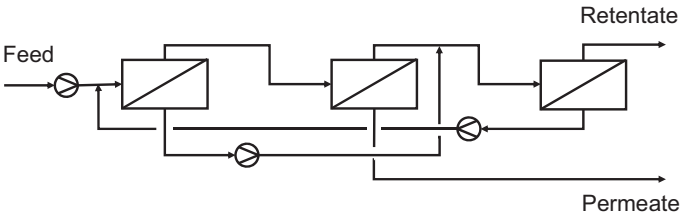

(a) Recovery rate: 0.8; Objective function: selectivity

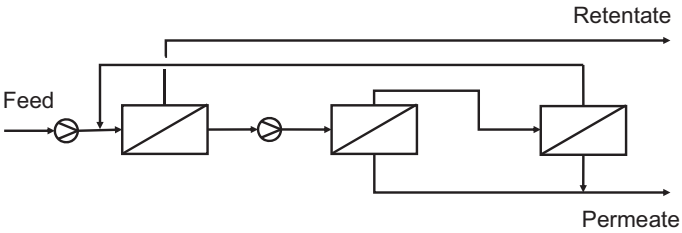

(b) Recovery rate: 0.9; Objective function: selectivity

Figure 3.7: Resulting additional module configurations from the optimizations of the increasing recovery scenario without consideration of the power demand.

Figure 3.7 presents other resulting configurations with a recovery rate of 0.8 and 0.9 if the power demand is not included in the optimization variable. At a recovery rate of 0.8, the permeate of the third stage is fed back before the first stage (Figure 3.7a). With 0.9 recovery, the feed of the first stage is generated from the process feed and the recirculation of the retentate from the third stage. The permeate of the first stage forms the feed of the second stage while the retentate leaves the process. The retentate of the second stage is the third stage feed. The second and third stage permeate are mixed and exit the process (Figure 3.7b). In addition to the new configurations, this variant of the objective function changes the distribution of the arrangements from Figure 3.4a and Figure 3.4b concerning the recovery rate. The setup from Figure 3.4a is only optimal for 0.7 recovery. The configuration from Figure 3.4b is the optimal configuration for recovery rates from 0.1 to 0.6.

The curves (dotted lines) in Figure 3.6 show similarities with the results

discussed above from the optimizations with the previous objective function. Especially the selectivities and stage cuts are similar (Figure 3.6a). The curves of power demand and total membrane areas are identical regarding their shape. However, the dotted lines are shifted to higher recovery rates because of the differences in configuration changes (Figure 3.6b). With Table 3.4, it is verifiable that both values (power demand and total membrane area) are, in some cases, more than twice as high compared to the other objective function.

The compared values of Table 3.3 and Table 3.4 show how expensive a small increase in selectivity can be. The respective stage cuts are only slightly higher than in the situation discussed above. It is striking that the simple configuration (Figure 3.4a) is always determined as optimum for selectivities below 3. However, in the case of specified recovery, stage cuts are rather above the $20\,\%$ defined in the other scenarios. The consideration of the power demand in the optimization leads to a faster reduction of the selectivity depending on the stage cut (Figure 3.6). Simultaneously, the required membrane area is kept low by the optimization concerning the power demand at comparable high yields.

The new configuration with a recovery rate of 0.8 (Figure 3.7a) differs only slightly from the previous arrangement with the same recovery rate (Figure 3.5a). The new setup with a recovery rate of 0.9 (Figure 3.7b), on the other hand, is distinctly different from the setup using the previous objective function (Figure 3.5b). However, both new configurations can only improve selectivity to a small extent due to the high stage cut. Furthermore, the focus is on ensuring the required material flows. Thus, the conflict between recovery rate or stage cut and selectivity remains decisive for the configuration. The definition of a stage cut at $20\,\%$, as specified in the other scenarios, corresponds to a low recovery rate. However, the performed selectivity optimizations have a broader scope for possible solutions.

Table 3.4: Resulting selectivities, stage cuts, power demands and membrane areas from the optimization of the increasing recovery scenario without consideration of the power demand.

Recovery case	Selectivity value [-]	Stage cut [-]	Power demand [W]	Membrane area Module 1 [m^2]	Module 2 [m^2]	Module 3 [m^2]	Total [m^2]
Optimal configuration is depicted in Figure 3.4b.							
0.1	156.80	0.12	8216	419.7	125.6	17.8	563.1
0.2	61.27	0.27	8803	315.0	282.7	40.8	638.5
0.3	27.39	0.44	9108	308.2	316.9	68.0	693.1
0.4	16.65	0.61	9408	249.8	402.0	94.8	746.6
0.5	6.77	0.74	9615	203.3	467.3	114.8	785.4
0.6	3.75	0.85	9781	200.7	484.4	131.2	816.3
Optimal configuration is depicted in Figure 3.4a.							
0.7	1.75	0.84	5181	144.2	136.2	128.8	409.2
Optimal configuration is depicted in Figure 3.7a.							
0.8	1.25	0.82	6074	179.0	126.3	178.8	484.1
Optimal configuration is depicted in Figure 3.7b.							
0.9	1.32	0.97	4617	229.0	94.0	55.6	378.6

Rising ΔR scenario

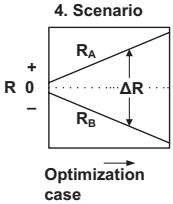

The fourth scenario contains hypothetical retentions for which the mutual distance of R_A and R_B is gradually increased. For the first case ($\Delta R = 0.2$), the optimization results in the configuration according to Figure 3.8a. The permeate streams of the second and third stage are each fed back and combined with the process feed, to feed the first stage. The retentate of the first and second stage form the feed of the respective subsequent stage. The retentate of the third stage and the permeate of the first stage are

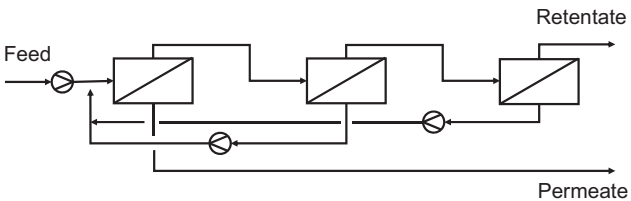

(a) ΔR = 0.2; Objective function: power specific selectivity

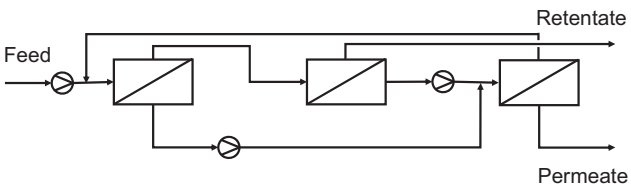

(b) ΔR = 0.4 to 0.6; Objective function: power specific selectivity

Figure 3.8: Resulting additional module configurations from the optimizations of the rising ΔR scenario.

leaving the process. Figure 3.8b shows the optimal configuration when ΔR has increased to 0.4 and 0.6. The permeate streams from stage one

and two are mixed and fed to the third stage. While the permeate of the third stage represents an outlet of the process, the retentate is recycled to the first stage. The retentate of the first stage is fed to the second stage. The second stage retentate is ejected. With all higher ΔR ($\Delta R = 0.8$ to $\Delta R = 1.8$), the optimization resulted in the configuration from Figure 3.4b.

Table 3.5: Resulting selectivities, power demands and membrane areas from the optimization of the rising ΔR scenario.

ΔR case	Selectivity value [-]	Power demand [W]	Membrane area Module 1 [m^2]	Module 2 [m^2]	Module 3 [m^2]	Total [m^2]
Optimal configuration is depicted in Figure 3.8a.						
0.2	1.24	2685	30.7	27.7	27.7	86.1
Optimal configuration is depicted in Figure 3.8b.						
0.4	1.67	2693	30.7	27.7	30.7	89.2
0.6	2.29	2785	36.8	29.7	30.8	97.2
Optimal configuration is depicted in Figure 3.4b.						
0.8	4.59	4093	106.1	75.4	30.7	212.2
1.0	8.51	4490	125.0	91.5	30.7	247.2
1.2	17.71	4836	140.8	106.1	30.7	277.6
1.4	58.78	5451	168.5	132.8	30.6	331.9
1.6	474.1	6167	196.8	167.8	30.6	395.2
1.8	1667	4300	113.6	86.4	30.6	230.7

As expected, the selectivity value increases with increasing ΔR (Figure 3.9). Initially, the increase is only marginal, but the growth becomes exponential as soon as $\Delta R > 1$. The power demand and membrane areas increase for $\Delta R < 0.8$ only slightly. Beginning at $\Delta R = 0.8$, the changed configuration results in a significant increase in the power demand and membrane areas for module 1 and 2. The single results from the optimizations are listed in Table 3.5. Only for the highest ΔR applied ($\Delta R = 1.8$), the power demand and membrane areas decrease considerably. This decrease is particularly noticeable as the configuration does not change.

Remarkable are the two configurations (Figure 3.8) of the first two ΔR cases ($\Delta R = 0.2$ and $\Delta R = 0.4$). They reach only a low selectivity ($S < 2$) but still do not correspond to the setup of Figure 3.4a. However, a closer

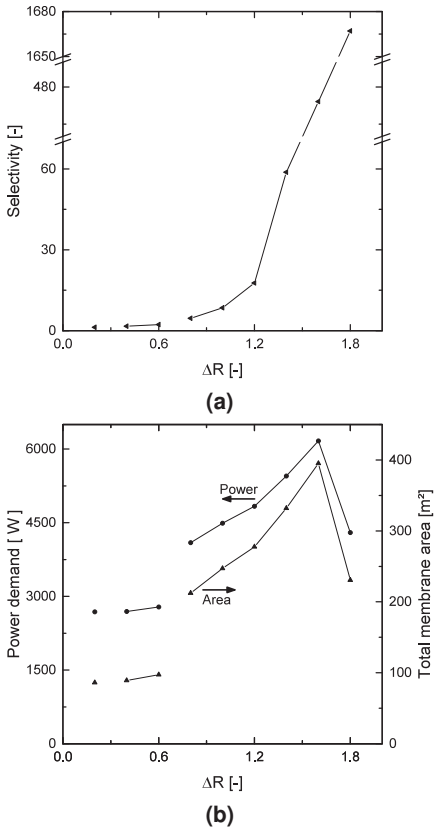

Figure 3.9: Resulting selectivity ◄ (a) as well as power demand ● and total membrane area ▲ (b) for the rising ΔR scenario. The lines are interrupted when the module configuration changes.

look reveals similarities between the configurations of Figure 3.8 and Figure 3.4a. In this way, the setup from the first case (Figure 3.8a) can also be understood as a single stage process. In this process, the permeate is split and partially recycled. The recirculation changes the concentration ratio in the feed to the advantage of selectivity. In the second case ($\Delta R = 0.4$), the first two stages can be combined to form a single membrane with the sum of the membrane areas. Finally, the third stage is different by using the permeate of the other stages as feed. The valuable substance is purified again to achieve the final permeate. The recycled retentate stream improves the concentration ratio in the feed of the first stage due to its composition. Eventually, the stream originates from the permeate of the pre-stages. In the first stage, the concentration of the desired substance increases and that of the undesired solute decreases.

The similar retention case (– –) from the second scenario (experimental measured values scenario) shows a lower selectivity and as optimal configuration Figure 3.4a. The most critical difference is undoubtedly the position of the ΔR on the retention scale. In this scenario (Rising ΔR scenario), the two retentions always have different signs, which means that only the desired solute is enriched in the permeate. The signs lead to a slightly higher selectivity, which allows a higher power demand and thus a different configuration. The general statement from the third scenario (increasing recovery scenario) that a selectivity below 3 always leads to the setup according to Figure 3.4a must, therefore, be revised. Instead, the combination of selectivity, stage cut, and location of the ΔR is responsible for the configuration.

The observation that the configuration according to Figure 3.4b is first given with an $\Delta R = 0.8$ as optimum, also supports this explanation. This result was unexpected as in the second scenario (experimental measured values scenario) the corresponding configuration is already considered as optimum with an $\Delta R = 0.45$. However, in this case, the signs of both solute retentions are positive, and the achieved selectivity is significantly higher. In this scenario (rising ΔR scenario), a comparable selectivity is not reached until $\Delta R = 1.2$ (cf. Table 3.2 and Table 3.5). Again, the position of the ΔR on the retention scale is decisive, although intuitively higher selectivities

would be expected at lower ΔR for different signs. The retention case (+ –) from the second scenario (experimental measured values scenario), on the other hand, achieves significantly higher selectivities than comparable ΔR from this scenario would suggest. In this case, the position of the ΔR is not symmetrical at $R = 0$. We assume that this is the reason for the considerable difference. The last scenario will provide clarity in this respect.

As already mentioned, the highest ΔR in this scenario remains striking. The selectivity is exceptionally high with $S = 1667$ (Table 3.5), which is almost four times as high as for the previous ΔR. Since the configuration does not change, only the membrane area is left as the control variable for the flux. The stage cut of the overall process and the pressure in the feed of the modules are fixed. The smaller membrane areas of the first two modules (see Table 3.5) lead to lower permeate flows. These lower flows explain the reduction in power demand. The recirculation of the retentates from the second and third modules is reduced. Accordingly, the amount of liquid in the overall process is smaller. The smaller amount of fluid is enabled by the increase in ΔR. The configuration as a reinforcing cascade increases the selectivity, whereby even small changes in the ΔR lead to significant improvements in selectivity. The variable space concerning the membrane area is limited since the total stage cut limits the permeate streams of the modules. The reason is that the product of the stage cuts of the individual stages results in the overall stage cut. Therefore, a smaller membrane area, and thus a smaller amount of liquid needs to be pumped, can lead to a better ratio between selectivity and power demand.

Shifting a constant ΔR scenario

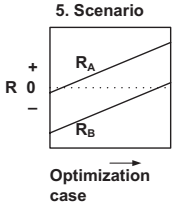

The scenario with constant ΔR shows the impact of the position of the ΔR on the retention scale. For the combinations $R_A/R_B = -0.1/-0.9$ and $R_A/R_B = 0.0/-0.8$ a configuration as shown in Figure 3.4a is optimal. The membrane areas are adjusted to the material streams required by the stage cut. The shift of ΔR gives the optimization a new scope to increase selectivity by recirculations or other configurations. If the position of the ΔR on the retention scale is changed to $R_A/R_B = 0.1/-0.7$, the configuration changes and is similar to Figure 3.8b. Due to a further shift of ΔR and change in configuration, the membrane surfaces of the first two stages and thus the internal material flows can be raised. For this purpose, only the permeate stream of the second stage is connected differently. The configuration in Figure 3.10 shows the optimum for the retention combination $R_A/R_B = 0.2/-0.6$. In this configuration, the feed of the first stage is composed of the process feed, the permeate of the second stage, and the retentate of the third stage. The first stage retentate is fed to the second stage feed while the first stage permeate becomes the third stage feed. The permeate of the third stage and the retentate of the second stage are respectively emitted from the process as output streams.

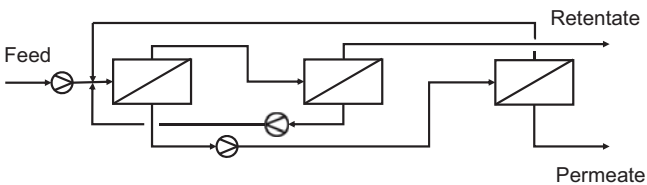

Figure 3.10: Resulting additional module configuration from the optimization of the shifting a constant ΔR scenario at $R_A/R_B = 0.2/-0.6$ in consideration of the power demand.

The new configuration (Figure 3.10) is of interest because both output streams of the first stage are fed into another membrane stage. The purification of the permeate is intensified in a second stage. The retentate, resulting from this separation, is used to adjust the concentration ratio for the feed of the first stage. The same applies to the second stage, which ejects the total retentate from the process. Here, the permeate stream containing a higher concentration of the desired solute is recycled. This recirculation also increases the concentration ratio before the first stage in favor of the valuable substance. However, even this configuration cannot be maintained if the ΔR moves further into the positive range. The total membrane area initially remains approximately constant. Since the optimization always evaluates the selectivity divided by the power demand, it can be assumed that a higher power demand would have been necessary for this configuration than for the configuration of Figure 3.4b. For the constellations from $R_A/R_B = 0.3/-0.5$ to $R_A/R_B = 0.9/0.1$, the optimization always resulted in the configuration as shown in Figure 3.4b.

In Figure 3.11, the selectivity, the power demand, and the total membrane area are plotted versus the retention of the undesired solute A. The results depicted with the solid lines are discussed first. For these results, the objective function was the selectivity related to the power demand. The selectivity hardly increases as long as the retention of R_A is below 0.6. Moving the position of ΔR further to higher values results in an exponential increase of selectivity. The power demand and membrane areas change as the ΔR passes 0.0, i.e., value R_A higher 0. From this point both increase until the lower retention value R_B also passes 0.0 and $R_A > 0.7$. While the power demand increases more or less constant, the total membrane area behaves in another way. Here, the change of configuration at $R_A/R_B = 0.1/-0.7$ and $R_A/R_B = 0.2/-0.6$ accompanies with significant higher values. Further shifting ΔR induces a more slight increase. Table 3.6 reveals that the first two stages mainly cause a change in the total membrane area. The membrane area of the third stage only increases rapidly at $R_A/R_B = 0.1/-0.7$. If the retention combination for the ΔR is completely positive, both power demand and total membrane area decrease rapidly.

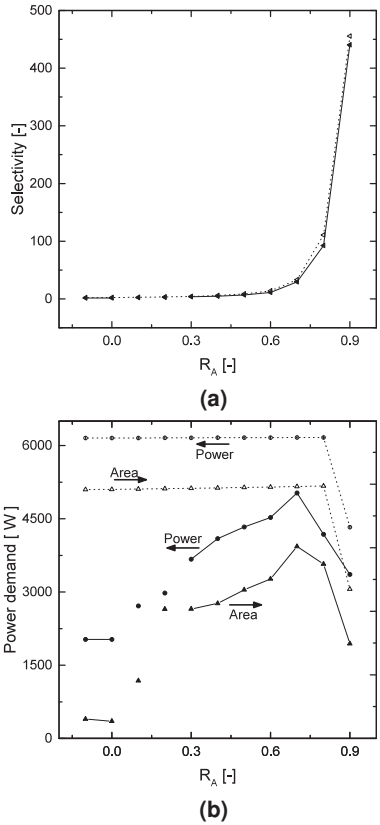

Figure 3.11: Resulting selectivity ◀, ◁ (a) as well as power demand ●, ○ and total membrane area ▲, △ (b) for the shifting a constant ΔR scenario.
Solid lines with closed symbols: objective function is the selectivity divided by the power demand.
Dotted lines with open symbols: objective function is the selectivity.
The lines are interrupted when the module configuration changes.

Table 3.6: Resulting selectivities, power demands and membrane areas from the optimization of the shifting a constant ΔR scenario in consideration of the power demand.

R_A/R_B case	Selectivity value [-]	Power demand [W]	Membrane area Module 1 [m^2]	Module 2 [m^2]	Module 3 [m^2]	Total [m^2]
Optimal configuration is depicted in Figure 3.4b.						
0.9/0.1	440.40	3361	59.0	59.0	31.1	149.1
0.8/0.0	92.37	4182	127.8	115.6	31.0	274.4
0.7/-0.1	29.36	5029	143.1	127.8	31.0	301.9
0.6/-0.2	11.23	4525	122.5	97.6	30.9	251.0
0.5/-0.3	6.80	4332	115.7	87.1	30.8	233.6
0.4/-0.4	4.59	4093	106.1	75.4	30.7	212.2
0.3/-0.5	3.59	3671	103.5	69.5	30.7	203.7
Optimal configuration is depicted in Figure 3.10.						
0.2/-0.6	2.92	2980	98.9	73.9	30.5	203.4
Optimal configuration is depicted in Figure 3.8b.						
0.1/-0.7	2.08	2716	32.7	27.6	30.6	90.8
Optimal configuration is depicted in Figure 3.4a.						
0.0/-0.8	1.62	2028	10.5	9.3	7.3	27.1
-0.1/-0.9	1.55	2028	10.9	10.2	9.4	30.5

Since the ΔR always remains constant and only the position was varied, changes must result from this position shift. With rising retentions on the retention scale, the selectivity of the membrane cascade increases exponentially. Considering that the change of the ΔR into the positive range equals an increase of the retention for both solutes simultaneously, this increase is plausible. When the selectivity is calculated (Equation 3.17), both denominator and numerator decrease, leading to an exponentially increasing function. This exponential change with the same configuration is comparable with that from the stage cut scenario and the increasing recovery scenario or rising ΔR scenario. Thus, the selectivity seems to be exponentially dependent on the factors stage cut/recovery, ΔR and location of the ΔR. The configuration only changes when the selectivity drops below 3. With a simple setup, sufficient power demand can be saved to achieve a more attractive relation between selectivity and power demand.

The configuration from Figure 3.4b results for all cases if the optimizations are performed without minimizing the power demand. In this situation, the objective function is defined only by the selectivity. The results are shown in Figure 3.11 as dotted lines and as individual values listed in Table 3.7. These optimizations achieve only slightly higher selectivity values. Furthermore, the results show significantly higher power demands and membrane areas. However, it is noticeable that the power demands and membrane areas change only slightly for all cases.

Undoubtedly, the configuration of Figure 3.4b always achieves high-

Table 3.7: Resulting selectivities, power demands and membrane areas from the optimization of the shifting a constant ΔR scenario without consideration of the power demand.

R_A/R_B case	Selectivity value [-]	Power demand [W]	Membrane area Module 1 [m^2]	Module 2 [m^2]	Module 3 [m^2]	Total [m^2]
Optimal configuration is depicted in Figure 3.4b.						
0.9/0.1	455.50	4329	119.7	84.0	31.1	234.8
0.8/0.0	110.80	6166	191.7	174.2	31.1	397.0
0.7/-0.1	33.24	6165	197.1	168.1	31.0	396.2
0.6/-0.2	13.93	6164	202.5	162.0	30.9	395.4
0.5/-0.3	8.62	6162	207.1	156.8	30.8	394.7
0.4/-0.4	5.97	6161	209.4	153.9	30.7	394.0
0.3/-0.5	4.46	6159	209.3	153.6	30.6	393.5
0.2/-0.6	3.53	6158	209.0	153.2	30.5	392.7
0.1/-0.7	2.92	6157	208.9	153.0	30.4	392.3
0.0/-0.8	2.49	6156	208.8	152.7	30.3	391.8
-0.1/-0.9	2.19	6155	208.7	152.5	30.2	391.4

est selectivities with $\Delta R = 0.8$. The noticeable similarity to the selectivity values from the previously discussed situation is due to the combination of the required stage cut and the solvent flux. The combination implies maximum values for the possible membrane area and power demand. As a result, a maximum amount of liquid is available in the internal process. The optimization cannot take any further countermeasures to get higher selectivities. This circumstance is depicted by the almost constant power demand and membrane area for the different optimization runs. If the

ΔR were broader, as shown in the rising ΔR scenario, this would result in larger membrane areas and power demands. Optimal selectivities with lower membrane areas and power demand are gained by shifting the ΔR to only positive values. The utilization of the maximum membrane areas and power demand is not necessary.

3.6 Conclusion

The presented optimization shows under which conditions already simple configurations of a process design change. A simplified model, as in Böcking et al. [Böck2019], was used for five different scenarios. The number of stages was limited to three in order to consider a possible control effort. It is the first optimization to study negative retentions in a cascade.

The most frequently selected configuration by the optimization is the amplification mode. In this process, the retentate streams are recirculated to the preceding stage (Figure 3.4b). The setup is not only dependent on different retentions, but also on the desired stage cut and the position of the retentions on the retention scale. The higher the retention of the undesired solutes and the broader the ΔR ($\Delta R = R_A - R_B$) and the smaller the required stage cut, the higher the achievable selectivity.

In each scenario, the configuration of the modules switches only at low selectivities. Accordingly, the process design only changes if high recovery rates and therefore, stage cuts are required. Other causes for a configuration change are a small distance between the solute retentions or retention values of the undesired solute close to zero or negative. For the last reason, a change in the process design is probable if solutes with only negative instead of positive retention should be separated. The lower selectivity can be slightly increased by changing the process design. However, there is always a field of low selectivity where a cascade offers no advantage compared to a simple membrane process.

Membrane cascades with low selectivities are just as meaningless as cascades with low stage cut. However, the demonstrated dependencies show that further factors need to be considered to achieve optimum pro-

cess control. Individual decisions must be taken for each real process since the different parameters limit each other or are partly given.

For further work, the modeling can be extended and enhanced. The available optimizations have been calculated for the case that the valuable solute is recovered in the permeate and has lower retention. It is also recommended to consider the reverse situation, where the desired solute has higher retention than the other. Furthermore, it is interesting whether the module configurations change with concentration-dependent retention. Besides the connection possibility can be extended to allow splitting of streams. A more precise cost function than the limitation of the power demand could provide more accurate results. Indeed Ohs, Falkenberg, and Wessling [Ohs2019] already explained that the economic optimum is of higher practical relevance as the energy demand.

4 Superimposing effects influence membrane characteristics in water-ethanol and water-NMP mixtures

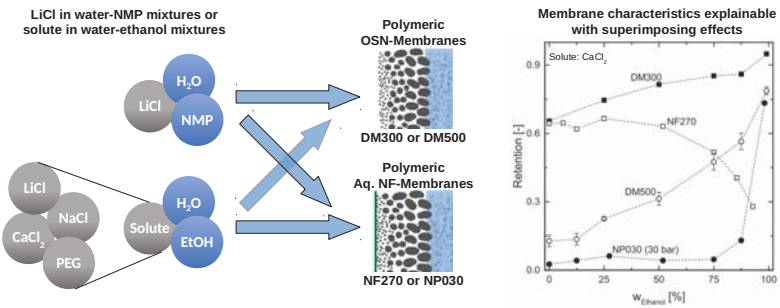

A systematic investigation of membrane characteristics in solvent tolerant nanofiltration reveals superimposed effects that influence mass transport, flux, and retention.

4.1 Introduction

Nanofiltration has become a well-established branch of membrane separation technology in recent decades with a growing number of publications. Generally, either a system of substances with water as solvent [Van 2008]; [Moha2015] or applications in organic solvents are considered [Vand2008]; [Marc2014]. Both research areas show different challenges that have to be overcome in order to be implemened as industrial process. Nowadays the number of realized processes and process possibilities increases continuously. Further applications emerge when the two variants are combined. These processes uses a homogeneous mixture of water and an organic solvent. Such process streams occur in the synthesis of pharmaceutical, agrochemical or specialty chemicals, for example. They are generated as process streams or waste streams that are either treated for discharge, for partial or complete recycling, or for recovery of value products. Their industrial relevance is contrasted by the limited number of scientific studies on nanofiltration of these complex aqueous-organic mixtures [Post2015]; [Mert2018]; [Marc2012]; [Marc2013]; [Laba2013].

Recently we asked whether PDMS membranes (developed for use in organic solvent nanofiltration (OSN)) also retain salts from water-methanol mixtures and compared the results with those of a commercially available nanofiltration membrane for aqueous applications [Post2015]. In continuation of this study, the present work is intended to broaden the knowledge for nanofiltration in aqueous-organic solvent mixtures. Since most nanofiltrations in research and, nanofiltration applications in industry are performed with polymeric membranes, we have selected commercially available polymer membranes for this study. We use flux and retention measurements as a function of the organic solvent proportion to investigate which effects occur and superimpose. Both, a common mixture of water-ethanol and a less researched but relevant solvent mixture of water-NMP is used. The discussion of the results is supported by the additional measurements of the zeta potential of the DuraMem300 membrane. The DuraMem membranes are also developed for OSN and their membrane charges are still unknown.

4.2 Background

Even though the nanofiltration of aqueous solutions is already being investigated in numerous studies and OSN is gaining in importance by increasing number of publications, the area in between is investigated rarely. Mertens et al. [Mert2018] names this area solvent tolerant nanofiltration (STNF). In their work, the retention of the dye Rose Bengal in various organic solvents and a DMF-water mixture is studied for self-produced PVDF membranes. High retentions of $99\,\%$ are obtained for the solvent mixture.

Postel and Wessling [Post2015] investigated salt retentions by nanofiltration in water-methanol mixtures. Silicone-based PDMS membranes for OSN and polyamide-based membranes for usage in aqueous solutions were used for the experiments. The decrease in salt dissociation explains higher retention in methanol-rich solutions. Also, they noted that the level of different salt retentions varies with the solvent mixtures.

In 2012, Marchetti, Butté, and Livingston [Marc2012] presented a phenomenological model for predicting solvent permeation using data from aqueous-organic solvent mixtures. In a follow-up study [Marc2013], significant negative retentions are determined depending on the composition of the solvent mixture water-ACN. Preferential solvation and affinities of the dissolved substances are used as explanations. In contrast to other investigations, Marchetti, Butté, and Livingston [Marc2013] and Marchetti, Butté, and Livingston [Marc2012] use ceramic membranes in their work.

Various binary solvent mixtures are also used in Geens et al. [Geen2005b]. The group performs the experiments with water, methanol, and ethanol. The membrane performance was explained by the polarities and viscosities of the solvents. Besides, it becomes clear that the retention and fluxes also depend on the properties of the membrane. Similarly, Hestekin, Smothers, and Bhattacharyya [Hest2001] assume that the increase in viscosity leads to a reduction in flux and, in addition, that the pores dewater as the proportion of organic solvents increases and therefore become narrower. Machado, Hasson, and Semiat [Mach1999] and Machado, Hasson, and Semiat [Mach2000] explain their obtained membrane behavior by changes

in viscosity and surface tension. Tsui and Cheryan [Tsui2004] report lower fluxes through the membranes and a minimum in flux corresponding to the change in viscosity through the addition of alcohol to the solvent. Furthermore, they stated that the molecular weight cut-off (MWCO) changes and that conditioning before the experiments do not lead to differences in the results for all membranes. The results concerning the MWCO confirmed the results of Yang, Livingston, and Dos Santos [Yang2001], which is also a challenge in the OSN. On the other hand, the conditioning results confirmed only to some extent the results of Shukla and Cheryan [Shuk2002], which used ultrafiltration membranes in water-ethanol mixtures.

Later Labanda, Sabaté, and Llorens [Laba2013] carried out measurements with up to 13 vol% ethanol. They emphasized that the results depend on the interaction between membrane, solvent and dissolved substances, as it is already postulated in the OSN by Stafie, Stamatialis, and Wessling [Staf2004] and Stamatialis et al. [Stam2006]. It becomes clear that in nanofiltration processes with aqueous-organic solution mixtures interactions between the components are of considerable importance.

Charge effects or electrostatic effects also need to be considered. Thus Zhao and Yuan [Zhao2006] explain that such effects are negligible in pure organic solvents, but their importance increases significantly as soon as the system contains water. A direct influence on membranes is described in Zhang, Xu, and Liu [Zhan2007] by measuring the streaming potential of porous charged membranes as a function of an organic-aqueous solution. The streaming potential of a membrane is directly proportional to the zeta potential. The zeta potential is the electrical potential that can be measured at the shear layer of a charged membrane surface if a liquid flows along it. This potential indicates the charge of a membrane. Zhang, Xu, and Liu [Zhan2007] reported a decrease of the streaming potential with increasing proportion of organic solvent. Zeta potential measurements with water-ethanol mixtures on commercially available nanofiltration membranes are shown in Pihlajamäki, Laakso, and Mänttäri [Pihl2012]. Their results clarify that changes in the zeta potential within organic-aqueous systems show distinct differences depending on the membrane material.

Related research can be found, for instance, in a study of Schwer and Kenndler [Schw1991]. They investigate the influence of organic solvents on electroosmotic velocity and zeta potential in fused-silica capillaries. Also in this study, the zeta potential decreases with increasing amount of organic solvent. The authors' explanation is the increase of organic solvents in the liquid near the surface layer and an influence on the adsorption of ions or charged molecules.

The comprehensive investigations of Zhukov [Zhuk2007] show zeta potential measurements of ceramic surfaces which are in contact with organic solvents. The results demonstrate that the surface is also charged in organic solvents. The interactions with the charged surface are determined by the type of solvent and are identified for alcohols as acid-base interactions. In addition to the solvent type, the solvation of the solutes/ions by the solvent and the concentrations influence the potentials. Lyklema [Lykl2013] provides a general overview of interactions in non-aqueous electrolyte solutions. Specific parameters and coefficients for the calculation of detailed models are currently only available to a minimal extent since knowledge about ions in such solutions is lacking. Parameter values from binary solvent mixtures are comparably easy to find, especially if water is one of the solvents. In 4.6, we show various relevant properties of the used solvent mixtures from literature.

Table 4.1: Membrane properties as provided by the suppliers.

Membrane	Type	Material		Max. pressure [bar]	Max. temp. [°C]	pH range [-]	MWCO [kg/kmol]
		Active layer	Support				
Filmtec™ NF270	TFC	PA	PSU/PE	41	45	2-11	200-300
Nadir® NP030	TFC	PES	PE/PP	40	95	0-14	500-600
DuraMem® 300	ISA	modified PI (P84®)		60	50	7	approx. 300*
DuraMem® 500	ISA	modified PI (P84®)		20	50	7	approx. 500*

TFC: thin film composite, ISA: integrally skinned asymmetric, PA: polyamide, PES: polyethersulfone, PSU: polysulfone, PE: polyethylene, PP: polypropylene, PI: polyimide

*Styrene oligomers dissolved in acetone. See [See 2007].

4.3 Materials and methods

Membranes

Four commercially available membranes were used in this study: the Filmtec™ NF270 membrane (The Dow Chemical Company) and the Nadir® NP030 membrane (Microdyn-Nadir GmbH) are thin film composite (TFC) membranes for water applications and the DuraMem® 300 (DM300) and 500 (DM500) membranes (Evonik Resource Efficiency GmbH) are integrally skinned asymmetric (ISA) membranes for usage in OSN. The OSN membranes are selected related to their performance in polar solvents. At least two membranes of the same kind are used per measurement. Important membrane properties are summarized in Table 4.1.

Solvents and solutes

Different mixtures of water and ethanol (Merck KGaA), as well as mixtures of water and N-Methyl-2-pyrrolidone (NMP) (Fisher Scientific GmbH, ACROS Organics™), are used in the measurements as solvents. The solutes, $CaCl_2$, LiCl and NaCl (Carl Roth GmbH + Co. KG), are diluted in water-ethanol to measure the salt retentions. LiCl is used as solute in water-NMP solvents. The solute (salt) concentration in the feed solution was $90\,\mathrm{mmol\,kg^{-1}}$. To investigate the influence of the solute concentration $5\,\mathrm{mmol\,kg^{-1}}$ $CaCl_2$ and NaCl are used as a variation of feed concentration.

Seven different polyethylene glycols (PEGs) ($200\,\mathrm{kg\,kmol^{-1}}$ to $2000\,\mathrm{kg\,kmol^{-1}}$, Sigma-Aldrich) are used as solutes in water-ethanol mixtures to observe the membrane characteristics for uncharged solutes using the DM500 membrane. The feed concentrations of each PEG was $1\,\mathrm{g\,L^{-1}}$. All PEGs are added simultaneously to the solvent solution. The purity of the solvents and solutes used is ACS grade. Table 4.2 and Table 4.3 list notable solvent and salt properties.

The membrane stability was investigated before starting the main experiments. These tests were necessary to be sure that the membranes are stable in the applied solvent solutions. Furthermore, the used membranes

Table 4.2: Solvent properties [Smal2012]; [Hans2007]; [Reic1994].

Solvent	Mw	Hansen Solubility Parameter				ϵ_r	Viscosity	Polarity	Elec. dipole moment
		δ_{tot}	δ_d	δ_p	δ_h				
	[kg/kmol]	[MPa$^{1/2}$]				[-]	[mPa s]	E_T^N [%]	[D]
Ethanol	46	26.52	15.8	8.8	19.4	22.4	1.19	65.4	1.7
NMP	99	22.96	18.0	12.3	7.2	32.5	1.80	35.5	4.1
Water	18	47.81	15.5	16.0	42.3	78.2	1.00	100	1.9

Table 4.3: Properties of the salts which are used for retention measurements [Pinh1996]; [Li2010]; [Bowe1997]; [Nigh1959]; [Li2014]; [Jass2002].

Salt	Mw	Solubility at 25 °C			Related ions			
		in water	in ethanol	in NMP	Stokes radius		Hydrated radius	
	[kg/kmol]	[g/L]			[nm]			
$CaCl_2$	111.0	740	162	61.7*	Ca^{2+}: 0.310	Cl^-: 0.121	Ca^{2+}: 0.412	Cl^-: 0.332
LiCl	42.5	832	197	57 .0	Li^+: 0.238		Li^+: 0.382	
NaCl	58.5	358	0.434	0.105	Na^+: 0.184		Na^+: 0.358	

* at 20 °C

consist of different polymer layers. The pretests reveal if different swelling behavior of the membrane materials can cause delamination of a single layer. Membrane degradation due to the solvent was not observed for all water-ethanol mixtures. Contrary, the NF270 and the NP030 membranes are only stable up to 50 wt% NMP in water-NMP solutions. DuraMem® membranes (in the used configuration T1) showed different swelling behavior of the active membrane layer and the carrier fleece in pure NMP. Therefore, the experiments with water-NMP mixtures are performed up to 87.5 wt% NMP.

Methods

A MetCell crossflow set-up (Evonik Resource Efficiency GmbH) with two membrane modules in series is used for flux and retention measurements. Each membrane module designed as round cell provides an active membrane area of 52.8 cm^2. The circulation pump conveys the feed solvent with ca. 60 L h^{-1}, the test system volume is 800 mL. Retentate and permeate are recycled. Nitrogen (grade 5.0) is applied to pressurize the system.

Depending on the applied membrane, three pressure levels are set. The maximum pressure values for the respective membrane can be found in Table 4.1. The temperature was kept constant at 25 °C. Fluxes are measured with a mass balance at steady state. Meanwhile, samples are taken to determine the retention.

Before usage of a new solvent composition, the set-up is exhaustively rinsed, and the membranes are pre-washed with the test solvent. The pre-washing procedure was carried out until minimum 5 mL cm^{-2} was collected, and the permeate liquid became colorless. This procedure is necessary to prepare the membrane for its usage, by removing the conditioning agent from the membrane surface. The pre-wash procedure is repeated for each solvent composition since the solubility of the conditioning agent is dependent on the solvent.

Concerning the experimental order, some experiments are conducted in a bidirectional manner and thereby rechecking the results. Next to single

salts, salt blends with 90 mmol kg^{-1} of each salt as solutes in water-ethanol mixtures are measured regarding flux and retention using the DM500 membrane. Further, experiments with PEGs as solutes are performed with the same kind of membrane. Sample composition of feed and permeate are measured to investigate the possibility of solvent separation. For this purpose, the refractive index of the feed solution and the permeate is determined with the refractometer DR301-95 (A.KRÜSS Optronic GmbH, Germany). If no difference between the two samples could be measured, no solvent separation appears.

Conductivity measurements were carried out for the solutions containing single salts as the solute. The salt concentration in the samples results from data of calibration curve measurements also considering differing solvent composition. Salt retentions were subsequently calculated by:

$$R_i = 1 - \frac{c_{i\,(Permeate)}}{c_{i\,(Feed)}}. \tag{4.1}$$

It is important to notice that the conductivity measurements are inappropriate to gain the retention values of salt blends in solutions. Therefore, cation exchange chromatography was used which is able to separate and quantify the different salt components. The samples are diluted in water with a dilution factor of 50:1 to avoid a possible damaging of the chromatography column by ethanol. The used system is an Agilent HPLC 1100 Series with a Metrosep C4 250x4 mm cation exchange column (Metrohm AG, Herisau, Switzerland) and a guard column.

The retention values of PEGs as solute are determined by gel permeation chromatography (GPC). Before analysis, the samples are evaporated at 55 °C and subsequently re-dissolved in pure water. Sodium azide (0.02 wt%) is added to align the composition of the eluent (pure water and sodium azide). The GPC device consists of two columns (Suprema, 30 Å pore size, 3 µm particles, 8.0x300 mm (ID x length), Polymer Standards Service GmbH, Mainz, Germany) and a refractive index (RI) detector. The analysis is carried out at 35 °C.

To identify the surface charge of the polyimide based DM300 membrane

the zeta potential is determined using an SurPASS Electrokinetic Analyzer (Anton PAAR GmbH, Graz, Austria) at 0.4 bar. Ahead of the measurement, the membrane is prewashed as described above. Following, the prewashed membranes are stored for minimum 24 h in the measurement solution. The measurement solution consists of 1 mmol L^{-1} KCl, wherein either KOH or HCl is titrated to obtain results from alkaline mixtures and acidic mixtures, respectively. The electric current (I) is measured four times. The Helmholtz-Smoluchowski equation was used to calculate the zeta potential ζ:

$$\zeta = \frac{dI}{dp}\frac{\eta}{\epsilon_r \cdot \epsilon_0}\frac{l}{A}. \tag{4.2}$$

In this equation η is the viscosity and ϵ_r the dielectric constant of the measuring solution. For *dp* the pressure (0.4 bar) and for ϵ_0 the vacuum permittivity is inserted. The membrane length is *l* and the cross-sectional area where the measurement solution flows through is *A*.

4.4 Results and discussion

Flux and retention measurements are performed to investigate the functional characteristics of the membranes in water-ethanol and water-NMP mixtures. By default, the experiments begin in ethanol with a subsequent increase of water proportion. However, several experiments are additionally conducted in reverse order (beginning in water with an increasing amount of ethanol). These experiments in a bidirectional manner show approximately equal results. For this reason, it is assumed that the order of solvent contact is not influencing the membrane performance in the experiments.

While the flux was determined by weighing the samples, the retention analysis required the quantification of the concentration. Except for flux and retention determination, samples were analyzed considering the refractive index. Only for water-NMP mixtures and water content up to 50 wt%, the refractive indices of permeate and feed samples deviated. Thus solvent separation for water-ethanol can be excluded but have to be taken into ac-

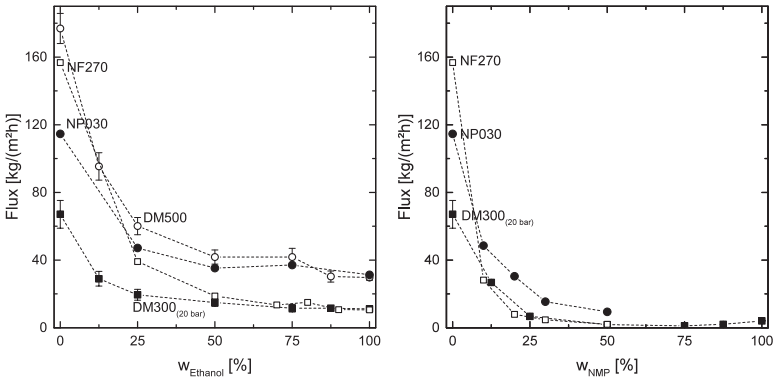

(a) Water-ethanol mixtures. **(b)** Water-NMP mixtures.

Figure 4.1: Solvent flux without solutes of four different membranes (□ NF270, ● NP030, ◯ DM500, ■ DM300) at 10 bar, exceptional for DM300 at 20 bar.

count for water-NMP. Using calibration curves of the refractive index the permeate composition can be determined. Salt retentions are calculated afterwards by interpolating in calibration curves of the conductivity versus the amount of NMP in solvent.

Hereinafter, results of solvent fluxes are discussed, followed by the results of salt and PEG retention. All measurements were performed at least twice considering the experimental effort. Therefore, the error bars in the diagrams show the measured maxima and minima. The results always show the same trend at the different pressure levels. Hence only one pressure level is shown in the figures. Effects caused by different pressure levels are mainly observed on the water-rich side of the solvent compositions. In general, it could be noticed for all membranes that the retention also increases with an increase in pressure. The fluxes through the membrane also increased as expected. Finally, zeta potential measurements of the DM300 are shown and discussed to discover the fixed charge of polyimide based membranes for OSN.

Solvent flux without solutes

Figure 4.1 presents the measured solvent flux without solutes as a function of the solvent composition for water-ethanol (Figure 4.1a) and water-NMP (Figure 4.1b). It is visible that the trend of the fluxes is similar for all membranes: Due to the addition of solvent the flux decreases. Figure 4.1a shows a pure water flux in the range of 70 to $180\,\mathrm{kg\,m^{-2}\,h^{-1}}$. The highest flux is found for the DM500 membrane followed by the NF270, NP030, and DM300. The DM300 was pressurized with 20 bar minimum because a flux through the membrane can only be detected when this pressure level is reached. The addition of ethanol leads to a reduction in flux, which is steep for small quantities of ethanol and decreases further with more ethanol, but less pronounced. The order of the membranes based on the flux (high to low) changed due to the addition of ethanol. In pure ethanol fluxes through DM500 and NP030 are similar as well as the fluxes through the NF270 and the DM300.

The observations from the experiments can be explained by interactions between membrane and solvents and interactions between the solvents themselves. The viscosity of the solvent mixture increases sharply up to $50\,\mathrm{wt\%}$ ethanol, which leads to a decrease in flux. In contrast to other studies ([Geen2005b]; [Tsui2004]), no increase in flux can be observed with high ethanol contents for any membrane. In these studies, this increase was explained by the decrease of the solvent mixture viscosity. We assume that in our case the viscosity effect on the flux is superimposed and compensated by effects with the membrane material. Further, the solvent properties of mixtures change concerning density and molar volume. While the density of the mixture continuously decreases, the molar volume increases [Khat2012] (cf. Figure 4.10a). Consequently, it supposedly becomes more difficult for the solvent to penetrate into the membrane.

Also, the polarity and the dielectric constant decrease, which can be deduced from [Schw1991]; [Peto2000]. The membranes for aqueous nanofiltration can be classified as polar or hydrophilic due to their primary field of application. The contact angle measurements of Qiao and Chung [Qiao2006] indicate a polar active layer for DuraMem® membranes. Therefore, it can

be assumed that the membranes permit fewer interactions in solvent mixtures than in water, resulting in lower affinity and flux.

Figure 4.1b presents the solvent flux without solutes for water, NMP and their mixtures. The pure water flux is comparable to the results measured during the water-ethanol experiments (Figure 4.1a). The presence of NMP in the solvent mixture results in a sharp decrease of the flux. The highest fluxes in the presence of NMP (up to $50\,\mathrm{wt}\%$) are obtained for the NP030 membrane, whereas the flux was close to zero for the DM300 and NF270 membrane. As stated before the NP030 and NF270 are not used for the whole range of solvent mixtures because of their limited chemical stability.

Similar to water-ethanol mixtures, the primary cause of flux reduction seems to be the viscosity. The viscosity rises significantly in water-NMP (about double as high as in water-ethanol) and has a maximum at approximately $70\,\mathrm{wt}\%$ NMP [MacD1971] (cf. Figure 4.11b). Since the measurements at higher NMP proportions were only possible with the DM300, it can be seen that the flux has a minimum and increases a few percents between 75 and $100\,\mathrm{wt}\%$ NMP. Nevertheless, the increase is marginal and we assume that higher increases are hindered by the reduction in solvent polarity. NMP is considerably less polar than ethanol, although the electric dipole moment is significantly higher than for ethanol or water (Table 4.2). The reason is that, contrary to water or ethanol, NMP is an aprotic solvent and is not able to form hydrogen bonds to the same extend as ethanol or water [Stri1997]. Therefore, the low fluxes of ca. $1.5\,\mathrm{kg\,m^{-2}\,h^{-1}}$ can be explained by the minor interactions of the NMP with the membrane. The polarity of the membrane material is dependent on the electric properties and on the properties of the solvent as a result of sorption of solvent molecules inside the polymeric matrix. Generally, the polymer polyethersulfone (PES) of the NP030 apply higher polarity than polyamide (PA) of the NF270 because of more mutual interactions in PA and a higher degree of solvent sorption in PES [Domi2012]. Therefore, higher fluxes also in less polar solvent mixtures could be the result. According to the results, similar properties to PA regarding polarity could be assumed for polyimide (PI) of the DuraMem® membranes. Nevertheless, the porosity of the membranes

also matters and, in this context, the NP030 has a higher porosity than the NF270 or DM300. The higher porosity is indicated by the molecular weight cut off (MWCO, Table 4.1) which marks the molecular weight at a retention value of 90 %. However, it should be noted that the measurement with pure NMP through the DM300 was only performed for the solvent flux measurement without solutes thereby the membrane remained stable. To avoid membrane stability issues, further experiments with water-NMP (salt retention) are performed up to 87.5 wt%.

Salt retention

Single salts in water-ethanol mixtures

Figure 4.2 presents the flux and retention measurements for four different membranes (NF270, NP030, DM500, DM300) in water-ethanol containing 90 mmol kg^{-1} salt as solute. Since the data of the set pressure levels show similar trends, only one pressure level is represented at a time. If the shown data refers to a pressure level that is not recommended for all membranes, representative data from a different pressure level are given for the respective membrane. The same method was applied if not enough results are obtained for a single measurement series because of failure during the experiment or sample analysis.

Figure 4.2a shows the measured flux, and Figure 4.2d shows the retention values for the tested membranes with LiCl as the solute in different solvent mixtures at 30 bar. The results of measurements with the DM500 membrane are depicted for the pressure level of 20 bar. Fluxes follow the same trend as solvent fluxes without solutes: The fluxes decrease exponentially with the increase of the ethanol content in the solvent. The influence of the salts on the viscosity is negligible at the used salt concentrations. This could be proven by random measurements of the viscosity. Strikingly, the measurement with the NP030 resulted in a flux plateau for the solvent mixtures with 25 to 75 wt% ethanol. The flux for the NF270 membrane decreases the most and is equal to the flux of the DM500 at 100 wt% ethanol. The DM300 membrane has the lowest flux in ethanol while the

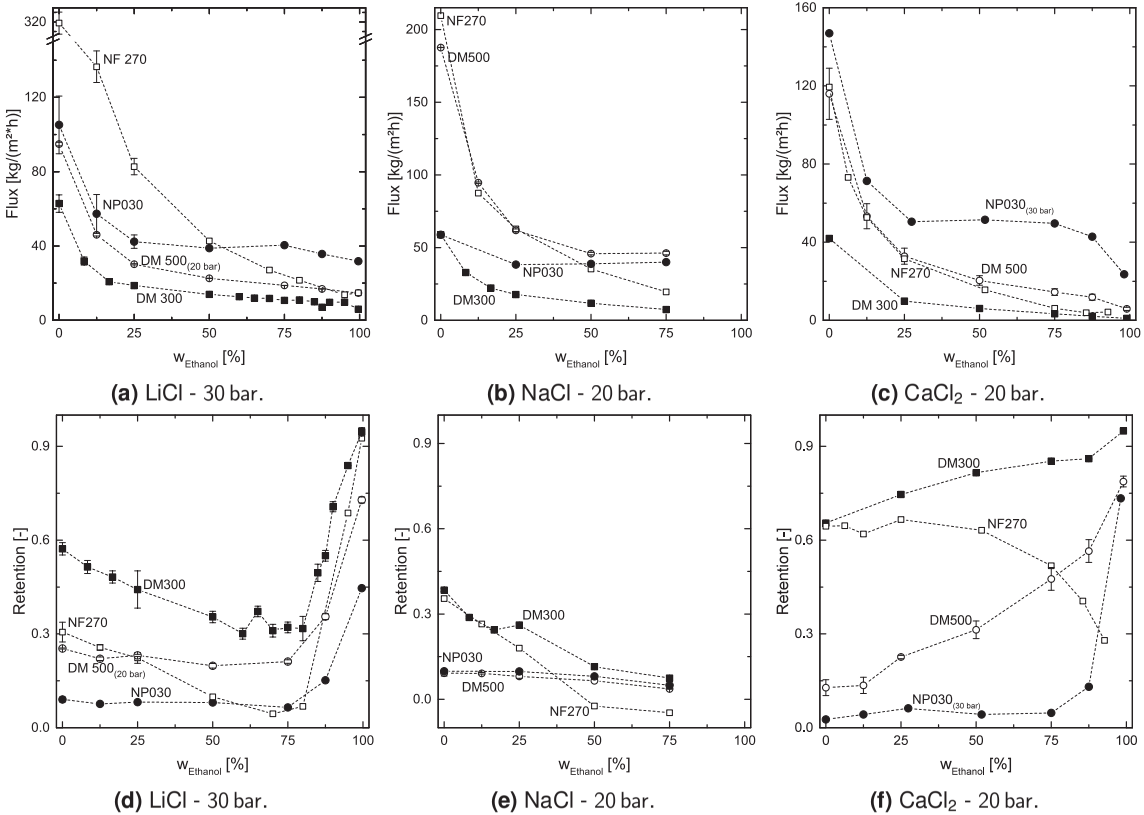

Figure 4.2: Flux (a,b,c) and retention (d,e,f) for four different membranes (□ NF270, ● NP030, ◯ DM500, ■ DM300) in water-ethanol containing 90 mmol kg^{-1} salt as solute.

NP030 has the highest.

LiCl is retained differently by the various membranes. The retention levels of DM500 and NP030 are in the water-rich solvents approximately constant and thus independent of the ethanol content in the solution. At the membranes DM300 and NF270 the retention decreases linearly with increasing ethanol concentration in the solvent. Between 60 and 80 wt% ethanol the retention has a local minimum, thereafter it increases strongly. In the same range of ethanol content, the retention of the DM500 and NP030 also increases sharply. All measured membranes show a maximum retention in ethanol.

Measurements with NaCl as solute with 90 mmol L^{-1} were only possible up to an ethanol content of 75 wt% due to the solubility in ethanol. The results of the measurements at 20 bar are shown in Figure 4.2b and 4.2e. The measurements result in similar diagrams as the results for LiCl as the solute. The fluxes decrease with increasing ethanol content of the solvent. Also for this salt, the fluxes through the NP030 are almost constant in the solvent mixtures. At 75 wt% ethanol, the fluxes through the NP030 and DM500 are in the same range ($\approx$ 40 kg m^{-2} h^{-1}), whereas the flux is halved through the NF270 and quartered through the DM300.

The NaCl retentions (Figure 4.2e) of the membranes NF270 and DM300 are towards 25 wt% ethanol very similar. The presence of more ethanol leads to further decrease in retention which is more pronounced for the NF270. On the contrary, the retentions of the NP030 and DM500 are comparable in all solvent mixtures and decline only slightly. The NaCl retentions at all membranes are below 10 % for solvents containing 75 wt% ethanol. Remarkably, the NF270 has slightly negative retentions from 50 wt% ethanol on.

Figure 4.2c and 4.2f show the flux and retention data from the tests with $CaCl_2$ as solute. Up to 25 wt% ethanol the fluxes decrease excessively, following the decline of the flux flattens. The flux through the NP030 is again, also for the third applied salt, stable in the range of 25 to 75 wt% ethanol. The value in ethanol for this membrane is around 24 kg m^{-2} h^{-1}, while the fluxes through the other membranes are below 6 kg m^{-2} h^{-1}.

Considering the retentions of $CaCl_2$, the differences to monovalent salts become evident. The DM300 retains more than $65\,\%$ $CaCl_2$ in water. The retention of this membrane increases continuously with increasing ethanol content and is over $90\,\%$ in ethanol. In contrast, the retentions of the membrane NF270 remain up to $50\,\mathrm{wt}\%$ ethanol constant at approximately $65\,\%$ and decline significantly below $30\,\%$ in ethanol-rich solutions. The retentions of DM500 rise with increasing ethanol concentration in the solvent in a similar way as of the DM300. However, the gradient is significantly higher, meaning the retention of marginally less than $15\,\%$ in water is increased to about $80\,\%$ in ethanol. In contrast to the other membranes, the $CaCl_2$ retentions of the NP030 are very similar to the LiCl retentions in dependence on the ethanol content in the solvent. Retentions on the water-rich side are low ($\approx 5\,\%$) and nearly constant. An ethanol content above $75\,\mathrm{wt}\%$ results in a sharp increase in retention to $75\,\%$ in ethanol.

Regarding the results, it becomes clear that individual effects alone cannot explain them. Instead, there is a superimposition of different effects that are dominant depending on the solvent composition or membrane material.

As for the fluxes, effects already discussed in the previous section remain effective. Besides, effects are triggered by the solutes, in these cases salts. The trend of fluxes remains the same compared to solvent flux measurements without solutes. The addition of salts generally slightly reduces the flux. Similar to the effect of pressure, this is more pronounced on the water side than on the ethanol side. A plausible explanation can be found in the osmotic pressure, which reduces the transmembrane pressure due to the salt and ethanol concentrations in the feed mixture. As expected from the degree of dissociation in combination with the van't Hoff factor [Moor2011], the effect is strongest for $CaCl_2$. The differences between the monovalent salts are minor in the respective pressure stage.

The retention values show the complexity of the interaction between the substantial effects. With the local minima between 60 and $80\,\mathrm{wt}\%$ ethanol, the retentions can be divided into the water-rich side and the ethanol-rich side. On the water-rich side, the Donnan effect affects the NF270 and DM300 membranes, resulting in higher $CaCl_2$ retention. With ethanol in

the solvent, the degree of dissociation of the salts and the Debye length of the ions decreases (Figure 4.8a and 4.9), weakening the electrostatic forces of the ions. However, the decrease in Debye length is small at salt concentrations of $90\,\mathrm{mmol\,kg^{-1}}$. The lower dissociation, on the other hand, leads to a reduction of the retention due to the lack of charge effects.

Simultaneously, ethanol slowly accumulates in the solvate shells of the ions. According to Marcus [Marc2007a] and Marcus [Marc2007b], there is always preferential solvation of water for Cl^- and Na^+, whereas this preference is continuously low for Na^+ up to $60\,\mathrm{wt\%}$ ($< 0.1\,\mathrm{mol\%}$). Li^+ ions are preferentially solvated by ethanol in this range. A statement on the preferential solvation of Ca^{2+} is currently not possible due to the available data in the literature. Though, also in this case, ethanol will certainly occur in the solvate casings. Ethanol enrichment in the solvate shells leads to a lower shielding of the electrostatic forces due to the lower permittivity [Schw1991]; [Peto2000]. This lower shielding leads to support of the Donnan effect and better transport of the monovalent ions through the membrane, increasing the distance between the retentions concerning the different salts.

Another effect that influences the retention is the disturbance of the water network formed by hydrogen bonds in the liquid caused by ethanol. According to Noskov, Lamoureux, and Roux [Nosk2005], this disturbance of the hydrogen bonds is maximal at approximately $63\,\mathrm{wt\%}$ ethanol. The effect increases the disorder in the liquid, the volume is reduced, which can be recognized from the excess volume [Grol1981], and we assume that the acid-base interactions with the membranes decrease. Such interactions determine the adsorption at the surface by the electron donor and electron acceptor principle [Fowk1978]. The resulting increase in mobility of the individual molecules inside the membrane could also lead to a reduction in retention. The decreasing retention of NaCl even reaches slightly negative values for the NF270. In other words, the salt permeates through the membrane faster than the solvent. This phenomenon may occur both in aqueous nanofiltration and in OSN. In OSN, the affinity between membrane and solvent or membrane and solute conduce as an explanation. Usually, the

differences of the Hansen solubility parameters are compared. However, these parameters are particularly difficult to determine for membranes.

Contrary, the NP030 and DM500 show relatively constant retention of LiCl, NaCl, and $CaCl_2$. This constancy could be attributed to the higher porosity and more open structure of the membranes, which seem to limit the surface effects already in the nanofiltration range. Besides, NP030 has higher swelling effects due to the material, which also results in more constant conditions inside the membrane using solvent mixtures [Domi2012].

On the ethanol side, the retention of LiCl increases strongly for all membranes and the retention of $CaCl_2$ for the DM300, DM500, and NP030. The reason for this could be the solvation, which more and more occurs by ethanol from 85 wt% ethanol onwards [Marc2007a]; [Marc2007b]. Furthermore, a network of ethanol molecules is increasingly built up in these solvent mixtures, which leads to a lower polarity of the liquid in the membranes [Nosk2005]. Correspondingly (due to the low shielding) the electrostatic interactions with the ions are stronger, and the retention increases. Besides, the membranes themselves have different swelling behavior in the different solvent compositions. It was already noted in '4.4 Solvent flux without solutes' that the membranes in ethanol swell less and are denser overall.

In contrast, the $CaCl_2$ retention in high ethanol concentrations decreases at the NF270 membrane. The interactions of PA with itself in water are already stronger than those of other membranes or with ions from the outside. Hypothetically, this effect is amplified by the less polar ethanol molecules in high concentration, and thus the Ca^{2+} can be retained less.

Single salts in water-NMP mixtures

NMP is a considerably harsher solvent than ethanol and can only be used to a limited extent due to the stability of the membrane materials. Figure 4.3 shows the flux and retention measurements when using LiCl as solute in water-NMP mixtures. The data of three membranes are presented, namely NF270, NP030 and DM300. All measurements confirm that the fluxes decrease exponentially in the presence of NMP (Figure 4.3a). The

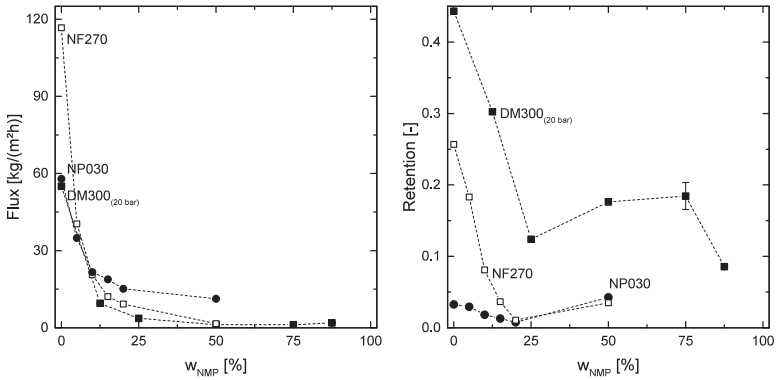

Figure 4.3: Flux (a) and retention (b) for three different membranes (□ NF270, ● NP030, both at 10 bar and ■ DM300 at 20 bar) in water-NMP containing 90 mmol kg^{-1} LiCl as solute.

decrease is extensive for the NF270 membrane and more gradually for the DM300 and NP030 membranes. The flux values from measurements with the DM300 are (except in water) roughly equivalent to the values from the measurement with the NF270. However, due to the chemical stability of the DM300, it is possible to measure with significantly higher NMP content in the solvent. Nevertheless, the low flux value (below 5 kg m^{-2} h^{-1}) remains constant at higher NMP content.

The retentions, presented in Figure 4.3b, decrease up to 25 wt% NMP in the solvent. The highest retentions are observed for the experiments with the DM300. In case the NMP proportion increases above 25 wt%, the retention increases. However, the measurement at 87.5 wt% NMP shows distinct lower retention. The experiments with water were subsequently repeated and thereby validated that the membrane is still intact. The two membranes NF270 and NP030 showed higher retentions when the NMP fraction is increased from 20 to 50 wt%. The retention at the membrane NP030 is for that solution slightly higher than in water. Rechecking the retention in water after the set of experiments verified membrane stability also in this case.

By comparing the fluxes with the solvent fluxes without solutes (Figure 4.1b), it is noticeable that as expected the values in water are lower with the salt as solute. The fluxes of the mixtures are approximately the same as those of the solvent mixtures without solutes. Up to $50\,\mathrm{wt}\%$ NMP fluxes decrease continuously. The gradient of the curves is striking high for low NMP concentrations in the solution. As already mentioned before, this results on the one hand from the sharp increase in viscosity [MacD1971] and on the other hand from the aprotic properties of the NMP, which allows only a few acid-base interactions with the membranes [Stri1997]. The slight flux increase in the NMP-rich solvents is probably due to the decrease in viscosity values which is not entirely compensated by the aprotic properties.

The LiCl retentions in water-NMP partly behave differently than in water-ethanol. Similar to ethanol, the addition of NMP to the solvent reduces the degree of dissociation (cf. Figure 4.8b) and thus the retention. The low retention in the water-NMP mixtures can also result from the aprotic polar property of the solvent.

Although the NMP can solvate the cations (here Li^+), it is not able to solvate the anions (Cl^-) [Stri1997]. Accordingly, the anions are entirely solvated by water and are shielded against the membrane. However, the solvate shells of the cations are increasingly occupied by NMP and less shielded (decreasing permittivity). Under the assumption that the membranes have a negative zeta potential for the used solutes, the cations can more easily penetrate into the membrane and permeate through it. It should be noted, however, that the membrane charge depends on the pH value of the surrounding solution, which in turn depends on the used salt and the amount of ethanol in the solvent. The assumption is supported by the knowledge of the pH values of our solutions (> 5.5) and the measurements of Niewersch et al. [Niew2008] for the NP030 as well as the measurements of Mänttäri, Pihlajamäki, and Nyström [Mänt2006] for the NF270. Since the zeta potential for the DuraMem® membranes was unknown, we measured it during this study. Beside the zeta potential, it is assumed that the easier penetration into the membrane is enhanced by

solvating the NMP molecules with water. An indication of such an effect is the negative excess volume [MacD1971], which also occurs in water-ethanol (cf. Figure 4.11b). This solvation competes with the solvation of the salt ions and disturbs the hydrogen bond network in the liquid.

The slight increase in retention above $50\,\mathrm{wt\%}$ can be explained by the further increases of NMP in solution which means that the remaining water cannot shield the Cl^- ions sufficiently. Therefore, the anions are retained slightly stronger by the permanent charge distribution of the membranes. After a further increase of the NMP content, the minimum of the excess volume (at approximately $78\,\mathrm{wt\%}$ NMP) is reached [MacD1971]. At higher NMP proportions in the solution, the solvation of the cations by the NMP molecules could have progressed so far (or the permittivity of the solution could have decreased so far) that the improved permeability of the cations would result in lower retention of the Cl^- ions.

Influence of the salt concentration

In addition to the measurements with $90\,\mathrm{mmol\,kg^{-1}}$ salt concentration, experiments with a lower concentration of $5\,\mathrm{mmol\,kg^{-1}}$ were conducted. These experiments were carried out with $CaCl_2$ and NaCl to determine the influence of the salt concentration on the flux and retention. At the lower concentration, both salts were soluble over the entire range of water-ethanol mixtures. Figure 4.4a shows the fluxes through the DM300 for two different salts and concentrations in water-ethanol mixtures at $20\,\mathrm{bar}$. Both the measurements with the high and the low salt concentrations show the typical trend of exponential flux reduction with increasing ethanol concentration in the solvent. In water, the fluxes for both salts are higher if the salt concentration is low. This behavior is obtained for the whole range of water-ethanol mixtures. It becomes apparent that the fluxes for the divalent $CaCl_2$ are in all cases lower than for the monovalent salt NaCl.

The retentions are shown in Figure 4.4b. NaCl is retained considerably higher with lower concentrations in the solutions. Comparable to the experiments with high salt concentration, the NaCl retention decreases up to

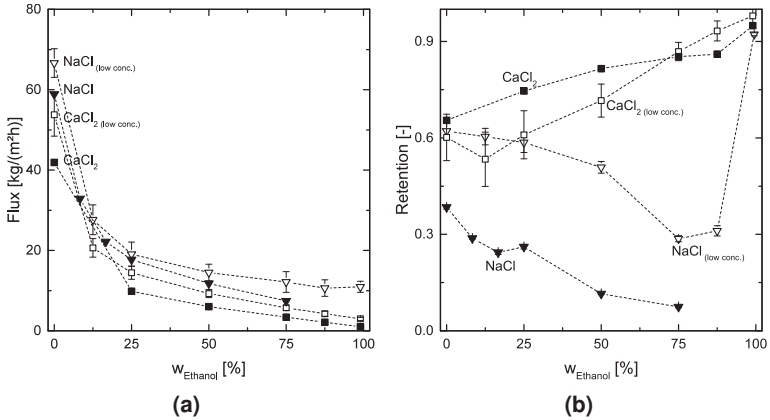

Figure 4.4: Flux (a) and retention (b) for the DM300 in water-ethanol containing 90 mmol kg^{-1} (closed symbols) and 5 mmol kg^{-1} (open symbols) $CaCl_2$ (■ / □) and NaCl (▼ / ▽) as solute at 20 bar.

4

an ethanol content of 75 wt%. Furthermore, the retention of solutions with higher organic solvent content (above 75 wt% ethanol) increases strongly resulting in a NaCl retention of over 90 % in ethanol. These retentions could not be measured with the high NaCl concentration due to the limited solubility. Though, they are similar to the retentions of LiCl. The retentions of $CaCl_2$ are closer together for both concentration levels than the values regarding NaCl. For both $CaCl_2$ concentrations, the retention increases with increasing ethanol fraction in the solvent. The curve slope appears higher for the lower salt concentration. The values measured in the water-rich solutions are lower for 5 mmol kg^{-1} whereas, in ethanol-rich solutions (above 50 wt% ethanol) the values from measurements with 90 mmol kg^{-1} are lower. In both cases, retention in ethanol exceeds 95 %.

The fluxes correspond to the expectations as the lower salt concentrations produce less osmotic pressure than the higher salt concentration [Meli2007]. Besides, similar effects that have already been described occur. Therefore, the curve shape of the different concentrations does not differ from each other. The lower concentrations lead to higher fluxes due to the lower osmotic pressures.

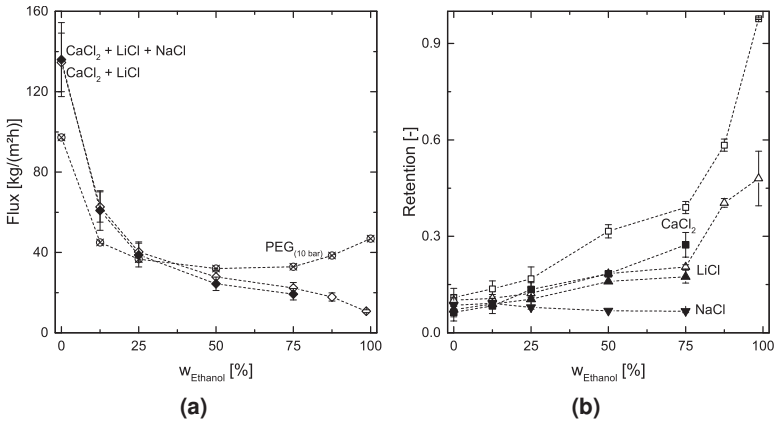

Figure 4.5: Flux (a) and retention (b) for the DM500 in water-ethanol containing salt mixtures consisting of $CaCl_2$ (■ / □), LiCl (▲ / △) and NaCl (▼) as solute at 10 bar. The mixture of all three salts (◆) are presented by closed symbols, whereas the mixture of $CaCl_2$ and LiCl (◇) are presented as open symbols. The flux graph (a) comprised also the measurements for the DM500 in water-ethanol containing PEGs (⊗).

NaCl retention at lower concentrations is expected to be higher than at high concentrations. The fact that the curve is similar to that of LiCl at high concentrations (Figure 4.2d) shows that the two monovalent salts react in the same way. Only the solubility of NaCl impeded the retention measurement with high concentrations in ethanol contents higher than 75 wt%.

The salts with divalent cations, on the other hand, are minor concentration dependent. Furthermore, the concentration effect is not apparent and also seems to depend on the solvent composition. For further statements other experiments with small bivalent cations are necessary.

Salt blends

Previously, only the fluxes and retentions of solutions with individual salts as solutes have been discussed. Experiments with more than one substance as solutes were also performed to investigate the influence of a multi-component solute on the flux and retention behavior of the membrane in water-ethanol mixtures. Figure 4.5 presents the results with salt blends

as solutes for the DM500 at 20 bar. Figure 4.5a also shows the flux measurements with the PEGs as solutes, which will be discussed later. The salt blend consisting of the salts $CaCl_2$ and LiCl were tested for the entire range of solvents mixtures, while the salt blend of $CaCl_2$, LiCl, and NaCl could only be studied up to an ethanol content of $75\,\mathrm{wt}\%$. Reason for this limitation is the solubility of NaCl in ethanol. The open symbols show the experimental results of the measurements with the 2-salts blend ($CaCl_2$ and LiCl), while the closed symbols show the results of the 3-salts blend ($CaCl_2$, LiCl and NaCl). As expected, the flux in these measurements follows the general trend by decreasing exponentially with an increase in the ethanol fraction. This is in line with the solvent flux without solutes and the flux measurements with single salts as solutes. The lowest flux value is accordingly measured at the highest ethanol content in the solution. Compared to the flux measurements with single salts, the values are similar to those obtained with $CaCl_2$. The increased osmotic pressure has a minor influence, in this case, caused by the more open structure or higher porosity of the membrane.

Retentions in Figure 4.5b are depicted for the individual salts from the salt blends. The analysis was performed with cation exchange chromatography, which is able to split the samples and evaluate the single salt concentration. Comparing to the results in Figure 4.2 few minor deviations can be observed. Similarly, the retention of $CaCl_2$ continually increases with the increase in ethanol concentration and reaches exceptional values on the ethanol-rich side (approx. $98\,\%$ in ethanol). In the 3-salts blend, the retentions of $CaCl_2$ and LiCl are lower overall compared to their retentions in the 2-salts-blend. This effect is due to higher total ion concentration and thus stronger charge screening (Debye length decreases). Hence, Donnan exclusion is weakened. The effect is more evident for $CaCl_2$ than for LiCl. In contrast to the single salt experiment, the retention of LiCl increases if the ethanol proportion in the solvent rises. This increase of up to $75\,\mathrm{wt}\%$ ethanol is only slightly but much more pronounced if the ethanol content continues to rise. The retentions of NaCl are also slightly different from those from the single-salt measurement. Here the retention decreases continuously and

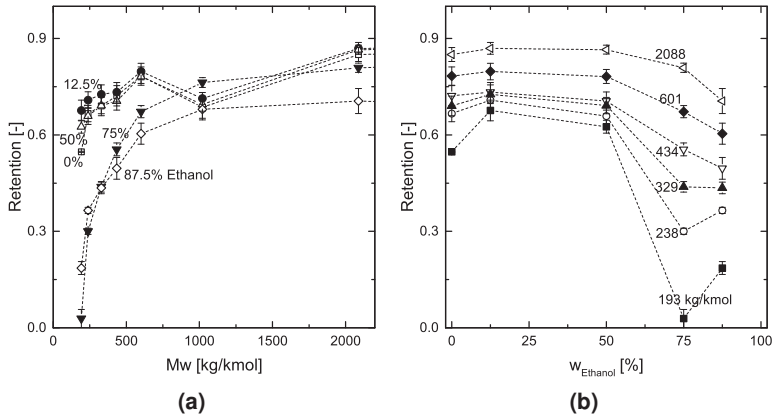

Figure 4.6: Retention dependent on the molecular weight (a) and the amount of ethanol in the solvent (b) for the DM500 in solutions containing seven different PEGs as solutes at 10 bar. The different symbols represent in graph (a) the solvent compilations and in graph (b) the molecular weights of the PEGs.

reaches a minimum value at 75 wt% ethanol in the solvent.

The lower retentions for the monovalent salts issue from the higher ion concentration and thus the Donnan effect [Meli2007]. Especially in ethanol, the LiCl retention is smaller than expected. The retention of $CaCl_2$, on the other hand, is slightly higher than in single salt measurement.

PEG retentions

Figure 4.5a shows the flux measurements by the usage of PEGs as solutes and Figure 4.6 the corresponding PEG retentions. The retentions are depicted as a function of the molecular weight (Figure 4.6a) and as a function of the ethanol fraction (Figure 4.6b). The measurements were carried out with the DM500 at 10 bar. PEGs in the range of 200 to 2000 kg kmol^{-1} with a feed concentration of 1 g mol^{-1} each were used.

The flux in water is almost 100 kg m^{-2} h (Figure 4.5a). The addition of 12.5 wt% ethanol causes a halving of the flux, which is further reduced to a minimum by adding ethanol at 50 wt%. In contrast to measurements with solvents without solutes or salts as solutes, a subsequent increase in

the ethanol content leads to a slight flux increase to about $45\,kg\,m^{-2}\,h$ with $100\,wt\%$ ethanol. Especially in water and on the water-rich side, the flux is significantly below the solvent fluxes without solutes. On the ethanol-rich side the difference is small, and in $100\,wt\%$ ethanol, the flux is slightly higher than for pure ethanol.

The lower fluxes on the water-rich side seem to have been amplified by concentration polarization effects [Meli2007]. This effect seems plausible since the PEGs were added in high concentrations ($1\,g\,L^{-1}$ each). The increase at 87.5 and $100\,wt\%$ ethanol in the solvent is indeed consistent with other measurements from the literature [Geen2005b]; [Tsui2004], yet the increase is low and does not permit a clear statement.

Figure 4.6a shows two main trends for retention, namely at ethanol concentrations lessor equal $50\,wt\%$ by weight and at higher ethanol concentrations. The measurements at $25\,wt\%$ and $100\,wt\%$ ethanol could not be adequately evaluated due to an error in sample preparation and are not presented here. The lower ethanol concentrations start at retention of approximately $60\,\%$ for $400\,kg\,kmol^{-1}$ and increase steadily to ca. $80\,\%$ at $2000\,kg\,kmol^{-1}$. The ethanol content (less or equal $50\,wt\%$) has only a minor influence on the retention values.

In contrast, significantly lower retentions are achieved for the lightweight PEGs at higher ethanol concentrations (e.g. $5\,\%$ at $75\,wt\%$ and $20\,\%$ at $87.5\,wt\%$ ethanol for the $400\,kg\,kmol^{-1}$ PEG). Retention increases strongly with the increase in molecular weight and is asymptotic for PEGs with high molecular weight. Retentions of maximum $80\,\%$ (at $75\,wt\%$ ethanol) and $70\,\%$ (at $87.5\,wt\%$ ethanol) are obtained.

Figure 4.6b shows once again the retentions of the PEGs, which are now shown versus the ethanol content of the water-ethanol mixture. In this context, it becomes clear that the retentions on the aqueous side remain almost constant and a local minimum for the retentions of the light PEGs is present at $75\,wt\%$ ethanol. For longer-chain PEGs, the retention decreases with a further increase in the ethanol proportion in the solvent. If the trend from the measurements with the salts as solutes is considered, it can be assumed that the retention for the light PEGs continues to increase and for

the heavy PEGs remains the same or only slightly decreases when ethanol is the solvent.

Similar to the salt retentions, it is possible to distinguish between a water-rich side and an ethanol-rich side. The reason that MWCO at 90 % retention is not achieved is probably concentration polarisation, which shifts the PEG retentions to lower values overall. The more or less constant retention values of the individual PEGs in different solutions with up to 50 wt% ethanol are significantly higher than those of the salts in the same solutions. However, it should be noted that the PEGs are also considerably larger than the salt ions and steric effects must be taken into account.

The extreme reduction in retention for small PEGs at 75 wt% ethanol is certainly astonishing. Similarly, the comparatively low values (even for large PEGs) surprises for solutions with an ethanol content of 87.5 wt%. As already mentioned, the most severe disturbance of the water network is at approximately 63 wt% ethanol [Nosk2005]. We assume that due to the disturbance, and thus the lack of interaction between the solvent and membrane, the PEGs themselves can interact more with the membranes (or adsorb on membrane material) and thus permeate better through them. Electrostatic effects of the membranes do not influence because of the electrical neutrality of the PEGs. At higher ethanol proportions in the solvent, a higher degree of order is restored in the liquid, and the ethanol network enlarges. However, the ethanol network can interact less with the membrane than a water network, so that there are more possibilities for the PEGs to interact and the retention is correspondingly lower.

Zeta potential

By measuring the zeta potential, conclusions can be drawn about the membrane charge. Since reliable information on the zeta potentials in water of the membranes NP030 and NF270 can be found in the literature [Niew2008]; [Mänt2006], only the zeta potential of the DM300 was determined for this work. For the DM500 we assume a similar zeta potential because the membranes are made of the same material and differ mainly

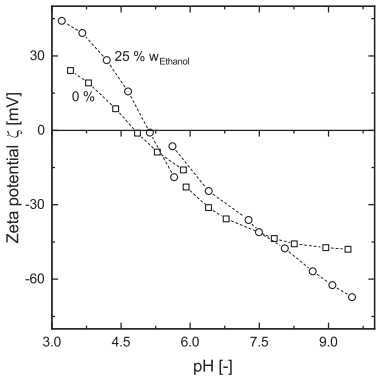

Figure 4.7: Zeta potential in water □ and in a solvent mixture with 25 wt% ethanol ◯ dependent of the pH value for the DM300.

in the degree of crosslinking. Figure 4.7 shows the results of the zeta potential measurements with the DM300 in water and a solvent mixture with 25 wt% ethanol. The measured zeta potentials show for the first time the charge of the DM300, representing polyimide membranes for applications in OSN. The potentials are plotted as a function of the pH value. Higher ethanol contents in the solvent could either not be realized due to the membrane fixation in the measuring device or did not provide reliable data. The discontinuity in the two curves shows the pH value of the measurement solution and marks the change from titration with HCl to KOH. In the acidic pH range, the membrane has a positive zeta potential of up to 25 mV in water and up to 45 mV in the mixture at a pH value of 3.5. With increasing pH value, the zeta potential decreases rapidly resulting in a negative zeta potential in the neutral and basic range. At a pH of 9.5, a zeta potential of −47.5 mV in water and −70 mV in the solvent with 25 wt% ethanol is measured. The isoelectric point, where the zeta potential is zero and the membrane is electrically neutral in the statistical mean, was measured in water at a pH of 4.8 and after the addition of ethanol at 5.1.

The pH values of the sample solutions from the salt retention experiments were always in the range of the negative zeta potential. The pH values of the solutions from the experiments with the monovalent salts as

solutes are between 5.5 and 6.5. The pH values for the solutions with $CaCl_2$ are at all times higher than the solutions with monovalent salts.

In the measured solutions negative charges of the membrane influence the fluxes and retentions with electrostatic effects. This result corresponds to our assumptions from the measurements with salts as solutes.

Although the addition of 25 wt% ethanol has only a minor effect on the zeta potential, we suppose that the effects may be more significant at higher ethanol contents. This hypothesis originates from Pihlajamäki, Laakso, and Mänttäri [Pihl2012], where a significantly flatter curve results in a solution with 70 % ethanol for a NF200 membrane. For strong statements on the corresponding effects on fluxes and retentions, as we have shown above, further zeta potential measurements in different solvent mixtures have to be carried out.

4.5 Conclusion

In this work, we report several STNF test results for the membranes NF270, NP030, DuraMem® 300 and 500 from measurements in water-ethanol and water-NMP mixtures. The experiments were performed with polymer membranes with different properties. Three salts ($CaCl_2$, LiCl, and NaCl) and PEGs were selected as solutes. The salts were used individually and in combinations and with two different concentration levels.

The measurements show different behavior in the solvent mixtures, which is caused by superimposed effects. The dominant effects depend on the respective solvent composition.

While in aqueous solutions the viscosity of the solvent mixture has a considerable influence on the flux, it is superimposed by polarity effects with increasing organic content in the solvent. Low fluxes imply that the membranes allow highly polar solvents to permeate better. This behavior also applies to the DuraMem membranes developed for utilization in OSN. A flux decrease due to osmotic pressures after the addition of salts could also be observed.

The retention properties of the different membranes are influenced by

further overlaying effects. In addition to known factors such as porosity, membrane cross-linking or Donnan effects, less investigated effects are visualized. These include the preferential solvation of ions and the disturbance of the hydrogen bonds in the liquid network by the organic components in the solvent mixture. The latter is reflected in the excess volume. The effects affect acid-base interactions as well as polarity and electrostatic effects. Swelling effects could also be recognized as an approach to explanation.

The superimposition of the effects can be seen even with uncharged solutes, and it becomes apparent that in solvent mixtures with an ethanol content of between 60 and 80 wt% the dominance of the substantial effects changes. However, the effects are minor for larger solutes than for smaller ones.

Since no data were available on the membrane charge of the DuraMem membranes, the zeta potential was measured for these membranes and it could proved that the polyimide-based membranes are charged. The addition of up to 25 wt% ethanol had little effect on the zeta potential, but we expect the effects to be significant at high ethanol proportions. Corresponding measurements and others, in particular concerning swelling effects, are of particular interest for the evaluation and investigation of aqueous organic mixing systems in the future. For instance, swelling effects of the membranes could indicate cononsolvency of the polymers with the solvent mixtures.

4.6 Appendix

Degree of dissociation of salts

The degree of dissociation of salts depends on the solution in which they are dissolved. The calculation of the degree of dissociation was carried out according to the method of Fu and Prieve [Fu2007], which was already used by Postel and Wessling [Post2015] to calculate dissociation degrees of methanol-water mixtures. For this purpose, calibration data are first de-

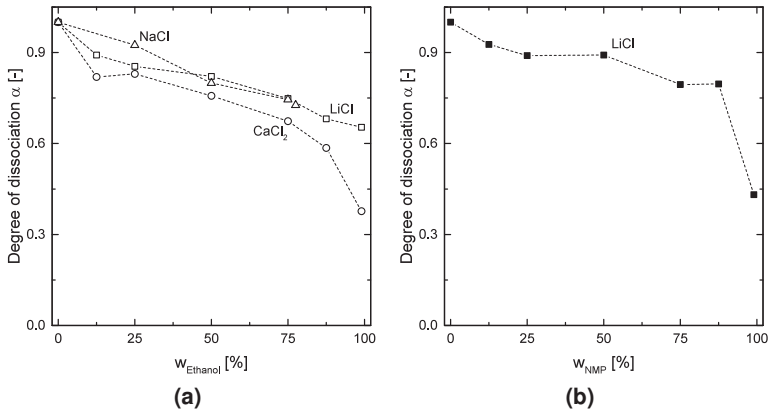

Figure 4.8: Degree of dissociation for $CaCl_2$ ◯, LiCl □, and NaCl △ in water-ethanol mixtures (a) and for LiCl ■ in water-NMP mixtures (b).

termined experimentally concerning conductivity L as a function of molar concentration c. Conductivity L is then plotted against c/L, and the conductivity in infinite dilution Λ_0 and the dissociation constant K are determined by equation 4.3. The degree of dissociation α is then calculated with equation 4.4 (Λ is the specific conductivity). In $100\,\mathrm{wt}\%$ water complete dissociation is assumed.

$$L = K\Lambda^2{}_0\frac{c}{L} - K\Lambda_0 \tag{4.3}$$

$$\alpha = \frac{\Lambda}{\Lambda_0} = \frac{L}{c\Lambda_0} \tag{4.4}$$

The graphs in Figure 4.8 show the calculated degree of dissociation for the salts $CaCl_2$, LiCl and NaCl in water-ethanol mixtures and for LiCl in water-NMP mixtures with a concentration of $90\,\mathrm{mmol\,kg^{-1}}$. The degree of dissociation decreases with increasing ethanol or NMP content in the solvent. The decrease in the mixtures is gradual. In solutions with high ethanol content ($>= 75\,\mathrm{wt}\%$) the decrease of the degree of dissociation for $CaCl_2$ is stronger and reaches approx. $40\,\%$ in ethanol. For monovalent salts, the

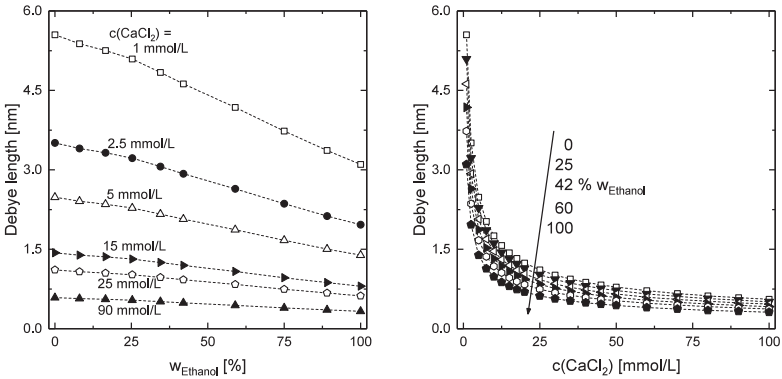

Figure 4.9: Debye length as a function of ethanol proportion in the solvent (a) and $CaCl_2$ concentration (b) at T = 25 °C.

value is significantly higher at approx. 65 %. In the mixtures of water-NMP, the decrease of dissociation for LiCl is lower compared to the mixtures of water-ethanol. However, the value drops sharply (to approx. 45 %) as soon as the solvent is 100 wt% NMP.

Debye length

The Debye length was calculated using the same method as applied in Marchetti, Butté, and Livingston [Marc2013]. Based on the Poisson-Boltzmann theory, the Debye length δ_D for electrolyte solutions is estimated using the following equation:

$$\delta_D = \left(\frac{\epsilon_r \cdot \epsilon_0 \cdot k_B \cdot T}{2 \cdot N_A \cdot e^2 \cdot I} \right)^{0.5} \tag{4.5}$$

Here ϵ_r is the permittivity, ϵ_0 the vacuum permittivity, k_B the Boltzmann constant and T the temperature. N_A is the Avogadro number, e the elementary charge and I the ionic strength of the electrolyte.

Figure 4.9 shows the calculated Debye lengths for $CaCl_2$ in different water-ethanol solutions and with different concentrations exemplarily. If the

Debye lengths are calculated for monovalent salts such as LiCl or NaCl, similar curves can be plotted. However, due to the lower ionic strength, the Debye length is longer, especially at low salt concentrations. Figure 4.9a clearly shows that the Debye length decreases linearly when the ethanol content in the solution increases. The salt concentration mainly determines the slope. If the salt concentration is high, the slope is higher than for low salt concentration. Figure 4.9b shows the dependence of the Debye length on the salt concentration. Here it becomes evident that the Debye length decreases exponentially by increasing the salt concentration.

Properties of water-ethanol mixtures

The data availability for water-ethanol mixtures is comparatively good compared to other binary mixtures. Khattab et al. [Khat2012] have measured several parameters for these mixtures, which also correspond well with other data from the literature. Figure 4.10 shows the graphs for density, surface tension, molar volume, molar excess volume and viscosity at 25 °C adapted from data of [Khat2012]. Also, the viscosity by Tsui and Cheryan [Tsui2004] at 22 °C is presented to get an impression of the temperature dependence of the viscosity. As the values from the publications are often given on other scales for the ethanol content (vol% or mol%), the scale for our graphs was adjusted suitably to wt%.

The surface tension decreases sharply on the water-rich side and continues to decrease moderately on the ethanol-rich side. The density and the molar volume behave differently. While the density decreases with increasing ethanol content, the molar volume increases. For both curves, the gradient on the ethanol rich side becomes larger. The molar excess volume is in the negative range and has a local minimum at about 63 wt% ethanol. If the ethanol content is further increased, the excess volume is raised rapidly. In contrast, the viscosity has a local maximum that can be measured with smaller ethanol contents. If the temperature is lowered, the viscosity increases and the maximum shifts to the water-rich side.

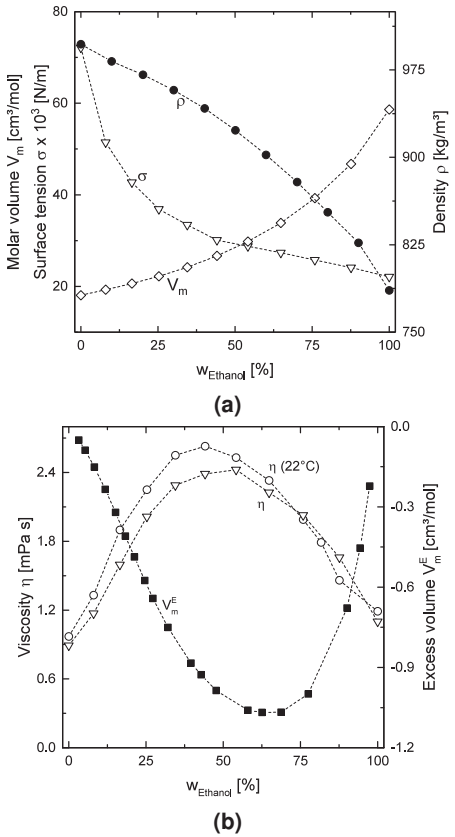

Figure 4.10: Molar volume, surface tension and density for water-ethanol mixtures (a) at 25 °C adapted from [Khat2012], viscosity and molar excess volume for water-ethanol mixtures (b) at 25 °C adapted from [Khat2012] and viscosity at 22 °C adapted from [Tsui2004].

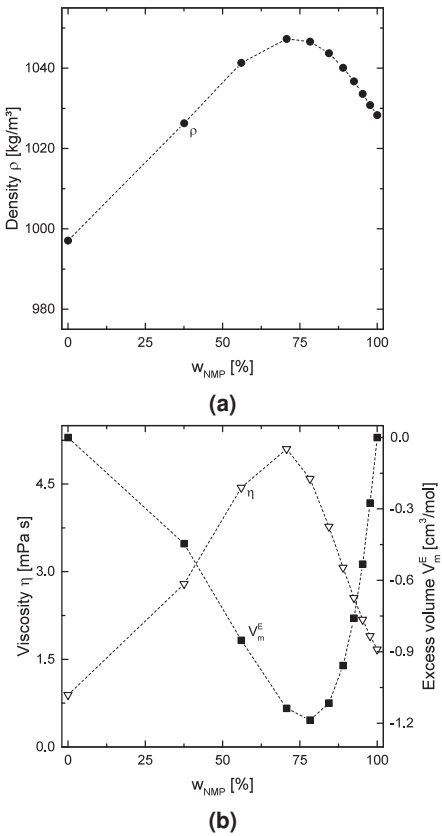

Figure 4.11: Density, viscosity and molar excess volume for water-NMP mixtures at 25 °C adapted from MacDonald et al. [MacD1971].

Properties of water-NMP mixtures

MacDonald et al. [MacD1971] measured the density, viscosity and excess volume for water-NMP at 25 °C. These data also coincide with other data from the literature, while considerably fewer data exist for these mixtures than for water-ethanol mixtures. Figure 4.11 shows the data from MacDonald et al. [MacD1971], with adjusted NMP content scale.

The density in the mixture shows a local maximum of approximately 65 wt% NMP. However, it should be noted that the resolution of the graph is very high and the density of water, NMP, and the mixtures are only slightly different in absolute terms. The situation is different for viscosity and excess volume. The viscosity increases significantly with the increase of NMP in the mixture and reaches a maximum that is about double that of water-ethanol. The maximum viscosity is around 70 wt% NMP. The excess volume of this mixture is also in the negative range and reaches a minimum at approximately 80 wt% NMP. The excess volume at this minimum is lower than that of water-ethanol and increases very strongly at higher NMP contents.

5 LbL membranes on ceramic supports applied in water-alcohol mixtures

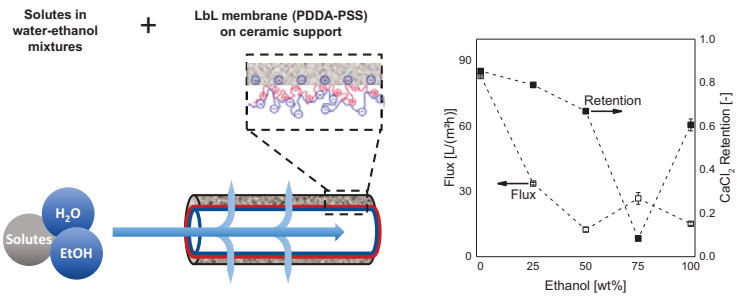

Tailor-made coatings on ceramic support membranes are used in solvent tolerant nanofiltration and achieve reasonable fluxes and salt ion retentions.

5.1 Introduction

Sustainability is currently an essential factor to plan new production plants and optimizing existing ones. This also includes the need to separate even trace substances from product or purification streams. Such compounds could be separated effectively with nanofiltration. This membrane process is widespread in water application and becomes more and more important in organic solvent permeation. Among these applications, another largely unexplored kind exists, where trace substances are required to be rejected from aqueous organic solvent mixtures.

Most of the membranes used in mentioned nanofiltration processes are polymeric membranes. Utilization of ceramic membranes could be advantageous because of their chemical stability and high fluxes through the membrane. The production of ceramic nanofiltration membranes is complex. Consequently, commercial ceramic nanofiltration membranes are hardly available especially for use in organic solvent nanofiltration (OSN). Therefore, we investigate the utilization of ceramic supports with Layer-by-Layer (LbL) membranes as a separation layer. These membranes with tailor-made polyelectrolyte multilayers are regenerative and backwashable. They are produced by coating commercially available ceramic membranes which is much more comfortable and flexible. We recently demonstrated the coating procedures and the performance of such membranes for aqueous nanofiltration [Menn2016b].

In this study, we conduct a broad range of experiments to characterize these membranes in the particular field of water-ethanol mixtures. The results lead to conclusions on the behavior and suitability of the membranes under different process conditions and with several solvent-solute systems.

5.2 Background

Applications and effects of nanofiltration

Membrane performances for nanofiltration in water processes are widely characterized with salt retentions regarding ion selectivity and retentions of uncharged organic compounds to determine the molecular weight cut off (MWCO, in most cases the molecular weight for which retention value is 90 %). Ion selectivity of the membranes is commonly explained by the Donnan exclusion mechanism, dielectric exclusion and differences in diffusion coefficients or molecular dimensions due to hydrated ions [Geis2014]; [Peet1998]; [Bous2006]; [Yaro2000].

In contrast to water applications, the membrane performance in organic solvent is strongly dependent on the interactions between solvent, solute and membrane [Staf2004]; [Stam2006]. Therefore, characterization methods of water applications cannot be transferred easily for OSN processes. It was found that MWCO values are dependent on every single solvent as well as on the solutes. According to the affinities of solvent and solutes to the membrane significant negative retentions occur [Post2013]. Furthermore, a large number of necessary compound data and membrane data are unknown as basis for reliable mathematical models. Nevertheless, the interest and knowledge on OSN processes is still growing since adequate solvent resistance membranes are available. The approaches to characterize solvent resistant membranes deal with different compound systems [Marc2014].

Studies for nanofiltration in aqueous organic mixtures are rare. The transfer of model conceptions to such solvent systems are complicated and limited. Next to charge and steric effects, also interactions known from OSN and solvent mixtures have to be taken into account (e.g. solute/solvent affinity to the membrane, polarity, viscosity). However, Postel and Wessling [Post2015] investigated salt retentions in mixtures of water-methanol for polydimethylsiloxane (PDMS) membranes and compared the results to those with an hydrophilic polyamid based membrane. The retention values vary between 10 % and 80 % depending on the composition of

the water-methanol mixture. Differences between the water rich and the methanol rich mixtures are explained by changes in dissociation of the solutes and the membrane material.

Geens et al. [Geen2005b] used different mixtures of water-methanol, methanol-ethanol and ethanol-water. They showed that interactions with the membrane surface and polarity become significant due to the narrow pores of the membranes. Furthermore, Labanda, Sabaté, and Llorens [Laba2013] studied nanofiltration as well as reverse osmosis retentions and fluxes of alcohol-water mixtures (max. $13\,\mathrm{vol}\%$ alcohol) with organic solutes. They concluded that membrane properties change due to the addition of alcohol to the solvent resulting in swelling and a decrease of polarity and dielectric constant. Tsui and Cheryan [Tsui2004] found a significant decrease of the flux for low ethanol concentrations and a slight increase in flux for high ethanol concentrations when measuring water-ethanol mixtures. This observations are explained by a local maximum of the viscosity of the solvent mixture. Next to the influence of the viscosity, Hestekin, Smothers, and Bhattacharyya [Hest2001] assume a dewatering of the membrane pores which become more narrow by increasing the amount of organic liquids in the solvent mixtures.

Ceramic nanofiltration membranes were tested in organic water mixtures by Marchetti, Butté, and Livingston [Marc2013]. In their study, main objectives were the solvent-solute competition related to the affinity to the membrane in combination with an understanding about the interplay of electrostatic and molecular affinity effects. They give a comprehensive literature review on several possible effects and found preferential solvation as important effect which changes depending on the composition of the solvent mixture. Negative retentions as in OSN were measured in some mixtures of water and organic solvents as well.

LbL membranes in applications with organic solvents

Tailor-made membranes assembled with Layer-by-Layer techniques are in many cases a promising alternative to conventional membrane materials

since properties can be adjusted to the requirements of the specific processes. For instance, polyelectrolytes could adsorb and form layers on high porous supporting materials with different properties than the support (or otherwise available membranes). The thickness of such single layer is a few nanometers. According to the choice of polyelectrolyte solution, the adsorption time and the coating method, it is possible to vary the performance properties as for example the selectivity of ions. Variables of the polyelectrolyte solution are, for example, the pH-value, ionic strength, molecular weight and concentration of the polyelectrolytes [Harr2000]; [Mala2005]; [Jose2014]; [Baow2012].

LbL membranes (not only consisting of polyelectrolytes) are widely useable for water applications. The applications include separation of trace substances [Kras2000]; [Jin2003]; [Raja2014], reduction of membrane fouling [Ba2010] or functional tasks by interlace of catalysts or reactants inside the layer [Ouya2010]. Furthermore, LbL membranes exist which are stable under harsh conditions, such as the presence of sodium hypochlorite (NaOCl) [Cho2015]; [Groo2015a] and in solutions with high or low pH-values [Menn2016b].

The utilization of LbL membranes in organic solvents is, in contrast to water applications, only little known. Li et al. [Li2008] investigated Polydiallyldimethylammonium chloride (PDADMAC) and sulfonated poly(ether ether ketone) sPEEK layers on polymeric support membranes in different solvents (even aprotic solvents) and their stability was reported. The retention values of charged molecules seemed to be influenced mainly by the charge of the membrane surface. The charge of the final layer account most relevant for selectivity. Further Ahmadiannamini et al. [Ahma2012b] found that PDADMAC and Poly(acrylic acid) (PAA) layers are stable in different organic solvents, among these tetrahydrofuran as most aggressive one. The manufacturing properties, such as pH-value and usage of salts as additives affected the retention and fluxes of solvents with dyes as solutes. Coating parameters were further investigated by Ilyas et al. [Ilya2016] with the polyelectrolyte combination Poly(allylamine hydrochloride) (PAH) and PAA. The variety of permeability was explained by the interaction of solvent

and membrane and the physico-chemical properties of the solvents. Ahmadiannamini et al. [Ahma2012a] investigated the combination of PDADMAC with both poly(sodium 4-styrene sulfonate) (PSS) and polyvinyl siloxane (PVS). The layers were stable in all used solvents. A fewer swelling in organic solvents and a dependency of the permeability by the ionic crosslinking density were concluded from the results. The related measurements were continued by Joseph et al. [Jose2015]. For PAA and polyethylenimine (PEI) layers, Tylkowski et al. [Tylk2013] observed increasing swelling in organic solvents with increasing layer number. The swelling of polyelectrolytes in water and in ethanol were also discussed by Miller and Bruening [Mill2005]. They found that swelling of the combination PDADMAC/PSS in ethanol is less pronounced than in pure water.

The performance of the LbL membranes used in this study was recently presented by Menne et al. [Menn2016b] for water applications. Menne et al. [Menn2016b] and Menne et al. [Menn2016a] produced the membranes in a newly introduced dynamic coating procedure. This work aims at studying comprehensively LbL membranes coated on ceramic supports in water-alcohol mixtures. In contrast to previous studies on LbL membranes coated on polymer supports and tested in organic solvents, we can identify exclusively the interactions of the organic solvents and solutes with the polyelectrolyte layers. Correspondingly, the ceramic supports are assumed to be chemically inert. To the best of our knowledge, we present for the first time LbL membranes tested in water-organic mixtures.

5.3 Membrane preparation

LbL membrane materials

Polyelectrolytes are grouped in strong and weak polyelectrolytes whether they are charged permanently or in dependence of the pH-value of the contacted solution [Sean2012]. Strong polyelectrolytes are selected concerning their low pH dependency on charge. Polydiallyldimethylammonium chloride (PDADMAC) with a molecular weight of 400 to 500 kDa is used as

poly-cation and poly(sodium 4-styrene sulfonate) (PSS) with a molecular weight of 1000 kDa as poly-anion. Both polyelectrolytes were obtained from Sigma-Aldrich. Membrane monoliths produced by Metawater (Japan) are provided by RWB Water Services B.V. (The Netherlands) as support material for the LbL layers. These ceramic monoliths consist of alumina with a nominal pore size of 100 nm and 55 channels. The length of the monoliths is 9.25 cm and each channel measures 2.5 mm in diameter resulting in a membrane surface of .04 m^2. Additional cross-linking agents are not used since no suitable agents were known for a PDADMAC/PSS combination. Also, stable layers and no stronger effects than the electrostatic interactions between the polyelectrolyte layer and membrane support are expected.

Coating procedure

The coating solutions consist of 1 g L^{-1} polyelectrolyte and 0.1 mol L^{-1} sodium chloride dissolved in pure water. Sodium chloride as additive ensures an even distribution of the polyelectrolytes on the support. The sodium chloride concentration is chosen on a low level to get a high degree of intrinsic charge compensation and ionic crosslinking between the polyelectrolyte charges. Consequently, the layers had denser pores and were thinner than for a high degree of extrinsic charge compensation [Groo2015b].

The surface modification of the ceramic support is performed in a dynamic coating procedure. Figure 5.1 shows a schematic representation of the dynamic coating procedure. On this occasion, a constant transmembrane flux of polyelectrolyte solution flew through the membrane at 30 L m^{-2} h^{-1} and after each coating step, the membrane was rinsed with water. Besides, pure water permeability was monitored between every layer. First, the poly-cation is applied to the membrane surface and adsorbs partly on top and partly inside the pores. Next, the poly-anion is applied to the first layer. By repeating these steps, several layers form a dense coating on the support. The so called bi-layer consists of a pair of positive and negative polyelectrolyte layers. The detailed coating procedure is described by Menne et al. [Menn2016a] and Menne et al. [Menn2016b].

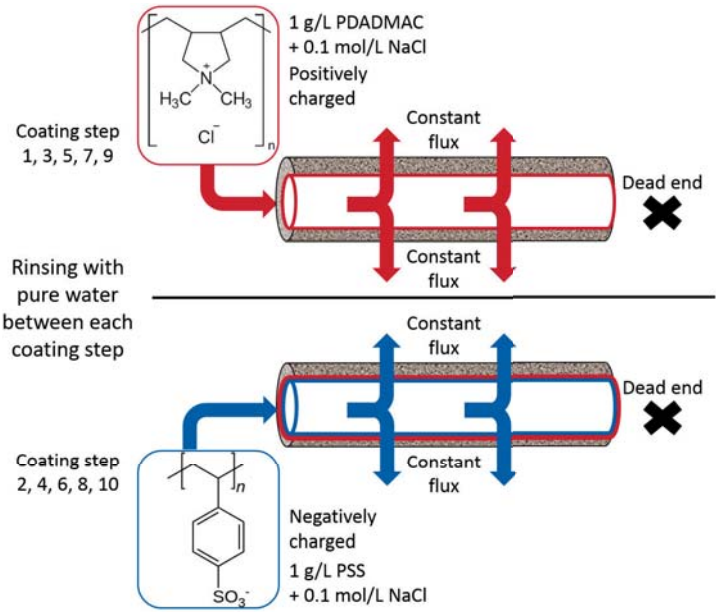

Figure 5.1: Schematic illustration of the dynamic coating procedure.

In order to determine the most promising amount of bi-layers for further experiments, membranes with 3, 5 and 10 bi-layers are pretested. The pretests include salt retention and flux measurements. Membranes with 5 bi-layers had higher retentions than membranes with 3 bi-layers. However, no consequently higher retention values are obtained with 10 bi-layers. With 5 bi-layers a complete pore coverage of the support is achieved. The obtained fluxes were all in the same range. Though, for membranes with 5 or 10 bi-layers the fluxes showed a better reproducibility. On account of these results and the faster coating procedure of 5 bi-layers, all further experiments are performed with 5 bi-layers coated on the ceramic support.

LbL Layer stability in organic solvents

Referring to stability, Ahmadiannamini et al. [Ahma2012a] showed that polyelectrolyte layers are permanently stable in different harsh solvents on poly-

meric membrane supports. The linkage of the adsorbed polyelectrolytes is based on ionic cross-linking and therefore electrostatic attraction and charge compensation are predominant [Jose2014]; [Mala2005]. Such linkage is relatively strong and in line with above mentioned studies [Li2008]; [Ahma2012b]; [Ilya2016]; [Ahma2012a]; [Jose2015] we did not expect conditions or effects where covalent linkage by cross-linking substances are needed. On that basis, rapid pretests for ceramic supported LbL-membranes were sufficient before starting the experiments. Therefore, pure water permeability was measured twice, first after coating procedure and second after storage of the coated membranes in an organic solvent for 48 h. Methanol, ethanol, butanone (MEK), ethyl acetate and n-methyl-2-pyrrolidone (NMP) were used as test solvents. The layer turned out to be credibly stable in each solvent since the difference between the two pure water permeability measurements was zero or insignificant.

Regeneration of the ceramic support

Layer removal from the ceramic support is mandatory if new coatings have to be tested, fouling occurs, or a new experimental series starts. The RCA cleaning (named after the founder the Radio Corporation of America) described by Kern [Kern1970] is a harsh treatment method which can deconstruct the layer. The applied mixture consists of ammonia solution (20 %), hydrogen peroxide (30 %) and pure water in a mass ratio of 3:2:9. The membranes are exposed to this solution at around 70 to 80 °C for 15 minutes.

Occasionally, this method could not reach a full deconstruction of the layers. In these cases, a thermal treatment was applied to remove the layers by heating the membranes up to 600 °C for 6 h. In this process, the ceramic supports are heated and cooled gradually to avoid destruction by thermal stress. The pure water permeability was measured after each layer removal treatment. The layer degradation succeeded if the permeability was closely above $1000\,\mathrm{L\,m^{-2}\,h^{-1}\,bar^{-1}}$.

5.4 Experimental procedure

All flux and retention measurements were conducted with at least two different membranes at three pressure levels: 5 bar, 7.5 bar and 10 bar. Two modules are connected in parallel in the cross-flow set up. A piston pump pressurized and a centrifugal pump circulated the solution at laminar flow (Reynolds number of 1000). The temperature was kept constant at 30 °C. Reynolds number and temperature are chosen by the account of the possible cooling and pump capacity of the set-up. The feed pressure, temperature, pressure loss inside the modules and mass flow in feed and permeate streams are recorded. Table 5.1 gives an overview of the performed experiments for this study.

Solvents and solutes

The flux of the pure solvent and its mixtures are determined. Pure water (Milli-Q) and pure ethanol (Merck KGaA) are applied as solvent. The amount of organic solvent in the mixtures of water and ethanol was set to 25 wt%, 50 wt% and 75 wt%.

Furthermore, flux and retention measurements are performed for these solvents containing a solute. Two different types of solutes are investigated, namely salts and polyethylene glycols (PEGs).

For salt retention measurements, respectively $CaCl_2$, LiCl and NaCl (Carl Roth GmbH + Co. KG) are applied with a concentration of 5 mmol L^{-1}. The salts are selected considering the solubility in pure ethanol. In order to investigate the dependency of flux and retention on salt concentration, additional experiments with 15 mmol L^{-1} and 25 mmol L^{-1} $CaCl_2$ are performed.

For PEG retention measurements, eight different PEGs (Sigma-Aldrich) in the range of 106 to 4000 kg $kmol^{-1}$ (weight average molecular weight) are dissolved simultaneously in the pure solvents and solvent mixtures. The concentrations of each single PEG was 1 g L^{-1}.

Table 5.1: Overview of performed experiments with 100 % H_2O, mixtures of H_2O with 25, 50 and 75 wt% EtOH and 100 % EtOH.

Solute	Measurement	Analysis	Process conditions
$CaCl_2$ (5, 15 and 25 mmol L^{-1})	Flux and retention	Flow meter Conductivity meter Refractometer	p = 5, 7.5 and 10 bar T = ca. 30 °C Re = 1000
LiCl (5 mmol L^{-1})			
NaCl (5 mmol L^{-1})			
PEGs (1 g L^{-1})	Flux and retention (MWCO)	Flow meter GPC	
-	Pure solvent flux	Flow meter Refractometer	
	Layer thickness	Ellipsometer	p = ambient T = ambient (ca. 25 °C)

Order of the solvent mixture

Shukla and Cheryan [Shuk2002] showed the effects of membrane conditioning for polymeric ultrafiltration membranes in ethanol-water mixtures. They recommend a gradual solvent exchange since rapid exchange with high organic concentrations leads to effects on flux and retention. Although the LbL membranes and ceramic support structure are stable in organic solvents, we expected that the contact order of solvent mixtures affects the measurements. Therefore, all measurements were performed in the same order. It was obvious to start each experimental series with water since the membranes were coated in aqueous solution. Afterwards, the experiments are continued with the solvent mixtures with increasing organic solvent concentration. Finally, the experiment with organic solvent was carried out.

On this occasion, the experimental effort should be recognized, in particular referring to extensive flushing of the set up between the measurements of different solvent mixtures. As a supplement, we investigated the effect of starting with ethanol for solvent flux and retention of $CaCl_2$.

The PEG retention measurements were performed with newly prepared membranes for each solvent mixture to exclude possible fouling effects.

Flux of pure solvents and mixtures

Solute free transmembrane flux measurements are performed at the given process parameter in steady state applying Coriolis flow meters (Table 5.1). Furthermore, the results are controlled by using a mass balance. Sample composition of feed and permeate are measured for every solvent experiment without solutes, to investigate the possibility of solvent separation.

The refractive index is an appropriate value to control the amount of solvents in two-component mixtures. Solvent separation occurred if the value of the permeate differs from the value of the feed. In this case, the ratio of the single solvents could be calculated with the single compound value. All samples of the pure solvent flux measurements were measured with the refractometer DR301-95 (A.KRÜSS Optronic GmbH, Germany).

After each flux and retention measurement, the pure water permeability

of the membranes was checked to determine if the permeation of organic-aqueous mixtures affects the polyelectrolyte layer. The feed inlet of each membrane module was connected to a pressure vessel filled with pure water. The measurements were performed at a constant pressure (2 bar) and were started when steady state was reached and minimum 0.5 L permeate was collected.

PEG Retention

PEG retention measurements are carried out to determine the pore sizes and the MWCO for solutes which are retained by size exclusion. The MWCO was defined as molecular weight retained by 90 %. The retention measurements provide insights into the quality of the coating and the density of the polyelectrolyte layer. Additionally, a change in the layer structure due to an increase of organic solvent content in the solution can be tracked. Samples from feed and permeate were simultaneously taken from each operating point.

The solvent mixture samples coming from the PEG retention experiments are prepared for analysis by evaporation at 55 °C followed by dilution in pure water. Sodium azide was added to align the concentration in the eluent. The prepared samples were analyzed with a gel permeation chromatography method at 35 °C. This method consists of a refractive index (RI) detector and two columns (Suprema, 30 Å pore size, 3 µm particles, 8.0x300 mm (ID x length), Polymer Standards Service GmbH, Mainz, Germany). Water with 0.02 wt% sodium azide was the mobile phase.

Salt-Retention

Salt retention can be measured with conductivity, although the relationship between conductivity and concentration is dependent on the amount of organic solvent in the mixture. Therefore, calibration curves for each used salt in each solvent composition are required. Figure 5.2 shows exemplary the conductivity measurements from various $CaCl_2$ concentrations in different solvent compositions resulting in the calibration curves. With this data and

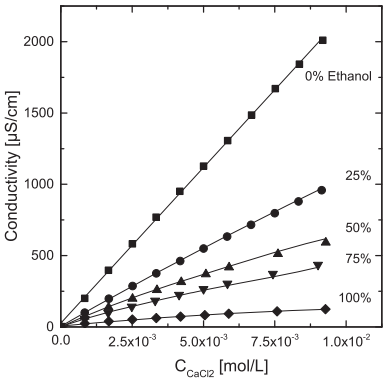

Figure 5.2: Conductivity calibration curves in each solvent composition for the determination of salt concentrations for experiments with 5 mmol L^{-1} $CaCl_2$.

the conductivity of the samples, their salt concentrations are determined, and the retention was calculated by:

$$R_i = 1 - \frac{c_{i\,(Permeate)}}{c_{i\,(Feed)}}. \tag{5.1}$$

Ellipsometry

The thickness of the polyelectrolyte layers was measured non-destructively with ellipsometry in the used solvent compositions. For this purpose, the layers were irradiated with polarized light. The reflected beam got detected, and the change in polarization was analyzed as described by Ogieglo et al. [Ogie2015]. The polyelectrolyte layers used for ellipsometry measurements were dip-coated on silicon wafer since ceramic supports did not reflect light sufficiently enough to be detected.

Silicon wafers were dipped into the respective polyelectrolyte solution for 20 minutes [Dodo2013]. The same polyelectrolyte solutions are used as for the coatings on the ceramic support. Between the coating steps with polyelectrolytes, the wafers were submerged in pure water for minimum 10 minutes. The coating steps are repeated until the required amount of bi-layers is obtained. Two different numbers of bi-layers are tested, namely 5

and 10 bi-layers. The second coating was chosen since the static coating procedure requires more layers to achieve the same performance as the dynamic coating on the ceramic support [Menn2016a]. The finished wafers were stored for at least 48 h in the measuring solutions to ensure no continuing changes of the polyelectrolyte layers properties. During measurements the wet wafers were inserted in glass prisms filled with the solvent composition.

The thickness is at least triple measured at different positions of all coated wafers. A 'J.A. Woollam Co. Spectroscopic Ellipsometer' was used for the measurements. The glass prism has a height of 5.15 mm and the slope of the walls is 70°. The height of the clean wafers is 0.7 mm and the measurement of the natural oxide layer of the wafer resulted in a thickness of 1.95 nm. The measured values from the ellipsometer were interpreted by the model of Cauchy which is a standard method for transparent polymeric layers [Ogie2015]. Thereby, the refractive index is depending on the wavelength λ of the reflected light in µm by:

$$n(\lambda) = A + \frac{B}{\lambda^2} + \frac{C}{\lambda^4}. \tag{5.2}$$

The constants in this equation are adjusted to the model whereby C is neglected due to minor influence on the result. From A and B the provided software (CompleteEase®) calculated the thickness of the coating.

5.5 Results and discussion

The functional characteristics of the LbL membranes on ceramic supports are investigated with flux and retention measurements. Results of pure solvent fluxes are discussed, followed by the results of solute retention. All measurements were performed at least twice considering the experimental effort. Therefore, the error bars in the diagrams show the measured maxima and minima. As described before, the order of the solvent mixtures influence the results. Accordingly, the supplemental tests of freshly coated membranes starting with ethanol are presented after the results of those

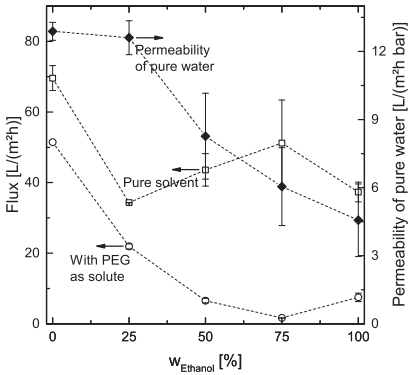

Figure 5.3: Pure solvent fluxes (□) and fluxes with PEGs as solute (◯) measured at 7.5 bar, 30 °C and $Re = 1000$. Pure water permeability (◆) measured between the pure solvent flux measurements with water-ethanol mixtures.

using the standard order of solvent mixtures (water-ethanol). The study is completed by a physical-chemical characterization of the polyelectrolyte layers using ellipsometry.

5

Pure solvent flux

Pure solvent fluxes are determined for water-ethanol. The fluxes differ according to the amount of ethanol in the mixture. Figure 5.3 shows the pure solvent fluxes for different ethanol concentrations at 7.5 bar and 30 °C. The pure water flux was approximately 70 L m^{-2} h^{-1}. Adding 25 wt% ethanol to the pure water resulted in a significant decrease in flux. Further increasing the proportion of ethanol lead to an unexpected increase in flux and a local maximum at 75 wt% ethanol. However, pure ethanol permeates through our LbL membrane with a satisfactory high flux of 37 L m^{-2} h^{-1}. The curve progression is similar for all tested pressure levels (5, 7.5 and 10 bar, not shown). A possible reason for the obtained trend (Figure 5.3) could be a change in the LbL structure due to the solvent mixture properties. Such influencing solvent mixture properties are the relative permittivity and the viscosity, for example. The LbL structure could further depend on the affinity to the solvent, on the amount of embedded salt, et cetera. Hence, a superimposition

of some effects on the LbL coating can be hypothesized. In contrast, we exclude a dependency of the support structure due to the chemical stability of the ceramic monolith.

Samples are taken during the pure solvent flux measurements to detect potential solvent separation. We realized with refractometry data consistent refractive indices of the solvents in permeate and feed. The results are in line with data from literature [Scot1946]; [Beld2005] and confirmed no solvent separation. Therefore, all subsequent experiments are performed with the assumption of equal solvent mixtures in permeate and feed. Nevertheless, this assumption was also rechecked during the retention measurements.

Besides the solvent flux, the permeability of pure water was checked after permeation of every solvent mixture. Figure 5.3 displays, after increasing the amount of ethanol above $25\,\mathrm{wt\%}$, a sharp decrease of pure water permeability from ca. 12.9 to $4.6\,\mathrm{L\,m^{-2}\,h^{-1}\,bar^{-1}}$. The change in permeability was found to be not completely reversible while testing the same membranes in reverse order of ethanol-water mixtures. These measurements strengthen our expectation about a change in swelling behavior of the polyelectrolyte layers. Obviously, the experimental order plays a crucial role to obtain consistent results.

MWCO measurements

For functional membrane characterization the MWCO at $90\,\%$ retention is a common value to describe a nanofiltration membrane used in aqueous solutions [Bous2006]. From findings in the field of organic solvent nanofiltration, it is known that the MWCO value is strongly dependent on the interactions between solvent, solutes and membrane [Staf2004]; [Stam2006]. Figure 5.3 shows next to the pure solvent flux versus ethanol concentration also the flux with PEGs as solutes. Each operating point results in lower flux compared to the pure solvent flux; additionally, the curve progressions differ from each other. Concluding, PEGs as solutes have a significant impact on the flux. With PEGs as solutes, the flux in water was $46\,\mathrm{L\,m^{-2}\,h^{-1}}$

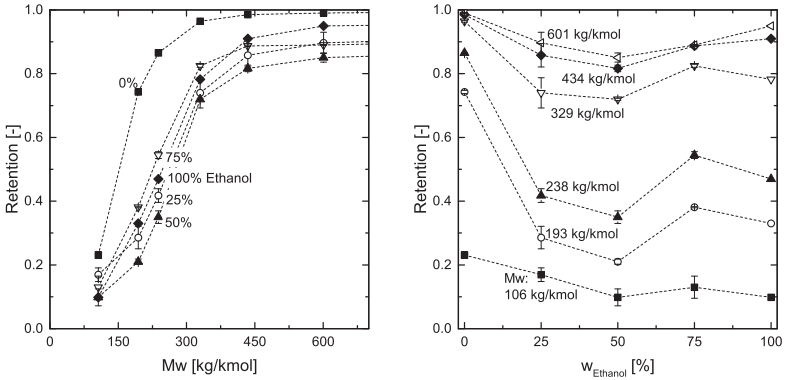

(a) Retention curves for PEGs in water-ethanol mixtures.

(b) Retention of individual molecular weights of the PEGs in water-ethanol mixtures.

Figure 5.4: MWCO measurements with PEGs with a molar mass ranging from 106 to 601 kg kmol^{-1} at 7.5 bar, 30 °C and $Re = 1000$.

and similar to the pure solvent flux the value decreases by increasing the amount of ethanol. On the contrary to pure solvent flux, there is no local maximum at 75 wt% ethanol but a local minimum (1.5 L m^{-2} h^{-1}). Using ethanol as solvent the flux increased to 6.7 L m^{-2} h^{-1}. In contrast to the pure solvent flux, the results for PEGs as solute show less deviation at each operating point for all measured pressures (not shown).

A change in the layer structure is expected to shift the MWCO. Figure 5.4a shows the retention curves for the dissolved PEGs at 7.5 bar. It is striking that the MWCO at 90 % retention is reached only by four feed compositions in the range of 106 to 601 kg kmol^{-1}. Increasing the molecular weights even further until maximum 4000 kg kmol^{-1} does not change the retention significantly compared to the value at 601 kg kmol^{-1}. Data from Figure 5.4a are depicted differently in Figure 5.4b in order to identify the influence of the solvent mixture composition on the retention for the different molar masses. Figure 5.4b shows the retention of the specific PEGs at their weight average molecular weight versus the amount of ethanol in the feed solution. Adding ethanol to the feed solution leads to a decrease of all PEG retention. The lowest retention values are in water-ethanol mixtures. In

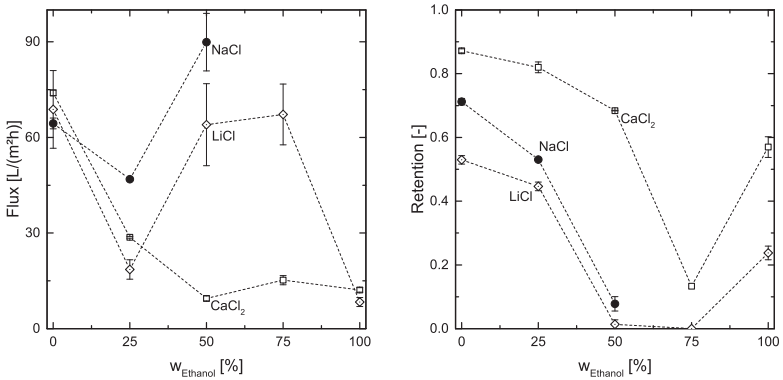

(a) Fluxes of salt containing solutions in water-ethanol mixtures.

(b) Salt retention in water-ethanol mixtures.

Figure 5.5: Measurements with $5\,\mathrm{mmol\,L^{-1}}$ salt (NaCl ●, LiCl ◇, $CaCl_2$ □) as solute in water-ethanol mixtures at $7.5\,\mathrm{bar}$, $30\,^{\circ}\mathrm{C}$ and $Re = 1000$.

some of these retention curves, a local maximum at $75\,\mathrm{wt\%}$ ethanol arose. The MWCO at $90\,\%$ retention is reached in water near above $238\,\mathrm{kg\,kmol^{-1}}$ and ethanol close below $434\,\mathrm{kg\,kmol^{-1}}$. In a solution with $25\,\mathrm{wt\%}$ and $75\,\mathrm{wt\%}$ ethanol this $90\,\%$ boundary is exceeded near to $601\,\mathrm{kg\,kmol^{-1}}$.

The differences in flux of pure solvent measurements compared to solvents containing PEGs (Figure 5.3) can be partly explained by concentration polarization. This effect arises from the cross-flow velocity in the laminar range (Re = 1000) and the high solute concentration. Bearing this effect in mind the flux and retention values of the MWCO measurements could slightly be underestimated. However, the conclusions from the results remain. It was shown by Menne et al. [Menn2016b] that the LbL membrane is suitable for nanofiltration. Here, we showed a successful application in water-ethanol mixtures and ethanol. As mentioned before, the polyelectrolyte layers change their structure (probably their porosity) based on the applied solvent mixture. Meaning, the retention of the uncharged solutes (PEGs) is mainly dependent on the solvent mixture.

Salt retention

Flux and retention values of solvent-solute systems with monovalent and bivalent ions are typical characteristics for nanofiltration membranes [Geis2014]; [Peet1998]. The results are similar for all measured pressure levels. Henceforth, only one pressure level is representatively shown. Results from flux measurements with three different salts as solute (NaCl, LiCl, $CaCl_2$) at 7.5 bar are depicted in Figure 5.5a. The fluxes with water as solvent are approximately equal to the pure solvent fluxes (Figure 5.3). These results indicate that based on the low salt concentrations (5 mmol L^{-1}) no concentration polarization occurs. However, the fluxes for solutions with $CaCl_2$ decrease by increasing the amount of ethanol. At 75 wt% ethanol in the solvent a local maximum was obtained which is not as strongly pronounced as for the pure solvent measurements. In contrast to the fluxes containing $CaCl_2$, the fluxes for LiCl and NaCl solutions start increasing above 25 wt% ethanol. Partly the fluxes are higher compared to water and also show a local maximum at 75 wt% ethanol. Though, the fluxes in ethanol are significantly lower and for all solutes approximately equal around 10 L m^{-2} h^{-1}. The flux curves with LiCl and NaCl in solution are similar in shape to the pure solvent fluxes. On the contrary, the curve of the $CaCl_2$ solution resembles the flux curve with PEGs as solute. Similarly to the observations using PEGs, the error bars for the results of the $CaCl_2$ solution show a small deviation at each operating point.

Figure 5.5b shows the retention values using salt as solute. The retention of $CaCl_2$ decreases from 87 % in water due to the addition of ethanol. Remarkably, an extreme minimum (13 %) is found at 75 wt% ethanol. In ethanol, the retention increased to 57 %. In comparison, the retention curves for the monovalent salts LiCl and NaCl decrease stronger with already lower amounts of ethanol in the solvent. Retentions for these salts are almost zero if the ethanol content was 50 wt% or 75 wt% in the solvent. The results from the measurements with NaCl as solute were only up to 50 wt% ethanol evaluable or reproducible. However, in ethanol, the retention of LiCl rises to 24 %.

It is conspicuous that the highest flux values are related to the low reten-

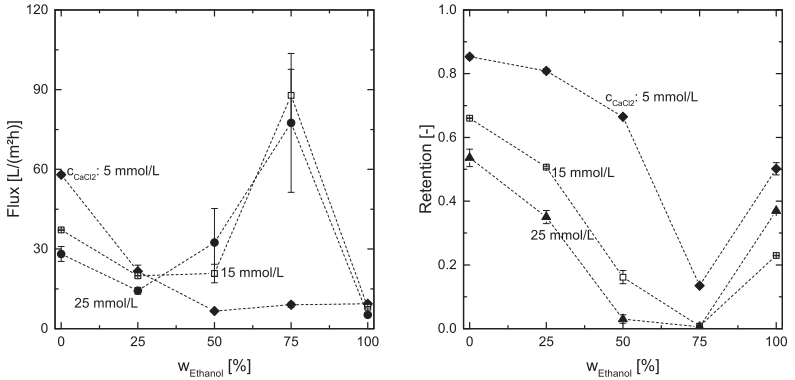

(a) Total fluxes of $CaCl_2$ containing solutions in water-ethanol mixtures.

(b) Retention of $CaCl_2$ diluted in water-ethanol mixtures.

Figure 5.6: Measurements with $CaCl_2$ at different concentrations 5 ◆, 15 □ and 25 mmol L^{-1} ●, 5 bar, 30 °C and $Re = 1000$.

tion values of the monovalent ions while the flux only slightly increased for the related minimum retention value of $CaCl_2$. Besides, flux and retention values both decrease if 25 wt% ethanol is added to water. During the pure water permeability tests between the operating points, the polyelectrolyte layers are still intact and not degraded.

In addition to the measurements with 5 mmol L^{-1} salts, experiments with higher concentrations of $CaCl_2$ were performed. Figure 5.6 comprises the results of flux and retention measurements at 5 bar for the salt concentrations: 5, 15 and 25 mmol L^{-1}. As expected, the fluxes in water decrease by increasing the salt concentration (Figure 5.6a). While the fluxes further decrease by adding 25 wt% ethanol, the differences in flux between the used salt concentrations reduce. With 50 wt% ethanol as the solvent the flux order is reversed. In contrast to 5 and 25 mmol L^{-1} $CaCl_2$, the flux of the 15 mmol L^{-1} $CaCl_2$ solution remained almost constant. The curve progression of the flux measurements for the low concentrated solutions (5 mmol L^{-1}) are similar for all measured pressures. Increasing the concentration lead to a change in the curve progression, which resembles the one with monovalent cations (cf. Figure 5.5, LiCl and NaCl).

For both higher concentrated solutions, the local maximum flux at 75 wt% ethanol is pronounced than for the low concentrated solution. The fluxes exceeded values of the measurements with water to 77.5 and 88 L m^{-2} h^{-1} on average for 15 and 25 mmol L^{-1}, respectively. For all solutions the fluxes in ethanol are close to each other in the range of 5 and 10 L m^{-2} h^{-1}.
The retention curves (Figure 5.6b) are similar in shape for all salt concentrations. As expected, more salt can permeate through the membrane at higher concentrations. The trend of retention decrease by adding up to 50 wt% ethanol to the solvent is steeper for the solutions with higher salt concentrations. However, all retention measurements with 75 wt% ethanol as solvent result in a local minimum. The retention values in ethanol were correspondingly higher, with the exception of 25 mmol L^{-1} $CaCl_2$ ($R \approx 37\,\%$) which retention is higher than for 15 mmol L^{-1} $CaCl_2$ ($R \approx 23\,\%$). The retention value for the solution with 5 mmol L^{-1} reached for ethanol as solvent 50 %. Therefore, the curve shapes from the measurements with $CaCl_2$ for higher concentrations align on the curve shapes measured with the monovalent salts.

In consideration of the extensive and partly unexpected results, it can be reasoned that several effects overlap. The flux reduction at 25 wt% (and partly at 50 wt%) ethanol is probably due to the interaction between the hydrophilic polyelectrolyte layers and the solvent, which becomes less polar. Also, a cononsolvency effect, as described by Scherzinger et al. [Sche2014] and Edmondson et al. [Edmo2010], can be assumed which affects the layers in this solvent mixture. If that assumption is correct, the layers swell less in the solution so it should become evident with the ellipsometry measurement.

The retentions of the salts in water are in line with the expectations for a nanofiltration membrane. The Donnan effect can explain the differences between monovalent ions and bivalent ions. Furthermore, the Donnan effect continues to be active after the addition of alcohol to the solvent. It is also known that the network of ordered water molecules is disturbed by the addition of ethanol [Nosk2005]. This disturbing is reflected in the excess volume of the solution. At approximately 63 wt% ethanol the ex-

cess volume has a local minimum since in this composition the hydrogen bonds between water molecules are most effectively disturbed. Therefore the water network in the liquid ceases. As a result, it is assumed that the molecules are more agile and interactions between the solvent and polyelectrolyte layers decrease. While solvent molecules of water or ethanol attach to the membrane wall within the pores, the mixed solvent molecules compete with each other [Edmo2010]. This competition prevents complete deposition of solvent molecules on the membrane wall within the pores of the polyelectrolyte layers similar to Tanaka, Koga, and Winnik [Tana2008]. With a complete deposition within the pores, the layers are widened, and at the same time, the effective pore radius is reduced by the solvent. If no complete deposition appears, the layers will become thinner and the effective pore radius larger (Figure 5.7). This results in better shielding of the diluted ions and thus lower retention and generally higher fluxes.

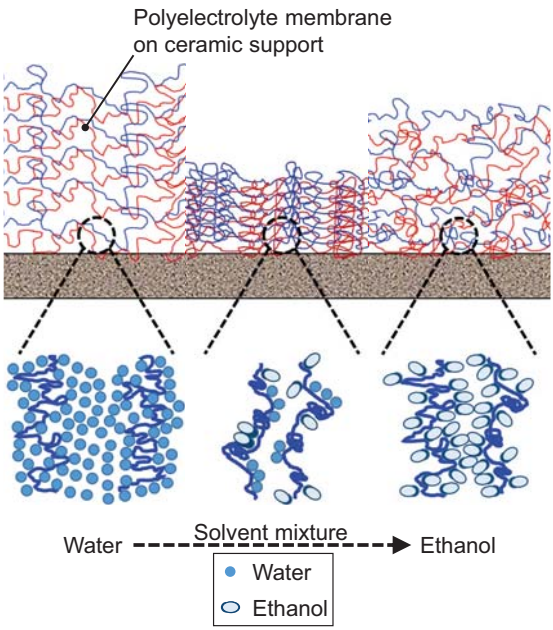

Figure 5.7: Schematic representation of the observed cononsolvency effect.

Besides, it can be hypothesized that the salts can slightly shift the point of greatest disruption of hydrogen bonds by ethanol. Thus the chaotropic effect of Na^+ and Li^+ would shift the point to lower ethanol contents and the more cosmotropic Ca^{2+} to higher ethanol contents. Marchetti, Butté, and Livingston [Marc2013] explain similar results with preferential solvation and the emerging competition between the affinities of solvent-membrane and solute-membrane. However, they state that the preferential solvation in water-ethanol mixtures is weak and, therefore, the influence low.

Increasing the $CaCl_2$ concentration leads to a decrease of the Debye-length and therefore a decrease of the electrostatic forces [Isra2011]. This results in an easier permeation of the ion and lower retention. Further, Ca^{2+} ions less counteract the disturbance of the hydrogen bonds by ethanol anymore. The water molecules become more disordered with lower amounts of ethanol in solution. Both, the disruption of the hydrogen bonds of the water molecules and the lower Debye-length, lead to a higher flux.

In ethanol, the flux decreases drastically since the layers remain hydrophilic and the polarity of the solvent decreases clearly. Therefore, the retention of the ions increase. Since the Donnan effect is still apparent, the retention is significantly higher in $100\,\mathrm{wt\%}$ ethanol for the lowest salt concentration (higher Debye length). The hydrogen bond network of ethanol is not disturbed by another solvent, so nothing is counteracting low fluxes.

Order of the solvent mixture

As already mentioned, the experimental order is expected to influence the measurements. The results from flux and retention measurements indicate changes in the layer. Hence, we measured the pure ethanol flux as well as flux and retention in ethanol with $5\,\mathrm{mmol\,L^{-1}}$ $CaCl_2$ directly after coating. Figure 5.8a shows the transmembrane flux depending on feed composition at $5\,\mathrm{bar}$. With regard to pure solvent flux, the curve progression is similar for all pressure levels. We observe initially a decrease in flux by adding ethanol. Continuing the addition of ethanol, the flux increases with a maximum at $75\,\mathrm{wt\%}$ ethanol. For pure ethanol the flux is around $26\,\mathrm{L\,m^{-2}\,h^{-1}}$. In

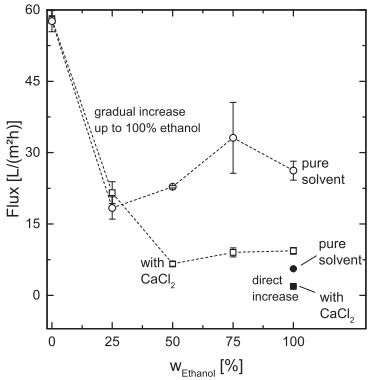

(a) Fluxes of pure solvent ◯, ● and solvent with diluted $CaCl_2$ □, ■ depending on gradual (open symbols) or direct increase (filled symbols) up to 100 % ethanol).

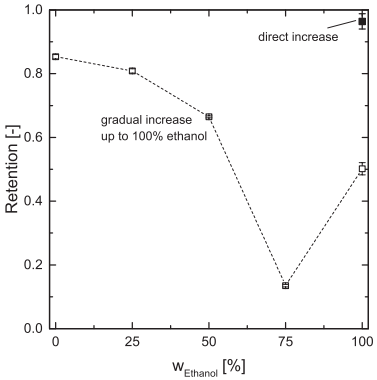

(b) Retention of $CaCl_2$, measured in solvents with gradual increase of ethanol proportion □ and measured directly in ethanol ■ after coating procedure.

Figure 5.8: Comparison of gradual increasing and direct ethanol contact with the membrane for pure solvent measurements and measurements with 5 mmol L^{-1} $CaCl_2$ as solute at 5 bar, 30 °C and $Re = 1000$.

contrast, the flux is significantly lower (around 5.6 L m^{-2} h^{-1}) if the membrane is contacted directly with pure ethanol after the coating procedure. The flux is significantly lower for measurements with more than 25 wt% ethanol as solvent by using 5 mmol L^{-1} $CaCl_2$ as solute. In 100 % ethanol, the flux value reached 9.4 L m^{-2} h^{-1}. For the same feed composition, only 2 L m^{-2} h^{-1} is obtained if the membrane was directly used in ethanol. Thus, we found in both cases, with and without salt, reduced fluxes if the LbL membrane gets in contact with ethanol as solvent directly after the coating procedure.

Next to the fluxes, the experimental order also influences the retention of $CaCl_2$. Figure 5.8b shows both retention values: on the one hand, from the above discussed measurements with a gradual increase of ethanol proportion in the solvent and on the other hand, retention values measured directly in ethanol as solvent after the coating procedure. As already mentioned, the retention values for the incremental increase of ethanol percentage in solvent rises to 50 % in ethanol. In comparison, all retention measurements

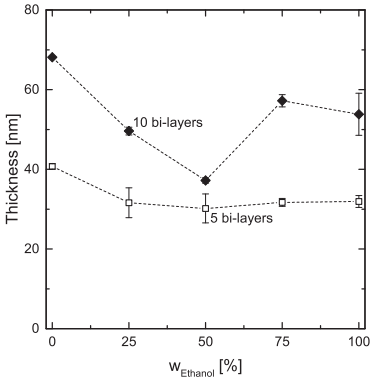

Figure 5.9: Thickness of polyelectrolyte layers (5 □ and 10 ◆ bi-layers) in water-ethanol mixtures.

in ethanol directly after coating result in high values (above 95 %). These retention values are higher than in water as the solvent. However, for applications the coincident low fluxes have to be considered.

5

Ellipsometry

Ellipsometry is used to determine the change in the polyelectrolyte layers thickness. By coating silicon wafers, the polyelectrolyte layers could be investigated independently of the support. Similar to the ceramic support, the silicon wafers do not influence the thickness by swelling. Figure 5.9 shows the thickness of the polyelectrolyte layers as a function of the containing weight percent of ethanol in the solvent. As mentioned before 10 bi-layers were measured beside 5 bi-layers since the static coating procedure requires more layers as the dynamic coating procedure to achieve similar characteristics. First, it becomes apparent that the polyelectrolyte layers thickness in water is 41 nm for 5 bi-layers and 68 nm for 10 bi-layers. Second, it can be seen that the thickness of 5 bi-layers decrease by adding ethanol to the solvent and is more or less constant for all ethanol containing solutions. For 10 bi-layers the thickness also decreases by adding up to 50 wt% ethanol. The thickness contraction is around 45 % from the value

in water compared to the value in a solution with 50 wt% ethanol. Further increasing the amount of ethanol in solvent resulted in swelling of the layer and therefore an increase in layer thickness.

In all ellipsometry measurements, the determined refractive index (Equation 5.2) was higher if the thickness was low. It is an indication that the layers are denser if they swell less. Though, a definite relation between refractive index and density could not be found. A lower thickness in ethanol than in water was expected since this result is in line with measurements of Miller and Bruening [Mill2005]. They suppose that the polyelectrolyte layers are less mobile in ethanol than in water and therefore the swelling degree is smaller. Results from the measurements with the mixtures show cononsolvency behavior for the layer and confirm the assumption concerning cononsolvency effect before. Consequently, the local minimum in the polyelectrolyte layers thickness for the solvent mixtures could be related to the mutual interaction of the solvent components and the solvent interactions with the polyelectrolytes.

Most of the interactions occur in water while ethanol is less polar but it still builds hydrogen bondings and forms a network. Thus, explaining the highest thickness of the polyelectrolyte layers in water, and the lower thickness in ethanol. Increasing the amount of ethanol in the solvent implies a replacement of embedded water inside the polyelectrolyte layers. Through the disruption of the hydrogen bonds in the water-ethanol mixtures, the solvent molecules could compete in the deposition at the membrane surface similar as described by Tanaka, Koga, and Winnik [Tana2008]. The swelling degree decreases as a result of the strong hydrophilic character of the polyelectrolyte layer (Figure 5.7).

The real reasons for cononsolvency are hitherto not clear and in literature controversy discussed [Mukh2014]; [Sche2014]; [Zuo2018]. In any case, the swelling degree decreases. However, usage of ethanol leads to thicker polyelectrolyte layers. The cononsolvency effect is not affecting anymore, and the swelling degree increases again to an approximately constant level. Generally, the swelling depends on the interactions of the solvent with the polyelectrolytes.

5.6 Conclusion

Nanofiltration processes, where solute traces need to be rejected from aqueous organic mixtures, are widely unexplored. In this study, LbL membranes coated on ceramic supports consisting of the polyelectrolytes PDADMAC and PSS are investigated in water, ethanol and their mixtures. Pretests showed the stability of the layers on ceramic support for various solvents and 5 bi-layers are found to be sufficient for the experiments.

The LbL membranes are characterized using flux and retention measurements with pure solvents, PEGs, and different salts as solutes. Refractometry measurements of feed and permeate samples proved that no solvent separation occurred. Pure solvent flux was lower in ethanol and water-ethanol mixtures than in pure water with a local maximum for 75 wt% ethanol.

Measuring the retention of PEG led to the MWCO in water at 238 kg kmol^{-1}, in the mixtures somewhat higher at 601 kg kmol^{-1} and in ethanol at 434 kg kmol^{-1}. Therefore, MWCO is clearly in nanofiltration range for all mixtures. Fluxes from these measurements showed a different curve progression than for pure solvent with a local minimum at 75 wt% ethanol.

Measurements with 5 mmol L^{-1} salts as solutes showed decreasing retention values by adding ethanol to the solvent. A significant minimum in retention and a local maximum in flux values were detected for solvent mixtures with 75 wt% ethanol. The sharp decrease in retention and increase in flux occur in measurements with monovalent salts as solute already for lower amounts of ethanol (50 wt%) in the solvent mixtures than in measurements with bivalent ions. The behavior observed for monovalent ions is also recognized for higher concentrations of the bivalent Ca ions. Donnan effect ensures higher retention values for bivalent ions than for monovalent ions. The curve shapes can be additional explained by the cononsolvency effect combined with the polarity effect of the solution. Cononsolvency can be possibly traced back to the disturbing of hydrogen bonds, and therefore, the interactions between the solvent, solute, and membrane.

Results from flux and retention measurements directly after coating pro-

cedure in ethanol result for both cases, with $CaCl_2$ as solute in solution and without, in lower fluxes. However, the retention is significant higher reaching more than $95\,\%$.

In addition to the retention and flux measurements, ellipsometry experiments are conducted to determine the thickness of the polyelectrolyte layers in the different solvent mixtures. The thickness is higher for measurements in pure water than in ethanol and mixtures of water and ethanol. We assume that the cononsolvency effect, as mentioned before, is the reason for this layer contraction. It is the first time a cononsolvency effect is observed for polyelectrolyte membranes.

Considering all results, we showed that LBL membranes on ceramic supports are suitable not only for nanofiltration in aqueous environment but also in water-ethanol mixtures and in ethanol. We measured significant flux and retention values of uncharged polymers and salts and discovered remarkable effects for the interaction of solvent, solute and membrane. For instance, such an effect with cononsolvency behaviour is widely unexplored in membrane science, although it probably appears in many applications of nanofiltration where solvents are mixed. Finally, this research field contains several exciting options for further investigation. Specifically, examination of other coatings and with additional test substances (solvents and solutes) will enlarge the knowledge swiftly and unravel questions resulting from the observed results.

6 Summary and outlook

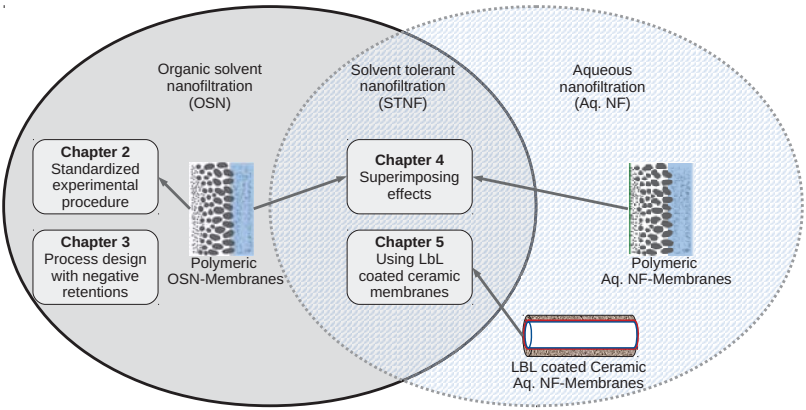

Outline of this thesis: The chapters follow the thematic path from organic solvent nanofiltration to solvent tolerant nanofiltration.

6.1 Summary and reflections

The present work covers different areas of nanofiltration with organic solvents. Compared to conventional separation processes, the use of these processes offers advantages concerning energy and resource efficiency. Thus, any improvement and dissemination of OSN and STNF will lead to a higher acceptance and widespread implementation of more sustainable processes.

To include the OSN as a standard application into the toolbox of separation processes, a standard procedure has been presented for measuring membrane characteristics such as retention and flux. For the first time, such a standard procedure was used and compared by several institutions to determine the statistical deviations. The proposed standard experimental procedure enables generating comparable and reliable membrane performance data. A superstructural optimization subsequently highlights the impact even small deviations can have on the whole process design. During these studies, further fundamental questions arose regarding the influence of negative retentions on the optimization of the process design. In five scenarios, a simplified model shows different approaches to these questions. A major result is differences in configurations of the membrane modules in a membrane cascade. The module configuration most frequently selected by the optimization algorithm was the amplification mode with retentate recirculation to the preceding stages. For a solution of two solutes diluted in a single solvent the following can be stated: The higher the retention of the undesired component and the broader the ΔR of the solutes, the higher is the selectivity. Also the required stage cut should be considered. A smaller stage cut generates a higher selectivity. However, the optimal configuration changes only at low selectivities.

Further experiments were conducted to characterize polymer membranes whereby water is added to the solvent system. As water is a strong polar solvent, ethanol or NMP are used as organic components. Thus the nanofiltration field changes from OSN to STNF. The investigations in this area are carried out both with uncharged solutes and with salts. The results show

that different effects superimpose each other when using polymeric OSN and aq. NF membranes. The intensity of the superimpositions and therefore the dominant effects change depending on the solvent composition. Besides, the influence of the superimposed effects decreases with increasing molecule size of the solutes. The viscosity mainly influences the flux in the aqueous medium. The effect is superimposed with polarity effects as the organic content of the solvent increases. In addition to the known forces (such as porosity and Donnan effect), less investigated effects have a considerable influence on the retention. These effects include the preferential solvation of ions and the disturbance of hydrogen bonds in the liquid network. The dominance of the crucial effects changes between 60 and 80 wt% ethanol content in the solvent.

In the the penultimate chapter, the LbL method developed by Menne et al. [Menn2016b] was taken up, and ceramic support membranes are coated with polyelectrolytes. These membranes, which have previously been extensively tested in aqueous nanofiltration, were used in this study for the first time in solvent systems consisting of water and ethanol. Since the membranes are prepared in an aqueous environment, ethanol has been added to the solvent system. Accordingly, the nanofiltration field is now changing from the aqueous nanofiltration to STNF. The experiments were conducted in the same way as the STNF experiments with the polymer membranes. Therefore, the superimposed effects were also observed with these membranes. However, in addition to the already known effects, the cononsolvency effect of the active separation layer could also be verified. This validation was possible with the method of ellipsometry.

Overall, the thesis describes various effects which occur during the performance of OSN and STNF. Several of these effects were up to now unknown or had not been described. The work offers new approaches for improving and researching the techniques. As a result of this further development and research of the processes, resistance, and doubts about the technology were reduced. A broader acceptance in the industry had been reached whereby the processes are considered in new designs or renewal of energy-efficient and resource-saving facilities. The STNF, in particular,

has received little attention so far, and this work puts into the focus of such investigations. Further studies in this field are an investment in a more sustainable future.

6.2 Outlook

The investigations conducted in this study provide numerous further opportunities for exciting research questions. Heuristic methods could promote and strengthen the standardized experimental method in Chapter 2. Results measured with the standardized method can help to reveal correlations in the complex solvent-solute-membrane system due to their high quality. The optimization model in Chapter 3 could further be applied to examine more retention cases. Besides, it could be extended to enable new possibilities in assessing process configurations and costs. For STNF processes further measurements, such as performed in Chapter 4, are necessary. Different chemical systems will lead to a better understanding of the effects detected and could support the investigation of other effects, such as the swelling of membranes. Also, other coatings on ceramic support membranes, similar to the coating in Chapter 5, with appropriate test systems will build up knowledge in this research field. In addition, the importance of ceramic membranes in nanofiltration processes could be promoted. Overall, an effort on generating a comprehensive understanding of challenges involving organic solvents and water in nanofiltration is needed. The combination of elements from aqueous nanofiltration and OSN is of central importance.

Accordingly, a standard procedure also for STNF should be developed as early as possible. The aim is achieving reliable results in this field which are directly comparable with ongoing investigations of innovations. Besides, this field requires comprehensive modeling, combining concepts from OSN and aqueous nanofiltration. The integration of possible experimental error sources which result in statistical deviations could lead to more accurate predictions.

Models used for designing processes can also be adapted to account for

statistical fluctuations of the parameters as they occur in real operations. This adaption would improve the prediction of successful processes and costs. Also, the connection to other process units could be improved in that way. Combinations of different retention cases through selectable membranes should allow greater flexibility. The combination and optimization sequences of different models have to be elaborated in a meaningful concept. Thereby the process design can be stabilized, and the acceptance of new membrane processes can be accelerated.

The exchange and combination of elements of aqueous nanofiltration and OSN are also beneficial for experiments. Such approaches have already been pursued in Chapter 4 and Chapter 5. Furthermore, membrane materials will play an essential role in the research of STNF. Beyond that, the LbL technique is promising for OSN and especially in combination with ceramic support membranes. The technology derived from aqueous nanofiltration can straightforward be used to apply tailor-made separating layers. If well compatible materials are selected, higher fluxes with high retentions should be feasible.

Bibliography

[Abej2014] R. Abejón, A. Garea, and A. Irabien. “Analysis and optimization of continuous organic solvent nanofiltration by membrane cascade for pharmaceutical separation”. *AIChE Journal* 60.3 (2014). (Cit. on p. 47).

[Adi2016] V. S. Adi et al. “Optimization of OSN membrane cascades for separating organic mixtures”. In *Computer Aided Chemical Engineering*. Vol. 38. Elsevier, 2016. Pp. 379–384. (Cit. on p. 48).

[AGEB2018] AGEB. “Auswertungstabellen zur Energiebilanz Deutschland 1990 bis 2017”. *Arbeitsgemeinschaft Energiebilanzen e.V.* (2018). (Cit. on p. 2).

[Ahma2012a] P. Ahmadiannamini et al. “Influence of polyanion type and cationic counter ion on the SRNF performance of polyelectrolyte membranes”. *Journal of Membrane Science* 403-404 (2012). (Cit. on pp. 124, 126, 127).

[Ahma2012b] P. Ahmadiannamini et al. “Multilayered polyelectrolyte complex based solvent resistant nanofiltration membranes prepared from weak polyacids”. *Journal of membrane science* 394 (2012). (Cit. on pp. 123, 127).

[Ande1952] T. W. Anderson and D. A. Darling. “Asymptotic Theory of Certain “Goodness of Fit” Criteria Based on Stochastic Processes”. *Ann. Math. Statist.* 23.2 (June 1952). (Cit. on p. 22).

[Ba2010] C. Ba, D. A. Ladner, and J. Economy. “Using polyelectrolyte coatings to improve fouling resistance of a positively charged nanofiltration membrane”. *Journal of Membrane Science* 347.1-2 (2010). (Cit. on p. 123).

[Baga1992] M. J. Bagajewicz and V. Manousiouthakis. “Mass/heat-exchange network representation of distillation networks”. *AIChE Journal* 38.11 (1992). (Cit. on p. 23).

[Baow2012] S. Baowei et al. “Preparation and performance of dynamic layer-by-layer PDADMAC/PSS nanofiltration membrane”. *Journal of membrane science* 423 (2012). (Cit. on p. 123).

[Bart2016] P. Barthelemy and E. Agyeman-Budu. “European chemical industry’s contribution to sustainable development”. *Current Opinion in Green and Sustainable Chemistry* 1 (2016). (Cit. on p. 1).

[Bast2017] M. Bastin, K. Hendrix, and I. Vankelecom. “Solvent resistant nanofiltration for acetonitrile based feeds: A membrane screening”. *Journal of Membrane Science* 536.Supplement C (2017). (Cit. on p. 12).

[Beld2005] R. Belda, J. Herraez, and O. Diez. “A study of the refractive index and surface tension synergy of the binary water/ethanol: influence of concentration”. *Physics and Chemistry of Liquids* 43.1 (2005). (Cit. on p. 135).

[Blum2015] S. Blumenschein, S. Druwe, and U. Kätzel. “The first of its kind OSN plant in a specialty chemicals company: a long and rocky journey”. In*Proceedings of the 5th International Conference on Organic Solvent Nanofiltration*. Antwerp, Belgium, 2015, 2015, p. 38 (cit. on pp. 11, 44).

[Blum2016] S. Blumenschein et al. “Rejection modeling of ceramic membranes in organic solvent nanofiltration”. *Journal of Membrane Science* 510 (2016). (Cit. on pp. 45, 46).

[Blum2017] C. Blum et al. “The concept of sustainable chemistry: Key drivers for the transition towards sustainable development”. *Sustainable Chemistry and Pharmacy* 5 (2017). (Cit. on p. 1).

[BMWi2010] BMWi and BMU. “Energiekonzept für eine umweltschonende, zuverlässige und bezahlbare Energieversorgung”. *Bundesministerium für Wirtschaft und Technologie (BMWi), Bundesministerium für Umwelt, Naturschutz und Reaktorsicherheit (BMU), Berlin* (2010). (Cit. on p. 1).

[BMWi2011] BMWi. “Forschung für eine umweltschonende, zuverlässige und bezahlbare Energieversorgung - Das 6. Energieforschungsprogramm der Bundesregierung”. *Bundesministerium für Wirtschaft und Technologie (BMWi), Berlin* (2011). (Cit. on p. 2).

[BMWi2018] BMWi. “Bundesbericht Energieforschung 2018 - Forschungsförderung für die Energiewende”. *Bundesministerium für Wirtschaft und Technologie (BMWi), Berlin* (2018). (Cit. on p. 2).

[Böck2019] A. Böcking et al. “Can the variance in membrane performance influence the design of organic solvent nanofiltration processes?” *Journal of Membrane Science* 575 (2019). (Cit. on pp. 44, 79).

[Bous2006] K. Boussu et al. “Characterization of polymeric nanofiltration membranes for systematic analysis of membrane performance”. *Journal of Membrane Science* 278.1-2 (2006). (Cit. on pp. 121, 135).

[Bowe1997] W. R. Bowen, A. W. Mohammad, and N. Hilal. “Characterisation of nanofiltration membranes for predictive purposes—use of salts, uncharged solutes and atomic force microscopy”. *Journal of Membrane Science* 126.1 (1997). (Cit. on p. 88).

[Caus2009] A. Caus et al. “The use of integrated countercurrent nanofiltration cascades for advanced separations”. *Journal of Chemical Technology & Biotechnology: International Research in Process, Environmental & Clean Technology* 84.3 (2009). (Cit. on p. 47).

[Cho2015] K. L. Cho et al. “Chlorine resistant glutaraldehyde crosslinked polyelectrolyte multilayer membranes for desalination”. *Advanced Materials* 27.17 (2015). (Cit. on p. 123).

[Chun2007] J. Chun-Te Lin and A. G. Livingston. “Nanofiltration membrane cascade for continuous solvent exchange”. *Chemical Engineering Science* 62.10 (2007). (Cit. on p. 47).

[Cupe2012] F. P. Cuperus. *How to run membrane experiments successfully*. Online brochure. Retrieved from http://www.solsep.com/Brochures/Pilotplantv21.pdf. 2012 (cit. on p. 12).

[Cupe2015] F. P. Cuperus. “Organic solvent nanofiltration applications: from lead to implementation”. In*Proceedings of the 5th International Conference on Organic Solvent Nanofiltration*. Antwerp, Belgium, 2015, 2015, p. 37 (cit. on pp. 11, 44).

[Dave2017] C. J. Davey et al. “Molecular weight cut-off determination of organic solvent nanofiltration membranes using poly(propylene glycol)”. *Journal of Membrane Science* 526.Supplement C (2017). (Cit. on p. 12).

[Dodo2013] S. Dodoo et al. “Effect of ionic strength and layer number on swelling of polyelectrolyte multilayers in water vapour”. *Soft Materials* 11.2 (2013). (Cit. on p. 132).

[Domi2012] H. Dominighaus, P. Elsner, and P. Eyerer. *Kunststoffe–Eigenschaften und Anwendungen*. 2012 (cit. on pp. 94, 100).

[Edmo2010] S. Edmondson et al. “Co-nonsolvency effects for surface-initiated poly (2-(methacryloyloxy) ethyl phosphorylcholine) brushes in alcohol/water mixtures”. *Langmuir* 26.10 (2010). (Cit. on pp. 140, 141).

[Euro2010] European Commission. *Europe 2020: A strategy for smart, sustainable and inclusive growth: Communication from the commission*. Publications Office of the European Union, 2010 (cit. on p. 1).

[Favr2010] E. Favre. “2.08 - polymeric membranes for gas separation”. In. *Comprehensive Membrane Science and Engineering*. Ed. by E. Drioli and L. Giorno. Elsevier, 2010, pp. 155–212 (cit. on p. 48).

[Fowk1978] F. M. Fowkes and M. A. Mostafa. “Acid-base interactions in polymer adsorption”. *Industrial & Engineering Chemistry Product Research and Development* 17.1 (1978). (Cit. on p. 99).

[Fu2007] R. Fu and D. C. Prieve. “Electrical Charges in Nonaqueous Solutions I: Acetone- Water Mixtures as Model Polar Solvents”. *Langmuir* 23.15 (2007). (Cit. on p. 112).

[Geen2005a] J. Geens et al. “Solute transport in non-aqueous nanofiltration: effect of membrane material”. *Journal of Chemical Technology & Biotechnology* 80.12 (2005). (Cit. on p. 11).

[Geen2005b] J. Geens et al. “Polymeric nanofiltration of binary water–alcohol mixtures: influence of feed composition and membrane properties on permeability and rejection”. *Journal of membrane science* 255.1-2 (2005). (Cit. on pp. 83, 93, 108, 122).

[Geis2014] G. M. Geise, D. R. Paul, and B. D. Freeman. “Fundamental water and salt transport properties of polymeric materials”. *Progress in Polymer Science* 39.1 (2014). (Cit. on pp. 121, 138).

[Grol1981] J.-P. Grolier and E. Wilhelm. “Excess volumes and excess heat capacities of water+ ethanol at 298.15 K”. *Fluid Phase Equilibria* 6.3-4 (1981). (Cit. on p. 99).

[Groo2015a] J. de Grooth et al. “Long term physical and chemical stability of polyelectrolyte multilayer membranes”. *Journal of membrane science* 489 (2015). (Cit. on p. 123).

[Groo2015b] J. de Grooth et al. “The role of ionic strength and odd–even effects on the properties of polyelectrolyte multilayer nanofiltration membranes”. *Journal of membrane science* 475 (2015). (Cit. on p. 125).

[Haen2012] R. Haensel et al. *Composite silicone membranes of high separation efficiency*. US Patent App. 13/513,225. 2012 (cit. on p. 53).

[Hans2007] C. M. Hansen. *Hansen solubility parameters: a user’s handbook*. CRC press, 2007 (cit. on pp. 14, 15, 88).

[Harr2000] J. J. Harris, J. L. Stair, and M. L. Bruening. “Layered polyelectrolyte films as selective, ultrathin barriers for anion transport”. *Chemistry of materials* 12.7 (2000). (Cit. on p. 123).

[Have2017] M. Haverkamp, M. Herbst, and J. Stegger. “Recent industrial OSN units: From process idea to industrial implementation”. In*Proceedings of the 6th International Conference on Organic Solvent Nanofiltration*. Saint-Petersburg, Russia, 2017, 2017, p. 40 (cit. on pp. 11, 44).

[Hest2001] J. Hestekin, C. Smothers, and D. Bhattacharyya. “Nanofiltration of Charged Organic Molecules in Aqueous and Non-aqueous Solvents: Separation Results and Mechanisms”. *Membrane Technology: in the Chemical Industry* (2001). (Cit. on pp. 83, 122).

[Hoff2015] S. Hoffmann. “A systematic investigation of transport phenomena in organic solvent nanofiltration”. Dissertation. Aachen: RWTH Aachen, 2015 (cit. on p. 17).

[Hoss2016] S. R. Hosseinabadi et al. “Solvent-membrane-solute interactions in organic solvent nanofiltration (OSN) for Grignard functionalised ceramic membranes: Explanation via Spiegler-Kedem theory”. *Journal of Membrane Science* 513.Supplement C (2016). (Cit. on p. 11).

[Ilya2016] S. Ilyas et al. “Weak polyelectrolyte multilayers as tunable membranes for solvent resistant nanofiltration”. *Journal of membrane science* 514 (2016). (Cit. on pp. 123, 127).

[Isra2011] J. N. Israelachvili. *Intermolecular and surface forces*. Academic press, 2011 (cit. on p. 142).

[Jass2002] M. Jassal and S. Ghosh. “Aramid fibres-An overview”. *Indian Journal of Fibre & Textile Research* 27 (2002). (Cit. on p. 88).

[Jin2003] W. Jin, A. Toutianoush, and B. Tieke. “Use of polyelectrolyte layer-by-layer assemblies as nanofiltration and reverse osmosis membranes”. *Langmuir* 19.7 (2003). (Cit. on p. 123).

[Jose2014] N. Joseph et al. “Layer-by-layer preparation of polyelectrolyte multilayer membranes for separation”. *Polymer Chemistry* 5.6 (2014). (Cit. on pp. 123, 127).

[Jose2015] N. Joseph et al. “‘Up-scaling’potential for polyelectrolyte multilayer membranes”. *Journal of Membrane Science* 492 (2015). (Cit. on pp. 124, 127).

[Kede1958] O. Kedem and A. Katchalsky. “Thermodynamic analysis of the permeability of biological membranes to non-electrolytes”. *Biochimica et biophysica Acta* 27 (1958). (Cit. on p. 45).

[Kell2017] S. Keller et al. “The Evolution of Data Quality: Understanding the Transdisciplinary Origins of Data Quality Concepts and Approaches”. *Annual Review of Statistics and Its Application* 4.1 (2017). (Cit. on p. 12).

[Kern1970] F. Kern. “Cleaning solutions based on hydrogen peroxide for use in silicon semiconducto technology”. *RCARev.* 31 (1970). (Cit. on p. 127).

[Khat2012] I. S. Khattab et al. “Density, viscosity, and surface tension of water+ethanol mixtures from 293 to 323K”. *Korean Journal of Chemical Engineering* 29.6 (2012). (Cit. on pp. 93, 115, 116).

[Kim2013] J. F. Kim et al. “When the membrane is not enough: A simplified membrane cascade using Organic Solvent Nanofiltration (OSN)”. *Separation and Purification Technology* 116 (2013). (Cit. on p. 47).

[Kras2000] L. Krasemann and B. Tieke. “Selective ion transport across self-assembled alternating multilayers of cationic and anionic polyelectrolytes”. *Langmuir* 16.2 (2000). (Cit. on p. 123).

[Laba2013] J. Labanda, J. Sabaté, and J. Llorens. “Permeation of organic solutes in water–ethanol mixtures with nanofiltration membranes”. *Desalination* 315 (2013). (Cit. on pp. 82, 84, 122).

[Li2008] X. Li et al. “Solvent-resistant nanofiltration membranes based on multilayered polyelectrolyte complexes”. *Chemistry of Materials* 20.12 (2008). (Cit. on pp. 123, 127).

[Li2009] X. Li et al. “Evaporative Light Scattering Detector: Toward a General Molecular Weight Cutoff Characterization of Nanofiltration Membranes”. *Analytical Chemistry* 81.5 (2009). (Cit. on p. 12).

[Li2010] M. Li et al. “Solubilities of NaCl, KCl, LiCl, and LiBr in methanol, ethanol, acetone, and mixed solvents and correlation using the LIQUAC model”. *Industrial & Engineering Chemistry Research* 49.10 (2010). (Cit. on p. 88).

[Li2011] G. Li et al. “Enzymatic synthesis of sucrose octaacetate using a novel alkaline protease”. *Biotechnology Letters* 33.3 (Mar. 2011). (Cit. on p. 16).

[Li2014] B. Li et al. “Determination and correlation of solubilities of lithium chloride and sodium chloride in NMP (氯化锂, 氯化钠在 NMP 中溶解度的测定与关联)”. *Journal of Chemical Industry and Engineering (China) (*化工学报*)* 65.12 (2014). (Cit. on p. 88).

[Lind2003] A. Linden and J. Fenn. “Understanding Gartner’s hype cycles”. *Strategic Analysis Report Nº R-20-1971. Gartner, Inc* (2003). (Cit. on p. 10).

[Liu2016] L. Liu, W. Chen, and Y. Li. “An overview of the proton conductivity of nafion membranes through a statistical analysis”. *Journal of Membrane Science* (2016). (Cit. on p. 10).

[Lopr2017] C. G. Lopresto et al. “Application of organic solvent nanofiltration for microalgae extract concentration”. *Biofuels, Bioproducts and Biorefining* 11.2 (2017). (Cit. on p. 44).

[Lykl2013] J. Lyklema. “Principles of interactions in non-aqueous electrolyte solutions”. *Current opinion in colloid & interface science* 18.2 (2013). (Cit. on p. 85).

[MacD1971] D. D. MacDonald et al. “Properties of the n-methyl-2-pyrrolidinone-water system”. *The Canadian Journal of Chemical Engineering* 49.3 (1971). (Cit. on pp. 94, 102, 103, 117, 118).

[Mach1999] D. R. Machado, D. Hasson, and R. Semiat. “Effect of solvent properties on permeate flow through nanofiltration membranes. Part I: investigation of parameters affecting solvent flux”. *Journal of Membrane Science* 163.1 (1999). (Cit. on p. 83).

[Mach2000] D. R. Machado, D. Hasson, and R. Semiat. “Effect of solvent properties on permeate flow through nanofiltration membranes: Part II. Transport model”. *Journal of Membrane Science* 166.1 (2000). (Cit. on p. 83).

[Mala2005] R. Malaisamy and M. L. Bruening. “High-flux nanofiltration membranes prepared by adsorption of multilayer polyelectrolyte membranes on polymeric supports”. *Langmuir* 21.23 (2005). (Cit. on pp. 123, 127).

[Mänt2006] M. Mänttäri, A. Pihlajamäki, and M. Nyström. “Effect of pH on hydrophilicity and charge and their effect on the filtration efficiency of NF membranes at different pH”. *Journal of Membrane Science* 280.1-2 (2006). (Cit. on pp. 102, 109).

[Marc2007a] Y. Marcus. “Preferential solvation of ions in mixed solvents. 5. The Alkali Metal, Silver, and Thallium (I) Cations in aqueous organic solvents according to the Inverse Kirkwood-Buff Integral (IKBI) approach”. *Journal of Solution Chemistry* 36.11-12 (2007). (Cit. on pp. 99, 100).

[Marc2007b] Y. Marcus. “Preferential solvation of ions in mixed solvents. 6: Univalent anions in aqueous organic solvents according to the inverse Kirkwood–Buff integral (IKBI) approach”. *The Journal of Chemical Thermodynamics* 39.10 (2007). (Cit. on pp. 99, 100).

[Marc2012] P. Marchetti, A. Butté, and A. G. Livingston. “An improved phenomenological model for prediction of solvent permeation through ceramic NF and UF membranes”. *Journal of membrane science* 415 (2012). (Cit. on pp. 82, 83).

[Marc2013] P. Marchetti, A. Butté, and A. G. Livingston. “NF in organic solvent/water mixtures: Role of preferential solvation”. *Journal of membrane science* 444 (2013). (Cit. on pp. 4, 82, 83, 114, 122, 142).

[Marc2014] P. Marchetti et al. “Molecular separation with organic solvent nanofiltration: a critical review”. *Chemical reviews* 114.21 (2014). (Cit. on pp. 4, 5, 11, 17, 44–46, 82, 121).

[Marc2017] P. Marchetti, L. Peeva, and A. Livingston. “The selectivity challenge in organic solvent nanofiltration: membrane and process solutions”. *Annual review of chemical and biomolecular engineering* 8 (2017). (Cit. on pp. 12, 13).

[Mart2012] M. B. Martınez et al. “Separation of a high-value pharmaceutical compound from waste ethanol by nanofiltration”. *Journal of Industrial and Engineering Chemistry* 18.5 (2012). (Cit. on p. 1).

[Mein2006] D. Meintrup and S. Schäffler. *Stochastik: Theorie und Anwendungen*. Springer-Verlag, 2006 (cit. on p. 22).

[Meli2007] T. Melin and R. Rautenbach. *Membranverfahren: Grundlagen der Modul-und Anlagenauslegung*. Springer-Verlag, 2007 (cit. on pp. 4, 104, 107, 108).

[Menn2016a] D. Menne et al. “Precise tuning of salt retention of backwashable polyelectrolyte multilayer hollow fiber nanofiltration membranes”. *Journal of Membrane Science* 499 (2016). (Cit. on pp. 124, 125, 133).

[Menn2016b] D. Menne et al. “Regenerable polymer/ceramic hybrid nanofiltration membrane based on polyelectrolyte assembly by layer-by-layer technique”. *Journal of Membrane Science* 520 (2016). (Cit. on pp. 4, 7, 120, 123–125, 137, 151).

[Mert2018] M. Mertens et al. “Crosslinked PVDF-membranes for solvent resistant nanofiltration”. *Journal of Membrane Science* 566 (2018). (Cit. on pp. 5, 82, 83).

[Mill2005] M. D. Miller and M. L. Bruening. “Correlation of the Swelling and Permeability of Polyelectrolyte Multilayer Films”. *Chemistry of Materials* 17.21 (2005). (Cit. on pp. 124, 145).

[Moha2015] A. W. Mohammad et al. “Nanofiltration membranes review: recent advances and future prospects”. *Desalination* 356 (2015). (Cit. on pp. 4, 82).

[Mont2016] V. A. Montesdeoca et al. “Modelling of membrane cascades for the purification of oligosaccharides”. *Journal of Membrane Science* 520 (2016). (Cit. on pp. 47, 58).

[Moor2011] W. Moore et al. *Physikalische Chemie*. De Gruyter, 2011 (cit. on p. 98).

[Mukh2014] D. Mukherji, C. M. Marques, and K. Kremer. “Polymer collapse in miscible good solvents is a generic phenomenon driven by preferential adsorption”. *Nature communications* 5 (2014). (Cit. on p. 145).

[Niew2008] C. Niewersch et al. “Potentials of using nanofiltration to recover phosphorus from sewage sludge”. *Water science and technology* 57.5 (2008). (Cit. on pp. 102, 109).

[Nigh1959] E. Nightingale Jr. “Phenomenological theory of ion solvation. Effective radii of hydrated ions”. *The Journal of Physical Chemistry* 63.9 (1959). (Cit. on p. 88).

[Nosk2005] S. Y. Noskov, G. Lamoureux, and B. Roux. “Molecular dynamics study of hydration in ethanol- water mixtures using a polarizable force field”. *The Journal of Physical Chemistry B* 109.14 (2005). (Cit. on pp. 99, 100, 109, 140).

[Oatl2017] D. L. Oatley-Radcliffe et al. “Nanofiltration membranes and processes: A review of research trends over the past decade”. *Journal of Water Process Engineering* 19 (2017). (Cit. on p. 4).

[Ogie2015] W. Ogieglo et al. “In situ ellipsometry studies on swelling of thin polymer films: A review”. *Progress in Polymer Science* 42 (2015). (Cit. on pp. 132, 133).

[Ohs2016] B. Ohs, J. Lohaus, and M. Wessling. “Optimization of membrane based nitrogen removal from natural gas”. *Journal of Membrane Science* 498 (2016). (Cit. on pp. 23, 48, 49).

[Ohs2019] B. Ohs, M. Falkenberg, and M. Wessling. “Optimizing hybrid membrane-pressure swing adsorption processes for biogenic hydrogen recovery”. *Chemical Engineering Journal* (2019). (Cit. on pp. 52, 80).

[Ouya2010] L. Ouyang et al. “Catalytic hollow fiber membranes prepared using layer-by-layer adsorption of polyelectrolytes and metal nanoparticles”. *Catalysis Today* 156.3-4 (2010). (Cit. on p. 123).

[Peet1998] J. Peeters et al. “Retention measurements of nanofiltration membranes with electrolyte solutions”. *Journal of membrane science* 145.2 (1998). (Cit. on pp. 121, 138).

[Peev2010] L. Peeva, M. Sairam, and A. Livingston. “2.05 - Nanofiltration Operations in Nonaqueous Systems”. In*Comprehensive Membrane Science and Engineering*. Ed. by E. Drioli and L. Giorno. Oxford: Elsevier, 2010. Pp. 91–113. (Cit. on pp. 5, 11).

[Peev2014] L. Peeva et al. “Continuous purification of active pharmaceutical ingredients using multistage organic solvent nanofiltration membrane cascade”. *Chemical Engineering Science* 116 (2014). (Cit. on p. 47).

[Peto2000] P. Petong, R. Pottel, and U. Kaatze. “Water- ethanol mixtures at different compositions and temperatures. A dieletric relaxation study”. *The Journal of Physical Chemistry A* 104.32 (2000). (Cit. on pp. 93, 99).

[Pihl2012] A. Pihlajamäki, T. Laakso, and M. Mänttäri. “Surface Charge of Nanofiltration Membranes in Different Ethanol/Water Mixtures”. *Procedia Engineering* -.44 (2012). (Cit. on pp. 84, 111).

[Pinh1996] S. P. Pinho and E. A. Macedo. “Representation of salt solubility in mixed solvents: a comparison of thermodynamic models”. *Fluid Phase Equilibria* 116.1-2 (1996). (Cit. on p. 88).

[Post2013] S. Postel et al. “On negative retentions in organic solvent nanofiltration”. *Journal of Membrane Science* 447 (2013). (Cit. on pp. 12, 16, 20, 27, 36, 44, 45, 51–54, 56, 121).

[Post2014] S. Postel et al. “Multicomponent mass transport in organic solvent nanofiltration with solvent mixtures”. *Journal of membrane science* 466 (2014). (Cit. on pp. 46, 47).

[Post2015] S. Postel and M. Wessling. “Do silicone-based membranes permeate or reject salts?” *Desalination* 357 (2015). (Cit. on pp. 5, 82, 83, 112, 121).

[Post2016] S. Postel, C. Schneider, and M. Wessling. “Solvent dependent solute solubility governs retention in silicone based organic solvent nanofiltration”. *Journal of Membrane Science* 497 (2016). (Cit. on p. 11).

[Qiao2006] X. Qiao and T.-S. Chung. “Diamine modification of P84 polyimide membranes for pervaporation dehydration of isopropanol”. *AIChE journal* 52.10 (2006). (Cit. on p. 93).

[Rahm1997] M. M. Rahman and Z. Govindarajulu. “A modification of the test of Shapiro and Wilk for normality”. *Journal of Applied Statistics* 24.2 (1997). (Cit. on p. 22).

[Raja2014] S. Rajabzadeh et al. “Preparation of low-pressure water softening hollow fiber membranes by polyelectrolyte deposition with two bilayers”. *Desalination* 344 (2014). (Cit. on p. 123).

[Raza2017] M. Razali et al. “Exploring and exploiting the effect of solvent treatment in membrane separations”. *ACS applied materials & interfaces* 9.12 (2017). (Cit. on p. 18).

[Reic1994] C. Reichardt. “Solvatochromic dyes as solvent polarity indicators”. *Chemical Reviews* 94.8 (1994). (Cit. on pp. 15, 88).

[Reno2018] T. Renouard, A. Lejeune, and M. Rabiller-Baudry. “Separation of solutes with an organic solvent nanofiltration cascade: Designs, simulations and systematic study of all configurations”. *Separation and Purification Technology* 194 (2018). (Cit. on p. 47).

[Roys1995] P. Royston. “Statistical Algorithms: Remark AS R94: A Remark on Algorithm AS 181: The W-test for Normality”. *j-APPL-STAT* 44.4 (1995). (Cit. on p. 22).

[Sche2014] C. Scherzinger et al. “Cononsolvency of poly-N-isopropyl acrylamide (PNIPAM): Microgels versus linear chains and macrogels”. *Current Opinion in Colloid & Interface Science* 19.2 (2014). (Cit. on pp. 140, 145).

[Schm2013] P. Schmidt, T. Köse, and P. Lutze. “Characterisation of organic solvent nanofiltration membranes in multi-component mixtures: Membrane rejection maps and membrane selectivity maps for conceptual process design”. *Journal of Membrane Science* 429 (2013). (Cit. on p. 11).

[Schm2014] P. Schmidt et al. “Characterisation of Organic Solvent Nanofiltration membranes in multi-component mixtures: Process design workflow for utilising targeted solvent modifications”. *Chemical Engineering Science* 115 (2014). (Cit. on p. 12).

[Scho2015] M. Scholz et al. “Structural optimization of membrane-based biogas upgrading processes”. *Journal of Membrane Science* 474 (2015). (Cit. on pp. 23, 48, 49).

[Schw1991] C. Schwer and E. Kenndler. “Electrophoresis in fused-silica capillaries: the influence of organic solvents on the electroosmotic velocity and the. zeta. potential”. *Analytical Chemistry* 63.17 (1991). (Cit. on pp. 85, 93, 99).

[Scot1946] T. A. Scott Jr. “Refractive Index of Ethanol–Water Mixtures and Density and Refractive Index of Ethanol–Water–Ethyl Ether Mixtures.” *The Journal of physical chemistry* 50.5 (1946). (Cit. on p. 135).

[Sean2012] B. Seantier and A. Deratani. “Polyelectrolytes at interfaces: applications and transport properties of polyelectrolyte multilayers in membranes”. *Ionic Interactions in Natural and Synthetic Macromolecules* (2012). (Cit. on p. 124).

[See 2007] Y. H. See Toh et al. “In search of a standard method for the characterisation of organic solvent nanofiltration membranes”. *Journal of Membrane Science* 291.1-2 (2007). (Cit. on pp. 12, 19, 86).

[Shap1965] S. S. Shapiro and M. B. Wilk. “An Analysis of Variance Test for Normality (Complete Samples)”. *Biometrika* 52.3/4 (1965). (Cit. on p. 22).

[Shi2015] B. Shi et al. “Performance of spiral-wound membrane modules in organic solvent nanofiltration – Fluid dynamics and mass transfer characteristics”. *Journal of Membrane Science* 494.Supplement C (2015). (Cit. on p. 16).

[Shi2017] B. Shi et al. “Will ultra-high permeance membranes lead to ultra-efficient processes? Challenges for molecular separations in liquid systems”. *Journal of Membrane Science* 525 (2017). (Cit. on pp. 12, 13).

[Shuk2002] R. Shukla and M. Cheryan. “Performance of ultrafiltration membranes in ethanol–water solutions: effect of membrane conditioning”. *Journal of Membrane Science* 198.1 (2002). (Cit. on pp. 84, 130).

[Siew2013a] W. E. Siew et al. “Continuous solute fractionation with membrane cascades–a high productivity alternative to diafiltration”. *Separation and Purification Technology* 102 (2013). (Cit. on pp. 47, 58).

[Siew2013b] W. E. Siew et al. “Molecular separation with an organic solvent nanofiltration cascade–augmenting membrane selectivity with process engineering”. *Chemical Engineering Science* 90 (2013). (Cit. on p. 47).

[Silv2015] J. da Silva Burgal et al. “Organic solvent resistant poly(ether-ether-ketone) nanofiltration membranes”. *Journal of Membrane Science* 479.Supplement C (2015). (Cit. on p. 12).

[Skib2012] M. Skiborowski et al. “Model-based structural optimization of seawater desalination plants”. *Desalination* 292 (2012). (Cit. on pp. 23, 24, 48).

[Smal2012] I. Smallwood. *Handbook of organic solvent properties*. Butterworth-Heinemann, 2012 (cit. on pp. 14, 15, 88).

[Solt2016] H. B. Soltane, D. Roizard, and E. Favre. “Study of the rejection of various solutes in OSN by a composite polydimethylsiloxane membrane: Investigation of the role of solute affinity”. *Separation and Purification Technology* 161 (2016). (Cit. on pp. 11, 44).

[Spie1966] K. Spiegler and O. Kedem. “Thermodynamics of hyperfiltration (reverse osmosis): criteria for efficient membranes”. *Desalination* 1.4 (1966). (Cit. on p. 45).

[Staf2004] N. Stafie, D. Stamatialis, and M. Wessling. “Insight into the transport of hexane–solute systems through tailor-made composite membranes”. *Journal of Membrane Science* 228.1 (2004). (Cit. on pp. 84, 121, 135).

[Stam2006] D. Stamatialis et al. “Observations on the permeation performance of solvent resistant nanofiltration membranes”. *Journal of membrane science* 279.1-2 (2006). (Cit. on pp. 11, 84, 121, 135).

[Step2004] M. A. Stephens. “Goodness of Fit, Anderson-Darling Test of”. In. *Encyclopedia of Statistical Sciences*. John Wiley & Sons, Inc., 2004, pp. 1–4 (cit. on p. 22).

[Stri1997] A. Striegel. “Theory and applications of DMAc/LiCl in the analysis of polysaccharides”. *Carbohydrate polymers* 34.4 (1997). (Cit. on pp. 94, 102).

[SusC2018] SusChem - The European Technology Platform for Sustainable Chemistry. “SIRA - Strategic Innovation and Research Agenda”. *Brochure* (2018). (Cit. on p. 1).

[Tana2008] F. Tanaka, T. Koga, and F. M. Winnik. “Temperature-responsive polymers in mixed solvents: competitive hydrogen bonds cause cononsolvency”. *Physical review letters* 101.2 (2008). (Cit. on pp. 141, 145).

[Thie2018] Y. Thiermeyer, S. Blumenschein, and M. Skiborowski. “Solvent dependent membrane-solute sensitivity of OSN membranes”. *Journal of Membrane Science* 567 (2018). (Cit. on pp. 27, 34).

[Tsui2004] E. M. Tsui and M. Cheryan. “Characteristics of nanofiltration membranes in aqueous ethanol”. *Journal of membrane science* 237.1-2 (2004). (Cit. on pp. 84, 93, 108, 115, 116, 122).

[Tylk2013] B. Tylkowski et al. “Permeation behavior of polysulfone membranes modified by fully organic layer-by-layer assemblies”. *Industrial & Engineering Chemistry Research* 52.46 (2013). (Cit. on p. 124).

[Unit2015] United Nations. “Transforming our world: The 2030 agenda for sustainable development”. *Resolution adopted by the General Assembly* (2015). (Cit. on p. 1).

[Van 2008] B. Van der Bruggen, M. Mänttäri, and M. Nyström. “Drawbacks of applying nanofiltration and how to avoid them: a review”. *Separation and Purification Technology* 63.2 (2008). (Cit. on pp. 4, 82).

[Vand2008] P. Vandezande, L. E. Gevers, and I. F. Vankelecom. “Solvent resistant nanofiltration: separating on a molecular level”. *Chemical Society Reviews* 37.2 (2008). (Cit. on pp. 5, 82).

[Volk2014] A. Volkov et al. “Application of negative retention in organic solvent nanofiltration for solutes fractionation”. *Separation and Purification Technology* 124 (2014). (Cit. on p. 44).

[Walt1997] E. Walter and L. Pronzato. *Identification of parametric models from experimental data*. Springer Verlag, 1997 (cit. on p. 21).

[Wypy2016] G. Wypych. “{PMMA} polymethylmethacrylate”. In*Handbook of Polymers*. Ed. by G. Wypych. Second. ChemTec Publishing, 2016. Pp. 467–471. (Cit. on p. 16).

[Yang2001] X. Yang, A. Livingston, and L. F. Dos Santos. “Experimental observations of nanofiltration with organic solvents”. *Journal of Membrane Science* 190.1 (2001). (Cit. on pp. 11, 84).

[Yaro2000] A. E. Yaroshchuk. “Dielectric exclusion of ions from membranes”. *Advances in colloid and interface science* 85.2-3 (2000). (Cit. on p. 121).

[Zeid2013] S. Zeidler, U. Kätzel, and P. Kreis. “Systematic investigation on the influence of solutes on the separation behavior of a PDMS membrane in organic solvent nanofiltration”. *Journal of membrane science* 429 (2013). (Cit. on p. 44).

[Zhan2007] Y. Zhang, T. Xu, and Z. Liu. “Streaming potential across a porous charged membrane in organic-aqueous solutions”. *Desalination* 212.1-3 (2007). (Cit. on p. 84).

[Zhao2006] Y. Zhao and Q. Yuan. “A comparison of nanofiltration with aqueous and organic solvents”. *Journal of membrane science* 279.1-2 (2006). (Cit. on p. 84).

[Zhuk2007] A. Zhukov. “Integrated investigations of the electrosurface properties of nonaqueous disperse and capillary systems”. *Advances in colloid and interface science* 134 (2007). (Cit. on p. 85).

[Zuo2018] T. Zuo et al. “Water/Cosolvent Attraction Induced Phase Separation: a Molecular Picture of Cononsolvency”. *arXiv preprint arXiv:1806.11109* (2018). (Cit. on p. 145).

[Zwij2012] H. J. Zwijnenberg et al. “Important factors influencing molecular weight cut-off determination of membranes in organic solvents”. *Journal of Membrane Science* 390-391 (2012). (Cit. on p. 11).